UNIVERSIDADE DE SÃO PAULO
INSTITUTO DE FÍSICA DE SÃO CARLOS

LAYLA PIRES

Optical strategies for diagnosis and treatment of melanoma

São Carlos
2017

LAYLA PIRES

Optical strategies for diagnosis and treatment of melanoma

Thesis presented to the Graduate Program in Physics at the Instituto de Física de São Carlos, Universidade de São Paulo to obtain the degree of Doctor of Science.

Concentration area: Applied Physics

Option: Biomolecular Physics

Advisor: Prof[a]. Dr[a]. Cristina Kurachi

Corrected version

(Original version available on the Program Unit)

São Carlos

2017

Cataloguing data revised by the Library and Information Service
of the IFSC, with information provided by the author

Pires, Layla
Optical strategies for diagnosis and treatment of melanoma / Layla Pires; advisor Cristina Kurachi - revised version -- São Carlos 2017.
159 p.

Thesis (Doctorate - Graduate Program in Biomolecular Physics) -- Instituto de Física de São Carlos, Universidade de São Paulo - Brasil , 2017.

1. Melanoma. 2. Photodynamic therapy. 3. 2-Photon PDT. 4. Optical clearing agent. 5. Optical diagnosis. I. Kurachi, Cristina, advisor. II. Title.

`

In memory of my grandfather,
diagnosed with melanoma in 1996.

All my love.

ACKNOWLEDGEMENTS

I must express my profound gratitude to my parents, Ramiro and Rosangela, for all efforts to provide me the best education possible. Without their unfailing support and unceasing encouragement through this Ph.D., this accomplishment would not have been possible.

I would like to thank my boyfriend, Paulo Augusto, for all support and encouragement since my undergrad. His partnership, mainly during my internship abroad, was crucial to conclude this Ph.D. Thank you for all your effort on visiting me as many time as it was possible while I was abroad.

I am grateful to my family for all love and support. In particular, I would like to thank my aunt Ane for her big efforts to visit me in Canada during my internship to make sure I wouldn't feel alone when I was far from home, bringing home to me.

I wish to express my sincere gratitude to Prof. Dr. Cristina Kurachi for supervising me since my undergrad. Thank you for your friendship, guidance and encouragement thru the last nine years. I could not have asked for having a better supervisor and mentor for my Ph.D.

A very special thanks to Prof. Dr. Brian C. Wilson, who accepted me as an international student and supported me during this Ph.D. Without your precious collaboration, it would not be possible to conduct this research.

I am also grateful to Prof. Dr. Vanderlei S. Bagnato for the valuable guidance and encouragement offered to me during this Ph.D.

I am also grateful to the collaborators from Princess Margaret Cancer Centre, Dr. Alex Vitkin, and from St. Michael's hospital, Dr. Yeni Yucel and Shireen Khattak. These collaborations were crucial for the completion of this study.

I wish to thank Prof. Pier Luigi Lollini, Universitá Di Bologna who kindly donated the amelanotic B78H1 cells for this project.

I must thank Dr. Francisco Guimarães, Dr. Leonardo de Boni and Dr. Ana Gabriela Salvio for the valuable discussions that definitely contributed to this thesis finalization.

I am also grateful to the Advanced Optical Microscopy Facility and staffs. James, Miria, and Judy, I appreciate all the support with the 2-photon experiments, mainly for the conjunctival tumors.

I am also grateful to the Animal Resources Center and the STTARR facilities and staffs from the Princess Margaret Cancer Research Tower. Roberto, Mafe, Maria, and Deborah, I appreciate all the training and support for the animal's studies.

A special thank for all the staff from Sao Carlos Institute of Physics, University of Toronto and University Health Network.

I thank my labmate fellows at UHN for the stimulating discussions and support during my internship abroad. I am particular grateful to Carl, Santa, Masood, Greg, Azusa, and Valentin. I really appreciate the time I spent with you guys.

I take this opportunity to express gratitude to all my friends from the Biophotonics lab, especially the ones involved in this thesis: Clovis, Sebastião, Renan and Lili. Thanks to you all!

I must thank my friends with whom I shared the *"Castle"* office the last years. Cintia, Mariana, Michelle, Mirian, Thereza, and Didi, I couldn't have asked for best friends.

I am grateful for the funding sources that allowed me to develop this project: Coordination for the Improvement of Higher Level Personnel - Capes, Council of Scientif and Technological Development (CNPq) – Science Without Borders Program and 305795/2016-3, UofT-USP joint project, FAPESP (Cepof – 2013/07276-1) and Princess Margaret Cancer Foundation.

“What we do for ourselves dies with us. What we do for others and the world remains and is immortal.”

Albert Pike

ABSTRACT

PIRES, L. **Optical strategies for diagnosis and treatment of melanoma.** 2017. 159 p. Thesis (Doctor in Science) - Instituto de Física de São Carlos, Universidade de São Paulo, São Carlos, 2017.

Melanoma is a pigmented tumor that originates from the melanocytes; pigmented cells present throughout the body, including skin and iris. The cutaneous form is the most common type, and it represents about 5% of the skin tumors diagnosed in Brazil. Although it does not have a high incidence, it represents about 80% to 85% of all skin tumor deaths. The second most frequent type of melanoma is ocular. It represents 5% of all melanoma cases and is a potentially lethal disease, especially when it causes metastasis. The main therapeutic approach for melanomas, in general, is surgery, with resection of the cutaneous lesion or enucleation in the case of ocular melanoma. Other techniques such as adjuvant immunotherapy, palliative chemotherapy, and radiotherapy are also used. However, they have low efficacy and several side effects. Photodynamic therapy is a therapeutic modality based on the interaction of light at specific wavelength and photosensitizer, in the presence of molecular oxygen, leading the cell to death. As melanoma is a pigmented cancer, it usually does not respond well to photodynamic therapy due to the high absorption of light on the surface of the tumor, making volumetric eradication impossible. This project investigated optical strategies for the diagnosis and treatment of melanoma. For the diagnosis, it was evaluated the fluorescence lifetime technique to differentiate melanoma and normal skin. A sensitivity of 99.4%, specificity of 97.4% and accuracy of 98.4% were achieved using linear discrimination analysis. For the cutaneous melanoma treatment, PDT combined to optical clearing agents (OCAs) was investigated. Vascular and cell-target photosensitizers were evaluated combined or not to OCAs. OCA improved PDT response in all pigmented tumors treated, but the best results were achieved when a dual-photosensitizer treatment combined to OCA was performed. The treatment of conjunctival melanoma was conducted using 2-photon excitation photodynamic therapy. The advantage of this technique is the use of infrared light, in a wavelength that melanin has a low absorption, improving the light penetration into the tumor. The tumor histology shows that apoptosis was

induced only at the treatment site, with no damage to the surrounding tissue. Additionally, a single TPE-PDT session could treat the entire tumor.

Keywords: Melanoma. Photodynamic therapy. 2-Photon PDT. Optical clearing agent. Optical diagnosis.

RESUMO

PIRES, L. **Estratégias ópticas para o diagnóstico e tratamento do melanoma.** 2017. 159 p. Tese (Doutorado em Ciências) – Instituto de Física de São Carlos, Universidade de São Paulo, São Carlos, 2017.

O melanoma é um tumor pigmentado que surge dos melanócitos, células pigmentadas presentes em todo o corpo, incluindo a pele e a íris. A forma cutânea é a mais comum e representa cerca de 5% dos tumores cutâneos diagnosticados no Brasil. Embora não tenha uma alta incidência, representa cerca de 80% a 85% de todas as mortes por tumor de pele. O segundo tipo de melanoma mais frequente é o ocular. Representa 5% de todos os casos de melanoma e é uma doença potencialmente letal, especialmente em casos de metástase. A principal abordagem terapêutica para melanomas, em geral, é a cirurgia, com ressecção da lesão cutânea ou enucleação no caso do melanoma ocular. Outras técnicas, como imunoterapia adjuvante, quimioterapia paliativa e radioterapia também são usadas, porém, apresentam baixa eficiência e muitos efeitos colaterais. A terapia fotodinâmica é uma modalidade terapêutica baseada na interação da luz em um comprimento de onda específico e um fotossensibilizador, na presença de oxigênio molecular, levando a célula à morte. Como o melanoma é um câncer pigmentado, geralmente não responde bem à terapia fotodinâmica devido à alta absorção de luz na superfície do tumor, impossibilitando a erradicação volumétrica. Este projeto investigou estratégias ópticas para o diagnóstico e tratamento do melanoma. Para o diagnóstico, foi avaliada a técnica de tempo de vida de fluorescência para distinguir melanoma de pele normal. Utilizando análise de discriminação linear, obteve-se uma sensibilidade de 99,4%, especificidade de 97,4% e precisão de 98,4%. Para o tratamento de melanoma cutâneo, a PDT combinada com clareadores ópticos (OCAs) foi investigada. Um fotossensibilizador que tem como alvo vaso sanguíneo e um fotossensibilizador de alvo celular foram avaliados combinados ou não com OCAs. OCAs são soluções hiperosmóticas que desidratam o tecido, diminuindo o espalhamento da luz e melhorando a penetração de luz em profundidade. OCA melhorou a resposta de PDT em todos os tumores melanóticos tratados, mas os melhores resultados foram obtidos quando a PDT foi realizada com a combinação dos fotossensibilizadores e clareador óptico em uma única sessão. O tratamento do melanoma conjuntival foi realizado utilizando a terapia fotodinâmica por excitação de

2 fótons (TPE-PDT). A vantagem desta técnica é o uso de luz na região do infravermelho, em um comprimento de onda que melanina tem baixa absorção, melhorando a penetração de luz no tumor. A histologia do tumor mostrou que a apoptose foi induzida apenas no local do tratamento, sem danos no tecido adjacente. Além disso, uma única sessão de TPE-PDT foi capaz de tratar todo o tumor.

Palavras-chave: Melanoma. Terapia fotodinâmica. TFD por absorção de 2 fótons. Agente clareador óptico. Diagnóstico óptico.

LIST OF FIGURES

LIST OF TABLES

LIST OF ABBREVIATIONS AND ACRONYMS

ABCD	Asymmetry, Border, Color, Diameter
ALA	Aminolevulinic Acid
ANOVA	Analysis of Variance
ATCC	American Type Culture Collection
DNA	Deoxyribonucleic acid
DMEM	Dulbecco's Modified Eagle's Medium
DMSO	Dimethyl Sulphoxide
DRS	Diffuse Reflectance Spectroscopy
DT	Doubling Time
ELM	Epiluminescence Microscopy
FAD	Flavin Adenine Dinucleotide
FDA	Food and Drug Administration
FRET	Forster Resonance Energy Transfer
H&E	Hematoxylin and Eosin
IRF	Impulse Response Function
LIFS	Laser Induced Fluorescence Spectroscopy
NAD	Nicotinamide Adenine Dinucleotide
OIDRS	Oblique-Incidence Diffuse Reflectance Spectroscopy
OCA	Optical Clearing Agent
OCT	Optic Coherence Tomography
PEG	Polyethylene Glycol
PMT	Photomultiplier
PS	Photosensitizer
PDZ	Photodithazine
PDT	Photodynamic Therapy
RNA	Ribonucleic acid
SDT	Sonodynamic Therapy
SGR	Specific Growth Rate
TCSPC	Time-Correlated Single Photon Counting
TEM	Transmission Electron Microscopy
TPA	Two-Photon Absorption

TPE	Two-Photon Excitation
TPE-PDT	Two-Photon Excitation Photodynamic Therapy
TUNEL	Terminal Deoxynucleotidyl Transferase dUTP Nick End Labeling
VIS	Visudyne

CONTENTS

CHAPTER 1 GENERAL OVERVIEW

1.1 INTRODUCTION

1.1.1 MELANOMA

Melanoma is a pigmented tumor that originates from the melanocytes; pigmented cells present throughout the body, including skin and iris. According to the National Cancer Data Base (NCDB – US), about 91.2% of the melanomas originate from the skin, followed by 5.2% from the eye and surrounding tissues, 1.3% from the mucosa and 2.2% from the unknown tissue.(1)

Cutaneous melanoma is the most aggressive type of skin cancer. It is characterized by pigmented lesions with high tissue invasion and metastasis rates. Annually, 2-3 million of nonmelanoma and 132 thousand of melanoma skin cancers are expected globally, according to the World Health Organization. Although melanoma is responsible for only 5% of all skin cancer, It represents about 80% to 85% of all skin cancer deaths.(2) It is estimated that in 10 to 15 years the incidence of cutaneous melanoma will double and that the survival will be around 69% considering the average world value and 56% for developing country.

Besides the tumor aggressiveness, the diagnosis at early stages increases the patient prognosis significantly, with high possibilities of cure. The first-line diagnostics include clinical analysis of the lesions, mainly the macroscopic characteristics of the lesion, known as ABCDEs, Asymmetry, irregular Borders, more than one or uneven distribution of Color, a Diameter of more than 6 mm and lesion progression. Excisional biopsy of lesions with 1-2 mm margins of normal skin should be performed in patients with suspected lesions, and the diagnosis confirmed by histopathological examination.(3) The main therapeutic approach for cutaneous melanoma is the surgery, with resection of the cutaneous lesion and, in some cases, with lymph node dissection. However, the recurrence rate varies from 7 to 51%, according to the tumor staging. (3,4) Adjuvant immunotherapy, palliative chemotherapy, and radiotherapy are also used, but they have a limited effect on patients' life expectancy.

Ocular melanoma is the second most frequent melanoma type following the cutaneous one, and it represents about 5.2% of all melanomas. (1) For ocular melanomas, 85% are uveal, 4.8% are conjunctival, and 10.2% occurs at other sites. It is a potentially lethal disease, especially when it causes metastasis. According to

the Melanoma Research Foundation, six people per 1 million will be diagnosed with ocular melanoma every year. In the majority of cases, ocular melanoma develops slowly from the pigmented cells of the choroid, but it also can develop from the pigmented cells of the iris and ciliary body. It can involve any of the three areas of the eye: iris, ciliary body, and choroid or posterior uvea. (5) The diagnosis is based on clinical examination of the tumor with biomicroscopy and indirect ophthalmoscopy followed by confirmation with ultrasonography, optical coherence tomography, and fundus angiography. Although biopsies are not indicated, fine-needle aspiration biopsy (FNAB) can be used to confirm the diagnosis. (5) The conventional treatments include brachytherapy, teletherapy, transpupillary thermotherapy, surgical resection (partial or full tumor removal), enucleation chemotherapy, radiation therapy, and immunotherapy, but recurrences are frequent with high morbidity depending on the initial tumor size. (5–7)

The lack of successful therapeutic options and the increase in melanoma incidence makes the development of non-invasive diagnosis techniques as well as the new treatments critical.

1.1.2 OPTICAL DIAGNOSTICS

Optical diagnosis relies on the analysis of light-tissue interactions to obtain optical tissue characteristics to differentiate normal and cancer tissues, for example. Some chromophores when absorbing light are excited, and when returning to its ground state emit light at a longer wavelength, that is called fluorescence.(8) These molecules, called fluorophores, are mainly excited at the ultraviolet/violet range of the spectrum. In the skin, the main UV absorbers are melanin and hemoglobin (330-400 nm) and some proteins (280-330 nm). Other molecules such as DNA, RNA, NAD/NADH and FAD also absorbs light in this spectrum range.(8) The fluorescence emission spectrum is characteristic of each chromophore and its near microenvironment, being considered an optical signature that can be used for disease diagnosis.

There are two main techniques used for steady-state fluorescence diagnosis, spectroscopy, and imaging. In both cases, the diagnosis is non-invasive and provide

real-time information about the target tissue, improving clinical lesion examination and reducing the need for biopsies and health system costs.

The steady-state fluorescence is widely used for nonmelanoma skin cancer diagnosis, although it is not as effective for melanoma. The light when interacting with tissues can be either absorbed or scattered.(8) Both processes are related to light attenuation and penetration in tissue depth. If the light is attenuated at the first layers of the skin, then the steady-state fluorescence will provide information only about these superficial layers and not for deeper structures or tumors, for example.(8) That is the case of melanoma. Melanin has a significant absorption in the violet-blue spectrum region, then when these wavelengths are used to excite the fluorophores present in the tissue, melanin acts as an absorber, preventing the light penetration in depth, and also will absorb the fluorescence emitted in its vicinity. Then, the steady-fluorescence technique is not able to provide information about the tissue and cannot be used to detect melanoma. A technique that has a potential to overcome these limitations is the fluorescence lifetime that provides real-time information targeting tissue metabolism status.

1.1.2.1 Fluorescence lifetime

The fluorescence lifetime of a molecule is the average time at which the molecule remains excited before its decay to the ground state through fluorescence emission. Measuring the lifetime of biological molecules provides valuable information about the tissue, especially about the metabolic condition of the cells.(9,10) The main fluorophores present in biological tissues used for lifetime fluorescence are NADH and FAD; cofactors in aerobic and anaerobic respiration pathways, the main difference between normal skin and most of the tumors.

The cofactor NADH has two distinct fluorescence lifetimes, a short and a long lifetime, which can be related to its free and protein-bound forms, respectively.(9) On the other hand, FAD protein-bound form has a shorter lifetime than its free form. Besides that, fluorescence lifetime can also provide information about the amount of NADH present in the mitochondria at the bond state, then related to the oxidative phosphorylation, or its free state at the membrane, related to the glycolysis, normal metabolism of injured tissue.(10) Although melanin still absorbs the light, using the fluoresce lifetime it is possible to differentiate melanin signal to the target

fluorophores, as NADH and FAD co-factors, and then acquire information about the tissue that can be used as a real-time and non-invasive diagnosis.

1.1.3 PHOTODYNAMIC THERAPY

Photodynamic Therapy (PDT) is a therapeutic modality based on the interaction between light and photosensitizer (PS), in the presence of oxygen, to induce cell death. The technique relies on photochemical reactions of the interaction of the excited photosensitizer with organic substrates and/or surrounding molecules generating reactive oxygen species such as hydrogen peroxide, superoxide radical and hydroxyl ─ "mechanism type I," promoting the oxidation of biomolecules. Another mechanism is the energy transfer between the photosensitizer and the oxygen present in the cell.(11) The photosensitizer is excited and transfer energy mostly to the molecular oxygen. Then, oxygen is excited to a singlet state, highly reactive and cytotoxic, generating oxidation of cellular structures such as mitochondria and membranes - the "Type II mechanism."(12)

The technique has been widely used for the local treatment of various cancers such as the uterine cervix, esophagus, gastric, bladder, and non-melanoma skin.(13–15) Clinical trials of photodynamic therapy in basal cell carcinoma showed complete response rates over 85%. For melanomas, there are not many trials that certify the effectiveness of the technique. In most of the studies, photodynamic therapy reduces the volume of the lesion but does not eliminate it, resulting in detrimental effects to the patient.

1.1.3.1 Melanoma resistance to PDT

According to Huang et al. 2013, PDT response on melanoma is limited mainly due to melanin optical interference, antioxidant effect of melanin, sequestration of PS inside the melanosomes, defects in apoptotic pathways and efflux of PS by the ATP-binding cassette.(16)

The optical interference is caused by the melanin, a pigment produced by the melanosomes with a high absorption in the entire visible spectrum. Besides that, melanin accumulates inside the cells in granules with different sizes, which implicates in not only an absorber component as a scatter too. These characteristics limit light

penetration in depth, restricting any optical technique to the most superficial layers of the tumor.

Melanin also plays a significant role in the cell photoprotection, acting as an antioxidant compound, preventing cell damages caused mainly by chemotherapeutic-induced reactive oxygen species.(17) This characteristic is also related to the PS sequestration by the melanosomes. During PDT, the photosensitizer absorbs light and goes to an excited triplet state then, transfer energy to oxygen present in the cell. The oxygen is excited to the singlet state that is highly reactive, causes oxidation of the cell organelles, membranes, proteins inducing the cell to death. If the photosensitizer is sequestered by the melanosomes, the reactive oxygen species produced will be neutralized by the melanin reducing the PDT effect. These characteristics of melanoma that limit PDT response may be overcome with strategies to change the tissue optical properties, combination of photosensitizers and maybe new light irradiation regimens, as two-photon excitation.

1.1.3.2 Strategies to enhance PDT response on melanoma

The high level of pigmentation in melanoma has made it unsuitable for PDT since the light is highly attenuated so that the full tumor thickness (typically few mm) is not homogeneously and globally irradiated. Thus, it is necessary to develop new methods to improve the light distribution into melanoma and guarantee the death of the entire tumor. In this study, the use of optical clearing agents and TPE-PDT was set as strategies to overcome the limited light penetration into melanoma.

1.1.3.2.1 Optical clearing agents (OCAs)

An approach to increasing PDT efficiency would be to change melanoma optical characteristics, especially related to absorbance and scattering, and improve light penetration in depth. OCAs are hyperosmotic non-toxic agents as glycerol, polyethylene glycol 400 (PEG-400), sucrose, dimethyl sulphoxide (DMSO), and others with a refractive index close to the one of the skin ~1.4. So, when applied to the skin, it effectively decreases the high light scattering caused by tissue microinterfaces. Then, OCA reduces the light attenuation and increases light penetration in depth.(18,19) OCAs are mainly used to improve tissue imaging using

confocal and 2-photon microscopy and also optical coherence tomography,(18,20) but there was none reported a study with the application OCAs combined to PDT, previously to the present one.

In this study, we aimed to evaluate the effect of the use of OCAs to reduce the light attenuation in melanoma and to increase the light penetration in depth and, thus, the efficiency of the photodynamic therapy.

1.1.3.2.2 Two-Photon excitation photodynamic therapy (TPE-PDT)

Two-photon excitation PDT is a new modality of PDT based on the 2-photon absorption process. Some molecules can absorb two photons of lower energy instead of one of higher energy so that they can be activated to the same excited state as by absorbing a single photon of twice the energy.

In the TPE-PDT, ultrashort (~10^{-13}s) long-wavelength (near-infrared) laser pulses are used to excite the photosensitizer, rather than low-intensity continuous light that is the standard clinical protocol. The main advantage of this technique is the use of near-infrared light, wavelength region where melanin presents a lower absorption when compared to visible light. The decrease in the tissue absorption, results in an increased light penetration into the tumor then, improving treatment response. Two-photon excitation PDT has also been described for *in vitro* and a few *in vivo* studies, but there is no report using TPE-PDT for melanoma treatment. In this study, the TPE- PDT effects were investigated in a conjunctival melanoma model.

1.2 STATE OF THE ART

1.2.1 MELANOMA

Melanoma is an aggressive type of cancer that origins from the melanocytes that migrate from the neural crest to the epidermis during embryogenesis. Because of this fact, melanoma presents a high metastatization capacity even in the initial phases, once the invasion and dissemination characteristics can be considered an innate feature of this cellular type. The most prevalent form originates in the skin, although it may arise from the mucous membranes or other sites to which the neural crest cells migrate as the eye.

Melanin is the pigment synthesized by the melanosomes when excited by the ultraviolet radiation that gives the pigmented characteristic to melanoma. (21) It has a major photoprotection function due to its antioxidative properties. Melanin synthesis involves the hydroxylation of L-tyrosine to L-dihydroxyphenylalanine (L-DOPA) and oxidation of L-DOPA to DOPA-quinone. Due to the cytotoxic byproducts of melanogenesis, all the process take place inside the melanocyte to avoid the cytoplasm exposure to these components. (22)

The term melanoma was first used to describe pigmented malignant lesion by Robert Carswell in 1838, that, 20 years later suggested a massive and depth surgical resection as the standard gold treatment. In 1907 Handley proposed the *en bloc* resection with a large margin. In 1969 Clark and collaborators (23) improved the staging systems for cutaneous melanoma using the tumor invasion of the dermis and subcutaneous fat as a prognostic criterion, that is known as Clark's level. (23) In 1970, Breslow (24) reported the importance of cutaneous melanoma invasion depth as a prognostic factor, that is known as Breslow's depth.(24) In 1992, Morton and co-workers (25) introduced the perioperative lymphatic tracking and selective lymphadenectomy that has now been incorporated as a routine procedure in most major cancer centers.(25)

Besides the primary treatment of cutaneous melanoma still is the surgery, for the ocular melanoma, the tumor management depend on the site, size of tumor and local extension. Then, the treatment varies from observation to enucleation, including plaque radiation therapy, transpupillary thermotherapy, laser photocoagulation, and radiosurgery. (26) According to Finger and collaborators (27), at the time of the ocular melanoma diagnosis, less than 4% of patients have detectable metastatic disease. Despite that, about half of the tumors will metastasize and lead the patient to death, due to the lack of effective systemic treatment.

The last world cancer statistics (Globocan/Iarc project), in 2012, revealed that 232,000 new cases of melanoma would be diagnosed in that year. Moreover, 55,000 deaths would be expected. The highest incidence was observed in Caucasians and over 80% of the cases and 65% of the deaths were in Oceania, Europe and North America.

According to the National Cancer Institute and the American Cancer Society, melanoma is the 5th most common type of cancer in the US and its incidence has rising for the last 30 years. For 2017, it is expected 87,110 new cases and 9,730

deaths related to melanoma, representing 1.6% of all cancer deaths. The 5-year relative survival varies from 98.5% for the localized tumor to 19.9% in cases of distant metastasis.

Karimkhani and collaborators(28) estimated the burden of melanoma globally for incidence, mortality, prevalence, years lived with disability, years of life lost and disability-adjusted life years. Australasia, North America and Western Europe have the highest incidence rate, ~54%, 21%, 15%, respectively. The highest mortality rates were found in Australia, North America and Eastern Europe – 5.62, 2.30, and 2.07, respectively.(28)

The rising melanoma incidence as well as the lack of therapeutic options for melanoma makes the development of new diagnosis and treatment technologies crucial. In this study, we aim to develop optical approaches for non-invasive diagnosis and treatment of cutaneous and conjunctival melanoma in *in vivo* models.

1.2.2 OPTICAL DIAGNOSIS

Optical diagnosis is a non-invasive technique based on tissue optical properties as fluorescence, reflectance, and Raman. The most investigated techniques include optical coherence tomography,(29) fluorescence,(8,30) and reflectance spectroscopy(31-32), Raman spectroscopy(33-34), and confocal microscopy.(29-30)

The fluorescence spectroscopy or imaging reflects the tissue biochemical composition, which is responsible for differentiating cancer and normal skin, for example. It is based on the interaction of light at a specific wavelength and a tissue fluorophore, that can be endogenous or exogenous. The endogenous fluorophores present in the skin are NADH, FAD, collagen, tryptophan, tyrosine, porphyrins, and melanin.(37) As these molecules are related to biological tissue physiology, they can provide a non-invasive real-time information about the skin and then classify the tissue as normal or diseased.

Borisova and collaborators investigated the light-induced autofluorescence spectroscopy (LIAS) to differentiated initial stages of skin cancer. They observed that basal cell carcinoma (BCC) show a lower fluorescence intensity when compared to normal skin. The opposite was observed for squamous cell carcinoma (SCC). LIAS also provided information about the lesion staging. Porphyrin-like signals were seen

in advanced stages of BCC and could assist the clinicians in cases of a patient with multiple lesions that cannot be treated at the same time. The choice was to treat first the lesion in the most advanced stage. Moreover, LIAS was used to monitor the electrochemotherapy response of tumors and showed promising results (30). Studies involving autofluorescence have been carried out for vitiligo (38), psoriasis, dysplastic and malignant lesions. (39-40) Panjepour and collaborators (41) evaluated the fluorescence spectroscopy for the detection of nonmelanoma tumors and compared its accuracy within the patients' skin phototypes. The system consisted of a laser emitting at 410 nm and an optical multichannel analyzer, connected to a fiber optic probe to excite the tissue and collect the fluorescence emission. They found that the variation in the skin pigmentation affected the classification method for normal skin, pre-cancerous and benign lesions(41), demonstrating that melanin may limit the efficiency of fluorescence spectroscopy.

In the most common skin cancer optical diagnosis technique, the aminolevulinic acid (ALA) is applied topically on the skin, resulting in the accumulation of Protoporphyrin IX in the cancerous tissue. Usually, it is used a light source at 405 nm to excite the fluorophore, and the fluorescence is collected mainly in the red range. Leeuw and collaborators(42) investigated the fluorescence imaging for the diagnosis of skin cancer at an early stage using endogenous and exogenous (protoporphyrin IX - PpIX) fluorophores. They used the commercial DyaDerm® fluorescence detection system, with an imaging area of 14 x 18 cm (252 cm^2). A pulsed LED (pulse duration: 5 ms; frequency: 1 Hz; and power: 1 W) emitting at 405 nm was used to excite the skin and the PpIX, and the fluorescence collection in the green range (autofluorescence) and in the red spectrum (PpIX) was separated by the system. The fluorescence was considered positive if the skin area showed a red center surrounded by a yellow halo. A total of 93 patients participated in this clinical trial. The positive fluorescence was detected in 61 patients. Comparing to the histology, the positive fluorescence could be related to pre-clinical benign lesions in 28 patients and pre-malignant lesions in 33 patients. Besides that, in five patients, the fluorescence diagnosis was more sensitive than the clinical examination, demonstrating the technical efficiency on detecting these pre-clinical lesions(42). As the system covers a large area, it reflects a potential for pre-clinical lesions screening.

Although several fluorescence detection techniques and setups have been developed for non-pigmented lesions, the steady-state fluorescence spectroscopy/imaging is still unsuitable for pigmented lesions due to melanin highly absorption at the visible range that prevents the distinction between melanin and skin endogenous fluorophores. In this context, the fluorescence lifetime technique provides information about the fluorescence decay of a molecule that is related to its microenvironment, for example, molecules in a free and a protein-bound state, allowing to differentiate melanin to other fluorophores.

1.2.2.1 Fluorescence lifetime

The fluorescence lifetime technique provides information about the molecules fluorescence decay. This is especially important due to the relation between the molecule fluorescence decay and its form and microenvironment inserted. (43-44)

Cancer in general are characterized by its metabolic rewiring. Metabolism in normal and cancer cells differs mainly due to the ‘aerobic glycolysis’ or Warburg effect. This effect was described in 1956 by O. Warburg(45) when stated that “cancer cells are impaired in respiratory chain function and very glycolytic” that is, even in the presence of oxygen, cancer cells produce energy mainly by glycolysis in the cytosol, four usually associated with an increase in the glucose uptake. It differs from normal cells that, in the presence of oxygen, the main respiration pathway is the oxidative phosphorylation followed by the pyruvate oxidation in the mitochondria – with a higher efficiency to produce ATP.

NADH and FAD co-factors are present in the glycolysis and oxidative phosphorylation pathways in two different forms: free and protein-bond. Both co-factors have two distinc fluorescence lifetime, a short and a long lifetime. In the case of NADH, the short and long lifetime are related to is free and protein-bound form, respectively. For the FAD co-factor, a shorter lifetime is observed to its protein-bound form when compared to its free form.(9) Besides that, fluorescence lifetime can also provide information about the amount of NADH present in the mitochondria at the bond state, then related to the oxidative phosphorylation, or its free state at the membrane, related to the glycolysis, normal metabolism of injured tissue.(10)

Tadrous and collaborators(46) investigated the fluorescence lifetime imaging on *ex vivo* breast cancer tissue. They observed that within individual patients, there

was a difference between the benign and malignancy-associated stroma. In a multivariate analysis they found a significant different between benign stroma, malignancy-associated stroma, blood vessels, and malignant epithelium, demonstrating the potential of the technique to detect breast cancer. (46)

Colasanti and collaborators(47) investigated the fluorescence lifetime technique in a *in vivo* model of fibrosarcoma and reported a shift of NADH from the bound to the.(47) In a study carried out by Pradhan and collaborators(48) in non-metastatic, metastatic and non-tumorigenic cell lines from different species. They used two lasers emitting at 310 nm and 350 nm to excite mainly tryptophan and reduced NADH, respectively. The tryptophan fluorescence lifetime was between 2.5 – 3.7 ns and the NADH lifetime was approximately three times lower in metastatic cells when compared to non-metastatic cells. (48)

Collagen fluorescence lifetime has also been used to differentiate tissue. Galletly et al.(49) investigated the fluorescence lifetime imaging in unstained excision biopsies of basal cell carcinoma (BCC), using a 355 nm laser. They observed a significant decrease in the fluorescence lifetime when compared tumor and its surrounding skin providing important information about the tumor borders.(49)

Dimitrow and collaborators(50) investigated the use of fluorescence lifetime imaging in combination with high-resolution multiphoton laser tomography to distinguish 46 *ex vivo* melanocytic lesions of the human skin. The fluorescence lifetime could differentiate keratinocytes to melanocytes and also correlate the intracellular amount of melanin. They also described a selective fluorescence of melanin for the 800 nm excitation that could be useful on detecting pre-malignant and melanoma lesions.(50)

The fluorescence lifetime method to detect melanoma remains experimental, and its development for *in situ* measurements/imaging is crucial. Melanoma is the most aggressive type of skin cancer and a non-invasive method to diagnose the lesion before the surgery would improve the patient prognosis.

1.2.3 PHOTODYNAMIC THERAPY FOR MELANOMA

Nelson and collaborators reported one of the first studies using PDT for melanoma treatment in 1988. They investigated the effect of PDT using a hematoporphyrin derivative for the treatment of both, non-pigmented and pigmented

tumors in mice. Pigmented tumors uptook more photosensitizer than the non-pigmented ones, although, the PDT response was more significant for the non-pigmented tumors. This lower effect in the pigmented tumor was then justified by the light absorption competition between melanin and the photosensitizer.(51) Based on these results, the subsequent studies were focused on developing new photosensitizers presenting a near-infrared excitation, at a wavelength that melanin has low absorption.(52) Even though some of them induced tumor necrosis at some level, no one could ultimately treat the lesion. Biolo and collaborators investigated a liposome delivered naphtalocyanine in a murine melanoma model. The photothermic measurements showed that, in the absence of the photosensitizer, the irradiation of pigmented tumors at 776 nm and 550 mW/cm^2 could increase the tumor temperature up to 6ºC, due to melanin absorption.(53) The best result for the PDT groups was achieved when two followed PDT sessions were performed: the first one the irradiation was carried out with 300 mW/cm^2 and 520 J/cm^2 and the second with 550 mW/cm^2 and 200 J/cm^2, reaching the tumor growth delay up to 13 days.

As only shifting the excitation wavelength was not enough to improve melanoma response, Busetti and collaborators evaluated the use of a high power peak pulsed laser emitting at 1064 nm to bleach melanin before the treatment and observed a delay in the tumor regrowth of 16 days, compared to the ten days when PDT was performed without pre-irradiation.(54) A benzoporphyrin derivative monoacid ring A (verteporfin) was also investigated as a photosensitizer in a murine melanoma model submitted or not to pre-irradiation at 1064 nm. The combination of 1064 nm irradiation with PDT improved the delay of tumor growth up to 28 days.(55)

Ma and collaborators investigated the combination of violet and red light-mediated PDT to pigmented melanoma in a murine model. They concluded that PDT with violet light could bleach melanin mainly in the superficial layers of skin and tumor, increasing the tumor sensitivity for the red light-mediated PDT and resulting in a more substantial tumor growth inhibition when compared to treatments in reversible order, that is, red-light followed by blue-light mediated PDT. (56) Sharma and collaborators published another study involving melanoma cells depigmentation. A reversible tyrosinase inhibitor was used associated with PDT treatment using hypericin as a photosensitizer. The association showed a significant increase in cell death when comparing the depigmented and untreated melanoma cells.(57)

Sonodynamic therapy (SDT) – a technique that uses ultrasound to excite the photosensitizer and induce the cell death was investigated *in vitro* and *in vivo* in a pigmented melanoma model, using Rose Bengal as a photosensitizer. No difference was observed between PDT and SDT on *in vitro* cell killing. However, SDF was more efficient in controlling melanoma regrowth.(58)

Kim and collaborators(59) reported an enhancement of PDT response for melanoma using bioluminescence as the light source. They called the technique as “bioluminescence-activated deep-tissue photodynamic therapy of cancer.” It was used chlorin e6 as a photosensitizer and conjugates of luciferin-quantum dots as the light source, and promising results in the reduction of the tumor were achieved. For the metastatic model, bioluminescent agents delivery via lymphatic vessels killed tumor cells present in the lymph nodes, improving animal survival.(59)

Upconversion nanoparticles have also been investigated for melanoma treatment with PDT. The upconversion process involves nonlinear optical absorption, that occurs when the nanoparticle converts near-infrared light (longer wavelengths) to visible wavelengths that can be absorbed by the photosensitizers. The advantage is the use of longer wavelengths to penetrate in the tumor and then locally generate the shorter wavelength needed to excite the photosensitizer. In a preclinical model, tumor growth inhibition was observed.

Most of the studies involving PDT for melanoma aims to improve light penetration into the tissue, whether by photosensitizers with absorption in the NIR region or photo/chemical melanin depigmentation. Alternative light sources have also been investigated as bioluminescence or FRET. Although some promising results have been achieved, an efficient protocol has not been established yet, and PDT for melanoma remains as an experimental option. To overcome melanoma’s resistance to optical treatments, we will investigate two techniques: a combination of PDT and optical clearing agent and the use of 2-photon excitation PDT (TPE-PDT).

1.2.3.1 Optical clearing agent

The tissue optical clearing method was proposed by Tuchin et al. (60) relies on the immersion of tissue into optical clearing agents to improve light penetration into the tissue. These hyperosmotic agents have a high refractive index like the indices for tissue components as collagen, elastic fibers, cells, and cell

compartments. The OCA replaces the water present in the tissue, inducing a refractive index matching between these tissue components and the extracellular fluid.(18,31) Then, the tissue scattering is reduced, improving the light penetration in depth. The most studied OCAs are glycerol, polyethylene glycol 400 (PEG-400), butanediol, glucose, dextrose, fructose, sucrose, and DMSO.

Wen and collaborators(61) published one of the first reports involving the optical clearing mechanisms *in vivo*. They performed the investigation in rat dorsal skin using different concentrations of glycerol, administered intradermally. After the OCA injection, the diffuse reflectance signal decreased, indicating a reduction in the tissue scattering. The second harmonic generation imaging showed a decrease in the dermis thickness and collagen fiber diameter. However, no damage to these fibers was observed. (61)

Shan and collaborators(62) have investigated the use of OCAs *ex vivo* to improve disease detection as fibroma, pigmented nevus, seborrheic keratosis, sebaceous cyst, and hemangioma. They observed that OCA's effect might differ between different tissue, probably due to the structure and composition of each tissue. For the fibroma, for example, OCA reduced the dermis thickness and the collagen fibril diameter, improving the light distribution into the tissue. On the other hand, they describe that the OCA could poorly diffuse into pigmented nevus due to its dense arrangement and then no improvement in the light penetration was seen. They then concluded that OCA might not be useful for all kinds of tissue.(62) To overcome this limited transdermal diffusion of OCA, Wen et al.(63) investigated a mix of PEG-400 and different chemical enhancers as thiazone and 1,2-propanediol combined to a physical enhancer (massage) to improve the OCA transdermal diffusion. The best result was achieved for the PEG-400 and 1,2-propanediol mix combined with the massage for 15 minutes, demonstrating that besides the use of different OCAs, the application route also plays an essential role in the clearing process. (63)

Various physical methods have been reported to improve the OCA transdermal diffusion as light irradiation and ablation, ultrasound, and mechanical compressions. Liu et al. (64) investigated the use of light sources as CO_2 and Nd: YAG pulsed lasers *in vivo* before the OCA topical application. They compared the reflectance signal before and after the OCA application and observed that in the pre-

irradiated experimental groups, the reflectance signal decreased up to 9 times more than the non-irradiated group.(64)

Stumpp and collaborators (65) studied the effect of heating to break the stratum corneum. They used a 980 nm laser to heat *in vivo* rat and hamster skin and added artificial absorbers on the surface to increase the heating on the stratum corneum. The OCA effect was assessed by OCT. They observed that 30-45 minutes after the OCA application, the OCT imaging depth was improved in 42%.(65) Xu et al.(66) studied 60% glycerol, 60% PEG-200 and assessed its effect on *ex vivo* porcine skin using OCT. A depth increased of 40% and 29% were observed, respectively. The authors also carried out experiments using ultrasound to improve the transdermal permeating and reached a depth increase of 56% for both OCAs. (66)

Tape stripping is another physical technique that might improve the OCA transdermal diffusion. It relies on the use of a tape that is gently applied to the skin surface and removed several times to break/remove the stratum corneum. (67) In this study, we investigated two OCAs (glycerol and PEG-400, 1,2-propanediol mix) associated with tape stripping and massage to improve its transdermal diffusion.

1.2.3.2 Two-photon excitation photodynamic therapy

The 2-photon absorption process was first theoretically predicted by Goppert-Mayer in 1931.(68) However, the theory was demonstrated experimentally only in the 1960s due to the lasers availability. The process involves the absorption of 2 photons of longer wavelengths and lower energy, instead of one with the equivalent double energy.

Marchesini and collaborators(69) published one of the first studies involving TPE-PDT in mice and *in vitro*. A nanosecond pulsed laser and a continuous wave Nd: YAG laser emitting at 1060 nm were used for *in vitro* and *in vivo* experiments, respectively. However no nonlinear absorption effect was obtained, probably due to the low efficiency of 2-photon absorption for non-focalized lasers.(69) Yamashita and collaborators investigated the pheophorbide-a-mediated TPE-PDT in a human hepatocellular carcinoma model *in vivo*. The tumors were irradiated interstitially with a Q-switched Nd: YAG laser at 1064 nm. However, the results suggested that the

protocol investigated was not enough to induce photodynamic effect, but thermal effects were observed.(70)

As the probability of the 2-photon absorption is much lower than the one-photon absorption, a large photon density should be delivered at the same time to the sample. It means that high power density is essential for 2-photon absorption. However, the increase in the laser power also increases tissue damage and then, its use for biological tissue become unsuitable. The advantage of using a pulsed laser is the possibility to have high instantaneous photon density and low average power density, that is, a large photon density is still delivered to the sample, but in a short period preventing tissue damage. In this context, most of the studies started using femtosecond pulsed lasers that are ideal for 2-photon excitation of biological molecules. During the 2-γ absorption, the molecule absorbs the first photon and is excited from the ground state to a virtual intermediate level, followed by the second photon absorption, reaching the excited state. The molecule capacity to absorb 2-photon is defined as 2-γ cross-section and is expressed in GM ($1GM=10^{-50}.cm^{4}.s/molecule.photon$).

The first studies using femtosecond pulsed Ti: sapphire lasers dates back to 1990s.(71,72) In 1999, Wachter and collaborators(73) investigated the use of NIR femtosecond lasers to activate melanin precursors as dihydroxyindole-2-carboxylic acid (DHICA) and induce tumor damage in a murine melanoma model. They reported that at 730 and 1047 nm increase in the tumor temperature up to 25ºC for 5 min could produce the cytotoxic effects. Necrosis and tumor contraction were observed within twenty-four hours and complete primary tumor clearance 18 days after the treatment. However, the growth of a secondary tumor was also noted. Besides that, poor response was obtained for the TPE at 800 nm due to the low absorption of melanin precursors.(73)

Although some studies have investigated the TPE with the conventional photosensitizers or its precursors as ALA,(74) protoporphyrin IX,(75) porphyrins,(76) and Visudyne,(77) recent research relies on the development of new photosensitizers with higher 2-photon cross-section to improve the TPE-PDT response. Collins and collaborators(78) developed high cross-sections anionic and cationic conjugates, more than two orders of magnitude greater than the commercial dyes. *In vitro* experiments demonstrate that the 2-photon engineered photosensitizers could 50% of the cells with half of the power density when compared to the Visudyne –

commercial photosensitizer. Moreover, they reported effective blood vessel closure using the pyridyl cationic conjugated porphyrin dimmer with no damage to surrounding tissue.(78) Zou et al.(79) developed a series of water-soluble bis(arylidene)cycloalkanone photosensitizer for TPE-PDT. The dye (Di(2,5,8,11,14-pentaoxahexadecan-16-yl)amino)benzaldehyde was effective in interrupting the blood flow of the target vessel in a mouse dorsal skinfold window chamber model. Besides that, in tumor-bearing mice, it inhibited the tumor growth and prolonged the animal survival.(79)

Two-photon excitation nanoparticles have also been developed. The nanoparticles, with large 2-photon cross-section, absorbs 2-photons and generate one photon with high energy right beside to the photosensitizer molecule, improving the PDT response for a more deep tissue.(80) Promising results have been achieved by Zhang and collaborators(81) that developed nanoparticles for photothermal and TPE-PDT. Experiments performed in a xenograft HeLa model showed high efficiency on the tumor growth inhibition.(81)

The TPE process is widely used in the microscope, but its use is still discrete for optical treatments. The development of ultrafast and more accessible lasers made the TPE-PDT a promising technique for the treatment of deeper and pigmented tumors.

This project was developed in collaboration with Dr. Brian C Wilson from Princess Margaret Cancer Centre/ University of Toronto through the Science Without Borders Program – CNPq and a USP-UofT joint grant.

1.3 OBJECTIVES

1.3.1 GENERAL OBJECTIVE

To develop optical strategies for the diagnosis and photodynamic therapy of *in vivo* cutaneous and conjunctival melanoma.

1.3.2 SPECIFIC OBJECTIVES

- to investigate the fluorescence lifetime technique as an optical diagnostic tool for cutaneous melanoma;

- to evaluate the effect of optical clearing agents as an enhancer of visible light penetration into the melanoma and its effect on OCT microvasculature imaging;

- to develop PDT protocols using single and dual-photosensitizers combined or not to optical clearing agents to improve photodynamic response;

- to investigate the effect of 2-photon excitation PDT (TPE-PDT) on melanoma cells *in vitro* and conjunctival murine melanoma model.

CHAPTER 2 MELANOMA OPTICAL DIAGNOSTICS USING TIME-RESOLVED FLUORESCENCE LIFETIME

2.1 OBJECTIVE

This chapter aims to evaluate the efficacy of the time-resolved fluorescence lifetime spectroscopy to detect cutaneous melanoma in an *in vivo* murine model.

2.2 MATERIALS AND METHODS

2.2.1 Animal model

Twenty-one nude athymic mice were anesthetized using 5% isoflurane for induction and 2% for maintenance. The melanoma lesion was induced by an intradermal injection of 10^7 B16F10 cells (American Type Culture Collection – ATCC, USA) in 100 µL of PBS into the right and left flank regions. All the animal procedures were approved by the Ethical Committee of the Universidade Federal de São Carlos – São Carlos/Brazil.

2.2.2 Time-resolved fluorescence lifetime system

It was used a device built with two diode lasers, emitting at 378 and 445 nm (BDL-375-SMC and BDL-445-SMC, Becker and Hickl, Berlin, Germany), to excite mainly NADH and FAD molecules. The lasers have a repetition rate of 20, 50, 80 MHz and a temporal pulse duration of 50-100 ps. For the measurements, a bifurcated fiber (Ocean Optics, Dunedin, Florida, USA) was used to both, deliver the light to the tissue and to collect the tissue fluorescence. The fluorescence signal was detected using a high-speed hybrid PMT detector (HPM-100-50, Becker and Hickl, Berlin, Germany) and then collected and processed using the TCSPC Software (Becker and Hickl, Berlin, Germany). The impulse response function (IRF) of the system is about 230 ps (Figure 2.1).

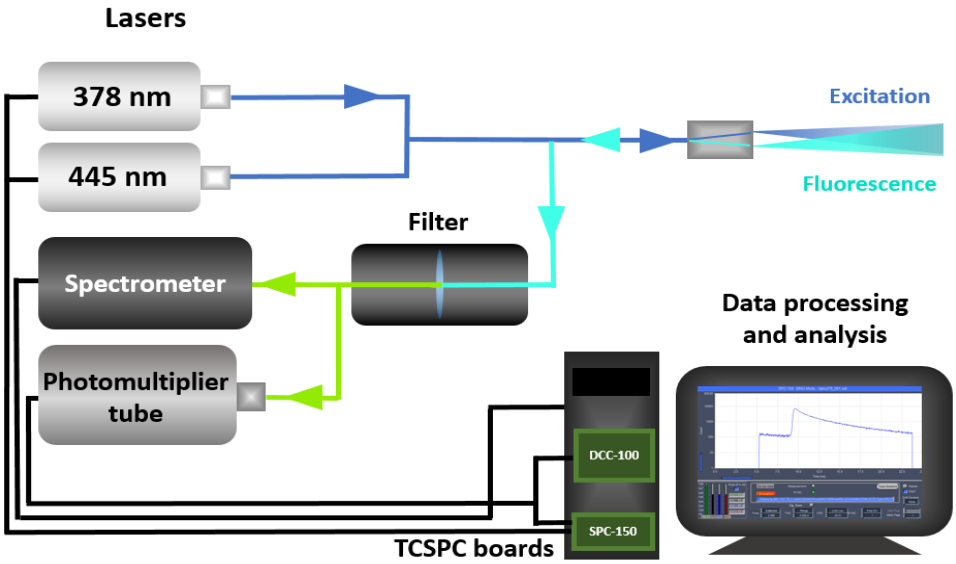

Figure 2.1 - Fluorescence lifetime spectroscopy system that consists of two pulsed lasers and a bifurcated optical fiber that is used to deliver the excitation light and collect the fluorescence data. A spectrometer, photomultiplier and TCSPC boards were used to collect and then analyze the data.
Source: NOGUEIRA (82)

2.2.3 Fluorescence lifetime measurements

The animals were monitored daily, and the measurements were acquired when lesions reached between 2 and 15 mm. The mice were anesthetized with 2% isoflurane using a mask. The optical fiber was placed on the experimental melanoma or the normal skin (far from the tumor), and the fluorescence measurements were collected. At least three measurements were taken from each lesion with each laser. A total of 42 tumors and 42 normal skin sites were investigated. After the measurements, the animals were sacrificed using a high dose of inhaled anesthetic and the tumor was removed for histologic analysis and H&E staining to confirm the tumor diagnosis.

2.2.4 Data processing

The software SPCImage (Becker and Hickl, Berlin, Germany) was used to process the raw data of the time-resolution photon counting as described by Pires et al. (2016).(83) In summary, from the first derivative of the increasing part of the fluorescence lifetime spectrum, the software estimates the IRF followed convolution

and exponential decay fitting. So, the decay curve of the model function was fitted by a bi-exponential function:

$$\boldsymbol{F(t) = a_1\, e^{-\frac{t}{\tau_1}} + a_2\, e^{-\frac{t}{\tau_2}}}, \quad (2.1)$$

using the average fluorescence lifetime values τ_1 and τ_2, corresponding to short and long lifetime components, respectively, and relative coefficients a_1 and a_2, where $a_1 + a_2 = 100$.

2.2.5 Statistical analysis

Statistical analysis was carried out by unpaired t-test. Exact p values were computed, all p values are two-sided, and a $p < 0.001$ was considered statistically significant.

2.2.6 Data analysis

A linear discriminant analysis was used to classify the combination of predictor variables that enhance the differences in the behaviors of the normal skin and cutaneous melanoma groups, using the software MATLAB® R2015a (Mathworks, USA). The classification algorithms were then evaluated based on sensitivity, specificity and accuracy values. Histopathology was used as the gold-standard for the classification.

2.3 RESULTS AND DISCUSSION

In this study, the experimental pigmented melanomas were induced in the superficial layers of the dermis. The tumor grew quite fast, reaching 0.7-0.9 mm thickness in 3 days after the cells injection (Figure 2.2-A). After that, it became nodular and started the vertical development in both directions (Figure 2.2-B). In most of the lesions, when the tumor reached the surface it started an ulcerative process in the tumor core, evidenced by tissue necrosis (Figure 2.2-C). For this reason, the measurements were performed when the tumor was tightly close to the

skin surface. However, a thin layer of normal skin was still covering the tumor (Figure 2.2-B).

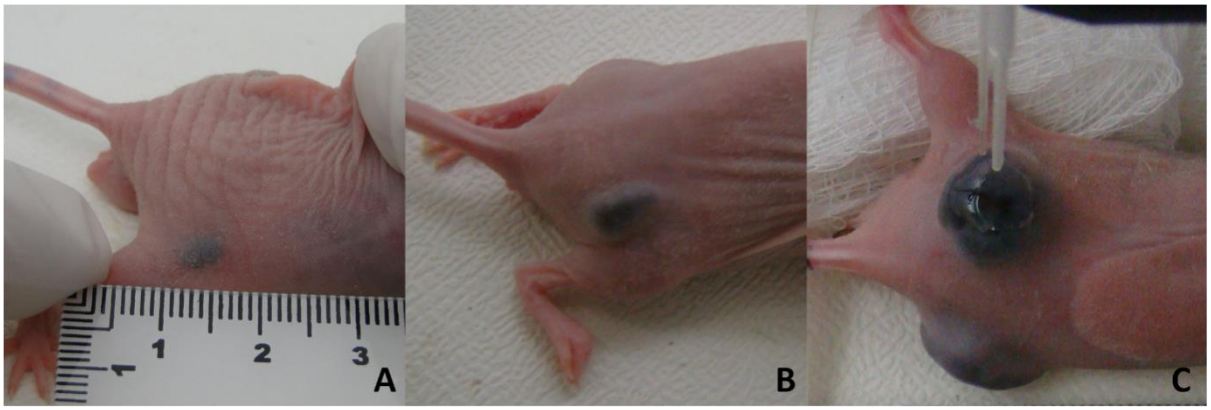

Figure 2.2 - Photographs of the experimental pigmented melanoma model in nude mouse. (A) Tumor at three days after the cell injection; (B) between 4-6 days and (C) 10 days after injection.

Source: By the author.

An example of the decay profiles mainly of NADH and FAD molecules is shown in Figure 2.3. At least 130 spectra were acquired for each melanoma and normal skin.

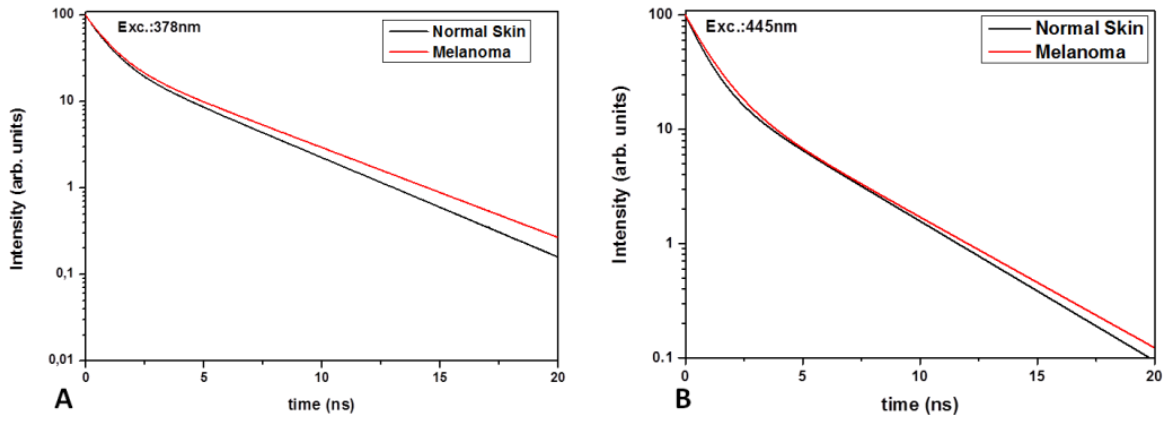

Figure 2.3 - Typical fluorescence decay of melanoma (red) and normal skin (black) when excited at 378 nm (A) and 445 nm (B).

Source: By the author.

The fluorescence decay was then processed using the software SPCImage (Becker and Hickl, Berlin, Germany). The parameters a1, a2, τ_1 and τ_2 obtained for normal skin and melanoma using laser excitation at 378 nm is shown in Figure 2.4.

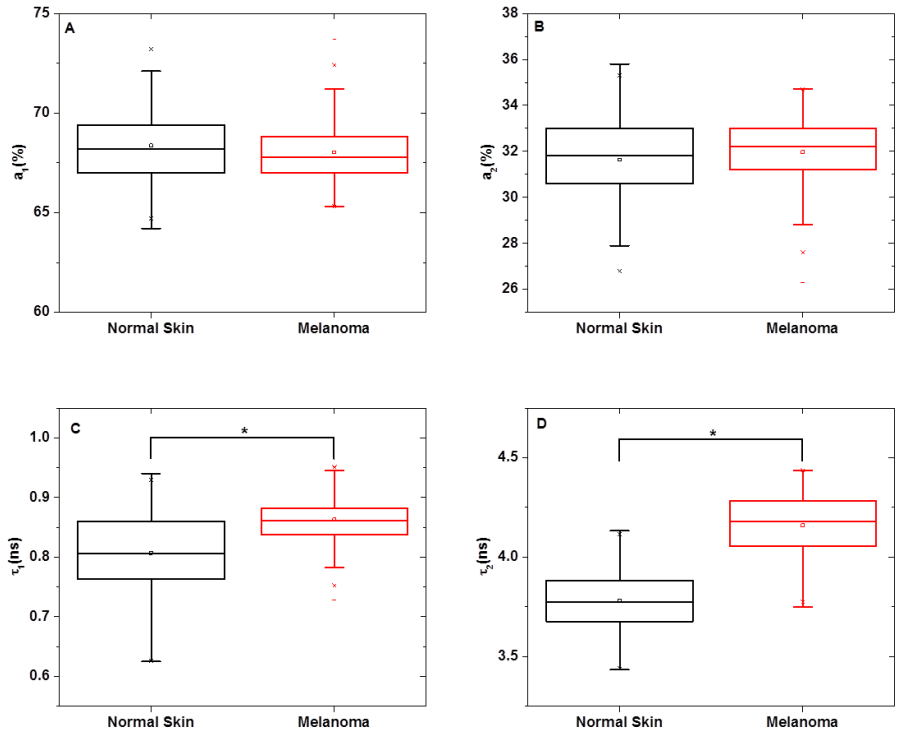

Figure 2.4 - Boxplot graph for the parameters achieved in the data analysis for 378 nm laser excitation: a_1, a_2, τ_1 and τ_2, respectively. Significant differences ($p < 0.001$) exist between normal vs. melanoma for the parameters τ_1 and τ_2(*).

Source: By the author.

No difference was observed between normal skin and melanoma for the parameters a_1 and a_2. Even with the tumor growth in the intradermal site, a thin layer of skin is still present on the top of the tumor, and it may induce changes in the measurements for the 378 nm laser once the high tissue absorption at this wavelength may prevent its penetration into the tumor. A significant statistical difference was observed only when compared short and long lifetimes. Melanoma showed higher short and long lifetimes when compared to normal skin. Following the Warburg effect, in the presence of higher concentration of free NADH molecules when compared to protein-bound molecules, the fluorescence lifetime would decrease. A hypothesis is that due to the melanoma development, it may not reach the stage in which the Warburg effect would be observed. Also, other molecules may contribute to this measurement as collagen and melanin.

Figure 2.5 shows the parameters obtained for both, normal skin and melanoma excited with a 445 nm laser.

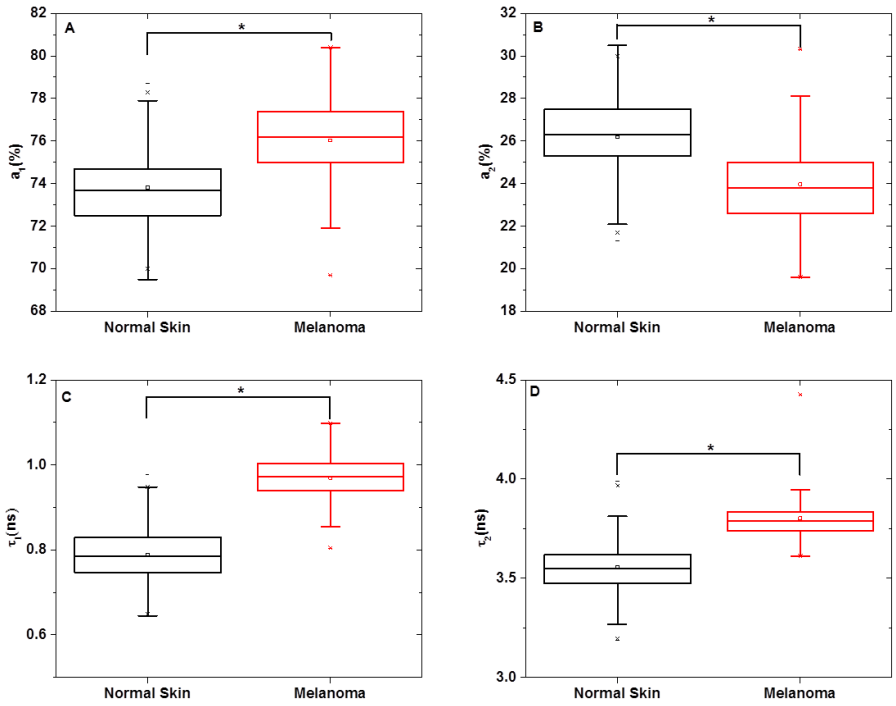

Figure 2.5 - Boxplot for the parameters determined by the data analysis for 445 nm excitation: a_1, a_2, τ_1 and τ_2, respectively. Significant differences p < 0.001) exist between normal skin vs. melanoma for all parameters (*).

Source: By the author.

For the 445 nm laser, all the parameters showed a significant difference when comparing normal skin and melanoma. The a1 and a2 parameters represent the relative quantities of FAD molecules in both states, protein-bound and free, respectively. In Figure 2-5A one can see that melanoma has more FAD protein-bound state molecules than normal skin. Moreover, the opposite is also true. a_2 shows that normal skin has more free FAD molecules than melanoma. If the normal glycolysis and oxidative phosphorylation ratio characteristic of melanoma were proved, a higher amount of free FAD would be detected in melanoma when compared to normal skin. However, the free and protein-bound measurements for FAD in normal skin agrees with the aerobic metabolism, expected for this tissue.

Considering the short and long lifetimes parameters, the protein-bound FAD has a shorter lifetime when compared to its free state. The increase in both lifetimes describes melanoma behavior tending to glycolysis once the FAD protein-bound state is related to the oxidative phosphorylation metabolism. As described by Scott et

al., melanoma increases the non-oxidative breakdown of glucose even in the presence of oxygen, that is, melanoma cells prefer glycolysis respiration pathway.

Normal skin and melanoma were classified by the linear discriminant analysis of the free FAD molecules, i.e., using short lifetime at 445 nm excitation and long lifetime at 378 nm excitation. Based on this classification, 99.4% of sensitivity, 97.4% of specificity and 98.4% of accuracy were achieved (Figure 2.6).

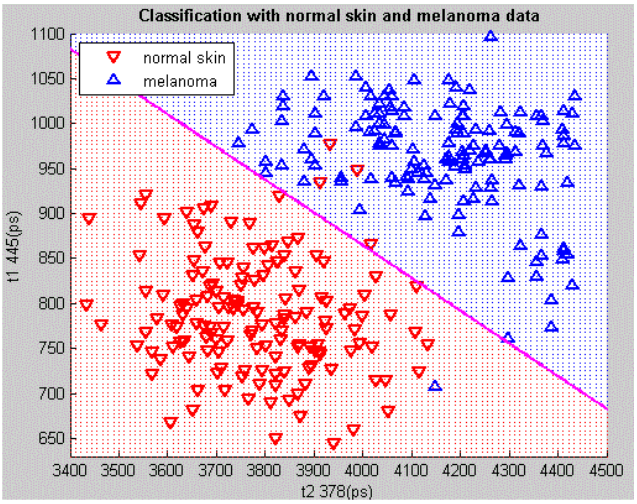

Figure 2.6 - Short lifetime component (τ_1) of 445 nm excitation against long lifetime component (τ_2) of 378 nm, the separating lines was performed using linear discrimination analysis.

Source: By the author

The standard melanoma diagnosis is based on the clinical analysis of the characteristics of the lesion, following the ABCD rules, that is, Asymmetry; Border irregularity; Color and Diameter greater than six mm.(3,84) In cases that the clinical examination suggests melanoma, a total lesion resection is performed with a large margin to prevent melanoma regrowth and metastasis. The combination of surgery and radiation therapy or chemotherapy is also indicated in cases with high risk of tumor spreading. However, clinical examination is highly subjective, where the diagnosis before surgery relies on the clinician training and expertise on recognizing a melanoma.(84) Morton & Mackie (1998) investigated the clinical accuracy of cutaneous melanoma diagnosis. The accuracy, sensitivity and positive predictive values were 80%, 91%, and 86%, respectively, for dermatologists with more than ten years of experience with melanoma. These values drop significantly for 3-5 years and

1-2 years of experience reaching accuracy values of only 62 and 56%, respectively.(85) Then, the developing of non-invasive and more objective techniques for melanoma diagnostics is crucial.

Argenziano and collaborators reported a clinical study of the use of epiluminescence microscopy (ELM) to not only detect melanoma as well as to follow its progression. They could correlate the ELM imaging with some histologic architecture of the lesion and estimate tumor thickness before surgery.(86) However, the diagnosis still relies on the clinic's previous experience. The oblique-incidence diffuse reflectance spectroscopy (OIDRS) has also been evaluated for *in vivo* melanoma diagnosis, achieving 90% of sensitivity and specificity.(87)

Raman spectroscopy and neural networks have also been investigated for melanoma diagnosis in biopsies, reaching 85% of sensitivity and 99% of specificity.(34) Other techniques as high-frequency skin ultrasonography,(88) fluorescence spectroscopy,(30) and positron emission tomography(89) were evaluated, but none of them has been established as a reliable technique for melanoma diagnosis.

To our knowledge, our study is the first report of the use of time-resolved lifetime fluorescence technique for melanoma diagnosis.(90) The main advantage of this method is the real-time assessment of tumor metabolism that is the principal difference between normal skin and cancers. Our results showed higher accuracy, specificity, and sensitivity than most of the non-invasive diagnosis methods, demonstrating the potential of the fluorescence lifetime as a tool to improve especially the diagnostic of melanoma at early stages.

The continuation of this study included the assembling, calibration, and characterization of a portable system for single-point measurements for clinical use.(82) The clinical investigation is in progress and involves the diagnosis of pre-malignant and malignant lesions in general.

2.4 CONCLUSIONS

The time-resolved fluorescence lifetime spectroscopy is a non-invasive, real-time technique that provides real-time information about tissue metabolism. The

standard gold technique for melanoma diagnosis is still the clinical evaluation of the lesion. However, it relies on the clinician previous experience and expertise. Then, the development of new technologies to support the clinical diagnosis is crucial. In this study, we aimed to establish the fluorescence lifetime parameters to distinguish normal skin and melanoma in a murine model. Using the time-domain fluorescence spectroscopy, we were able to detect the cutaneous melanoma with 99.4% of sensitivity, 97.4% of specificity and 98.4% of accuracy, demonstrating the potential of the technique for melanoma detection.

CHAPTER 3 EVALUATION OF THE COMBINATION OF OPTICAL CLEARING AND PHOTODYNAMIC THERAPY ON *IN VIVO* CUTANEOUS MELANOMA MODEL

3.1 OBJECTIVE

This study aims to investigate whether optical clearing agents can enhance the light distribution in cutaneous melanoma, improving light penetration and photodynamic therapy response.

3.2 MATERIAL AND METHODS

3.2.1 Cell line

The pigmented murine melanoma cell line B16F10 was purchased from American Type Cell Collection (ATCC), and the non-pigmented murine melanoma cell line B78H1 was kindly donated by Dr. Pier-Luigi Lollini, University of Bologna, Italy. Both cell lines were cultured in DMEM medium supplemented with 10% fetal bovine serum and 1% penicillin-streptomycin and kept at 37°C in a humidified 5% CO_2-enriched atmosphere.

3.2.2 Animal model

The animals were anesthetized with isoflurane 5% for induction and 2% for maintenance, and the tumor was induced by the injection of one million cells (B16F10 or B78H1) in 40 uL of PBS into the right flank of six-weeks nude athymic mice (J: NU, Jackson's lab) using a 30G needle. The tumors were assessed every other day using a photoacoustic system coupled to a high-resolution ultrasound (Vevo 2100: VisualSonics), 20 Hz and the LZ-550 transducer, operated between 32 and 56 MHz. For the photoacoustic imaging, it was used a tunable laser from 680 to 970 nm set up at 700 nm for the melanin excitation. The images were taken from the whole tumor with a step size of 0.076 mm, in triplicate to reduce the influence of breathing movements. Usually, an entire tumor was imaged in less than 10 minutes, depending on the tumor size. The treatments started when the lesions reached 1 mm in thickness. All the animals' procedures were approved by the Institutional Animal Care

Committees (University Health Network, Toronto, Canada, protocol 4401.1 and by São Carlos Institute of Physics, Brazil, protocol 03/2014). The animals were examined daily for excessive lethargy, hunched or abnormal posture, and seizure, which were the humane endpoints for euthanasia. Photographs of the tumor before the treatment are shown in Figure 3.1.

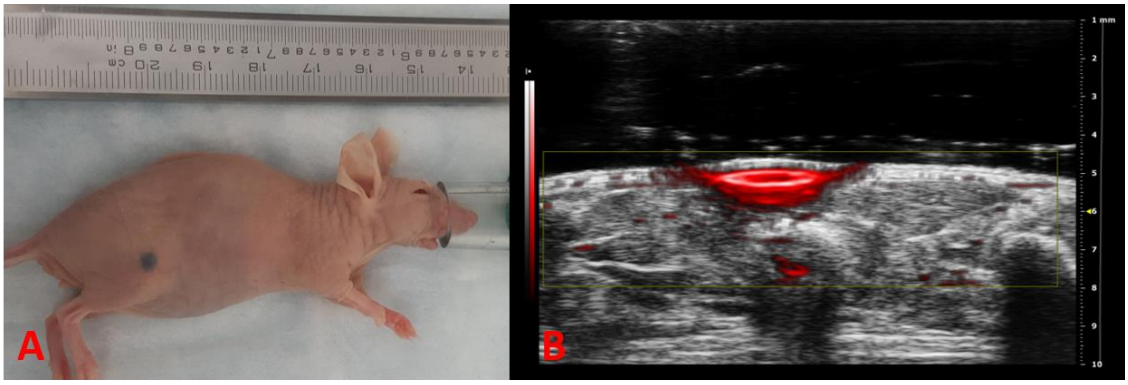

Figure 3.1 - Photograph of mice with a pigmented cutaneous melanoma and its corresponding ultrasound combined with photoacoustic imaging.

Source: By the author

3.2.3 Optical clearing agents (OCAs)

As it was the first time that an OCA was applied on melanoma, the clearing effects were investigated using a several of OCAs mix, involving glycerol in different concentrations and a PEG-400, 1,2 propanediol mix solutions. Glycerol, PEG-400, and 1,2 propanediol were purchased from Sigma-Aldrich®. The refractive indexes of glycerol 70%, PEG-400, and 1,2 propanediol are 1.42, 1.46, and 1.43, respectively. All of them presented a refractive index similar to the skin index of 1.4 and based on the induced tissue clearing; an OCA solution was chosen to be used in all the following PDT experiments. Also, the OCA solution (~300 uL) was always applied topically with previous tape stripping of the lesion and reapplied when needed.

3.2.4 Diffuse reflectance spectroscopy (DRS)

The animals were anesthetized using 5% of isoflurane for induction, and 2% for maintenance and the OCA was topically applied to characterize the clearing effect on melanoma. Two setups were used for the measurements: (1) a diode laser

emitting at 660 nm and an OceanOptics® spectrometer both coupled to two different optical fibers were used. The spectrometer was also connected to a computer using software OceanView (OceanOptics®). The fibers were then positioned on the top of the tumor using a holder attached to a nanometer. The diffuse reflectance was collected every 0.5 mm for 2 mm. (2) For the second setup, a fiberoptic reflectance probe with 520 µm source-collector separation and white light as described by Kim et al. (2010) was used. (91) In summary, the optical fiber probe was composed of 5 optical fibers with the same separation between each other (520 µm) connected to 3 white LEDs, a blue (405 nm) and red (630 nm) lasers. The distance between the excitation and the collection can be changed according to the measurements needed by the optical fibers positions. Due to the tumor absorption, it was used only the 520 µm source-detector separation using white light. The reflectance signal was acquired by the spectrometer (OceanOptics). The white-light DRS were acquired immediately after the topical application of OCA and every 15 min for 90 min in triplicate. Each measurement took around 5 seconds, including the triplicates. In both setups, the spectra were normalized by the first measurement, immediately after the OCA topical application.

Previous tape stripping was performed to remove stratum corneum and improve transdermal penetration of the OCA for both systems. The first measurements provided information about the total attenuation coefficient and the second ones, information about the tumor optical characteristics over the whole detected spectrum.

3.2.5 Optical coherence tomography (OCT)

The OCT studies were performed in collaboration with Dr. Alex Vitkin – Princess Margaret Cancer Center/ University of Toronto and were performed to evaluate the effect of OCA in pigmented melanoma. It was used a swept-source OCT system described previously.(92) In summary, images were acquired with a 36 kHz Fourier domain OCT system using a short-cavity swept laser source based on a tunable polygon filter. The axial and lateral resolutions in tissue were 8 and 13 µm, respectively. The animals were anesthetized using inhaled anesthesia (isoflurane 5% for induction and 2% for maintenance), and the paw was immobilized to the stage to reduce movement due to animal breathing during the OCT scanning. The first image

was acquired immediately after the OCA application and then every 30 min for four hours. Each image took approximately 5 min. Re-application of the OCA was performed when needed.

The histograms of signal intensity distributions within each ROI were fitted using a least-squares method following the equation:(93)

$$f(x,\alpha,\beta) = \frac{1}{\Gamma(\alpha)}\beta^{a}x^{a-1}e^{-\beta x} \quad [3.1]$$

The α and β parameters are related to the shape and scale of the gamma distribution, and its ratio represents the average signal brightness within a given ROI.

3.2.6 Microvasculature network imaging

The OCT B-scans were processed as described by Pires et al.(83) Briefly, the noise and artifact due to respiration movements were removed; a surface mask was used to correct the depth encoding and preserve the vessels structures; application of the Otsu's threshold method to retain the deep-vessel information and skin surface mask to flatten the surface. The obtained images were then compared before and after OCA topical application, and the effect of the OCA was quantified.

3.2.7 Photosensitizer kinetics

The PDZ kinetics in the melanoma model was performed using two different techniques: laser-induced fluorescence spectroscopy (LIFS) and chemical extraction. In both cases, the photosensitizer was intravenously injected into the tail vein at a concentration of 1.0 mg/kg. For the LIFS measurements, it was used a diode laser emitting at 408 nm, and a spectrometer (OceanOptics) coupled to a bifurcated optical fiber that was gently placed on the surface of the tumor for the measurements. After the spectra acquisition, the fluorescence intensity at 660 nm – corresponding to the dye emission peak - was used to determine the PS kinetics. The fluorescence intensity at 660 nm was normalized to the intensity at 500 nm for each measurement, that is, the photosensitizer fluorescence intensity was normalized by the highest

amplitude of the tissue autofluorescence in each measurement, to reduce interferences due to distinct light coupling between the probe and the tissue.

Based on the results of the laser-induced fluorescence spectroscopy, it was determined six timepoints to quantify the amount of photosensitizer in the tumor and normal skin. Two animals were sacrificed at each timepoint, and the tumor and normal skin were removed. Then, the samples were digested with 0.2 M de NaOH for four hours in a shaker at 50°C, followed by centrifugation at 3000 rpm for 10 min. Then, 10% de Triton X-100 and 1M HC were added. The concentration of the photosensitizer was determined by absorption spectroscopy and compared to a standard curve obtained with a known concentration of the photosensitizer as described by Peng et al.(94)

3.2.8 PDT protocol

The animals were anesthetized using inhaled isoflurane 5% for induction and 2% for maintenance. A chlorin-based (Photodithazine, Russia) and a verteporfin photosensitizer (Visudyne, QLC Inc.) at a concentration of 1.0 mg/kg and 44 mg/kg (that contains 0.8 mg/kg of verteporfin), respectively, were injected intravenously into the tail vein in a volume of 50 µL. The irradiation was performed 15 and 60 min after the injection for verteporfin and Photodithazine, respectively. The short light-drug interval used for Visudyne was based on clinical reports for age-related macular degeneration treatment.(95) Moreover, Photodithazine LDI was defined by the kinetics assays described above. The groups that received the OCA, it was applied 15 min before the irradiation with previous tape stripping. For the Photodithazine-mediated PDT, it was used a 670 nm diode laser as a light source, the irradiance of 100 mW/cm^2 and energy fluence of 100 J/cm^2. A diode laser emitting at 690 nm at 80 mW/cm^2 and 80 J/cm^2 was used for the treatment of the Visudyne-mediated PDT. For the dual-agent PDT, PDZ-mediated PDT was performed followed immediately by the VIS-mediated PDT. The photosensitizers concentrations, in this case, were of 0.5 mg/kg and 0.4 mg/kg for Photodithazine and Visudyne, respectively. The fluences were also reduced for 60 J/cm^2 for PDZ and 40 J/cm^2 for VIS. When the dual-agent PDT was combined with the OCA, the application protocol followed the description above. A summary of the treatment groups is shown in Table 3.2.

Table 3.1 - Summary of the treatment groups.

	OCA	Treatment group	Number of animals (n)
Non-pigmented and pigmented tumors	-	Control	3
	-	PDZ-PDT	3
	+	OCA + PDZ-PDT	3
	-	VIS-PDT	3
	+	OCA + VIS-PDT	3
	-	PDZ-PDT + VIS-PDT	5
	+	OCA + (PDZ-PDT + VIS-PDT)	5

Source: By the author.

3.2.9 Assessment of PDT response

The tumor volume was measured using ultrasound and photoacoustic imaging - as described in the section 3.2.2 -, every other day after the treatment for ten days when the animals were sacrificed by cervical dislocation under general inhaled anesthesia (isoflurane 5%). In the case of excessive lethargy, hunched or abnormal posture, ulcerative tumor or lesion over 1 cm diameter, the animals were immediately sacrificed. Then, the tumors were removed, sectioned and stained with H&E and for S100 protein expression. For the S100 staining, the specimens were incubated with a rabbit pAb to S100 (Z-0311, Dako – Agilent Technologies; 1:500) and WARP-Red chromogen – an Alkaline Phosphatase system to differentiate the staining and melanin present in the pigmented tumors.

3.2.10 S100 expression quantification

The protein expression was quantified using the MATLAB® R2015a (Mathworks, USA) software. The slides marked immunohistochemically for S100 protein were processed following the protocol: tumor area definition, color threshold and quantification of the amount of red in the image, related to the expression of S100. These were performed using MATLAB® image processing algorithms: Image Segmenter, Color Threshold, and Region Analyzer, respectively.

3.2.11 Tumor thickness

The slides stained for the S100 protein were used to assess the tumor thickness ten days after the treatment. The measurements were performed in triplicate for each tumor in the thickest area of the lesion, using the software Aperio ImageScope® v. 12.3.2.8013 (Leica Biosystems Imaging, Inc.).

3.2.12 Determination of the Specific Growth Rate (SGR) and Doubling Time (DT)

Specific growth rate

The SGR and DT were calculated as described by Mehrara and collaborators.(96) The SGR value was assessed using the volumes determined by the photoacoustic and ultrasound imaging(97) in a given moment. The tumor growth was considered exponential as outlined in the equations above:

$$SGR = \frac{1}{V}\frac{dV}{dt} \tag{3.2}$$

$$SGR = \frac{ln\left(\frac{V_2}{V_1}\right)}{t_2 - t_1} \tag{3.3}$$

Considering DT $V_2 = 2V_1$,

$$DT = \frac{ln(2)}{SGR} \tag{3.4}$$

SGR and DT were determined only for the experimental groups with remaining tumors in the immunohistochemically staining.

3.2.13 Statistical analysis

Statistical analysis was performed by one-way analysis of variance (ANOVA) with post-hoc comparisons with the Tukey test using software GraphPad Prism 7 (GraphPad Software, Inc., CA, USA). The value of $p<0.05$ was considered statistically significant.

3.3 RESULTS AND DISCUSSION

The experimental melanomas were observed two days after the injection and reached between 0.7-0.9 mm in thickness between days 3 and 4. Even with the fast-growing, no side effects or pain reaction were detected in the animals. Also, metastasis was not observed during the ten days evaluation period. Photographs of the pigmented tumor before and after topical application of OCA can be seen in Figure 3.2. In (A) it is possible to observe a blackish tumor covered with a thin layer of the normal epidermis. After topical application of OCA, the tumor becomes more visible, showing a higher visual definition and indicating the clearing of the superficial layer of normal skin. It means that the light attenuation on the normal epidermis was reduced, increasing the light penetration into the tumor and making it more visible.

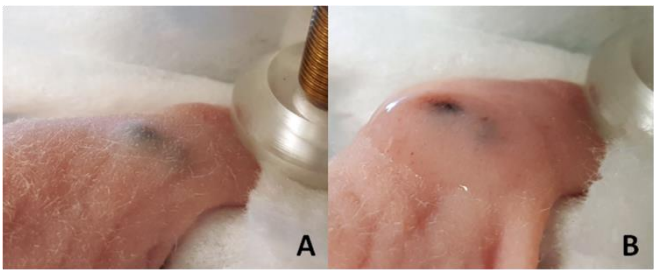

Figure 3.2 - Photographs of cutaneous pigmented melanoma before (A) and after (B) topical application of OCA.

Source: By the author

3.3.1 Diffuse reflectance spectroscopy (DRS)

The diffuse reflectance measurements as a function of the source-detector distance revealed a considerable heterogeneity within the same tumor, as well as between tumors (Figure 3.3). This heterogeneity is a factor that also changes the light distribution in the tumor, making the entire tumor treatment using PDT a

challenge. In Figure 3.3-A, it is possible to observe the diffuse reflectance decrease as a function of the source-detector distance for five different animals. From these curves, the tissue total attenuation coefficient was estimated, which for melanoma, ranged from 0.3 to 3 mm^{-1}, as can be observed in Figure 3.3-B (representation of the results of 15 animals). In addition to the significant difference in the total attenuation coefficient of each tumor, it is possible to observe the large error bars associated with the measurements, due to the heterogeneity observed in each tumor.

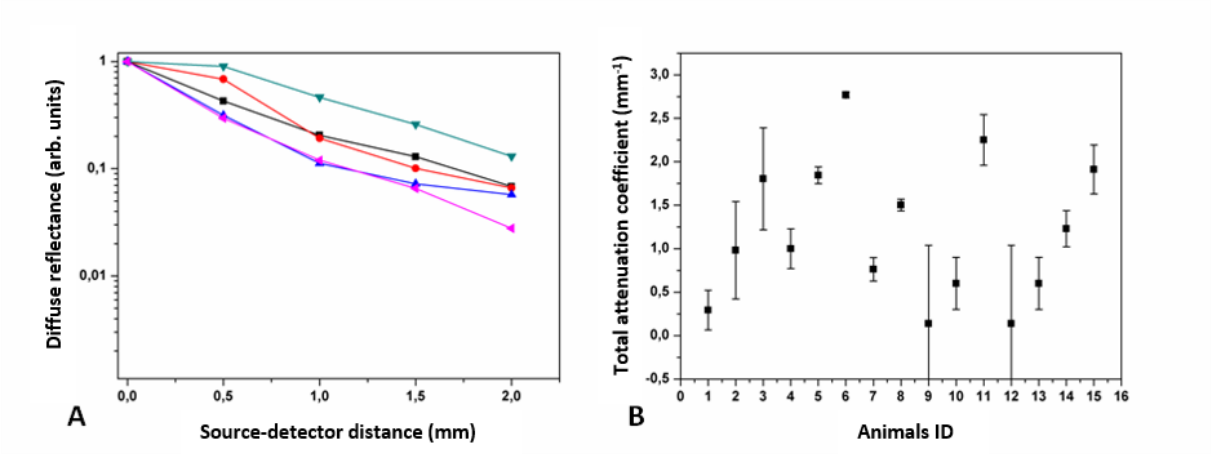

Figure 3.3 - DRS measurements as a function of the source-detector distance (A) and its corresponding total attenuation coefficient (B).

Source: By the author.

The experimental model was very similar to the melanoma lesions seen in the clinic. In addition to the pigmented characteristic, the tumors are quite heterogeneous both in relation to the pigmentation and the light distribution. The assays to determine the total attenuation coefficients before and after the application of the optical cleaning were performed in five replications, due to the variation in the optical characteristics observed in each tumor. These features will profoundly disturb any optical-based technique for diagnosis or treatment of melanoma. Specifically, for PDT, a homogenous light distribution within the tumor is one of the most relevant factors to achieve to result in successful treatment.

Glycerol is one of the most common optical clearing agent used to improve diagnostic imaging techniques. At low concentrations (20-50%) there is no significant optical clearing, whereas at high concentrations (above 75%) edema and scar tissue were reported after application. Also, at high concentration, glycerol may also promote significant changes in the structure of the biological tissue, and may even

obstruct blood vessels.(98) Based on these characteristics, glycerol 70% in water was investigated (Figure 3.4).

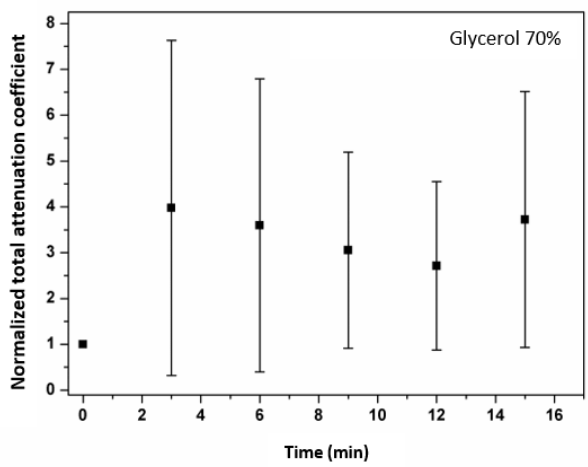

Figure 3.4 - Total attenuation coefficients calculated using the DRS technique before and after the topical application of glycerol 70%.

Source: By the author.

The measurements showed an average decrease in the DRS measurements, probably due to the tissue scattering reduction and, thus, the increase in tumor transmittance and/or absorbance, with an average increase of 380% when compared to the tissue total attenuation coefficient before OCA application. These results agree with those obtained by Wen and colleagues. They described that the increase in the glycerol concentration had a more significant reduction in the DRS signal. Also, histological analysis revealed that 75% glycerol could change the diameter of the collagen fibers when compared to the control group.(61)

Polyethylene glycol (PEG) is a hyperosmotic agent widely used as an OCA. Associations of PEG with agents that facilitate the transdermal diffusion in the tissue such as DMSO and propanediol are also investigated.(63) The association of PEG and propanediol in a ratio 19:1, respectively, showed an average decrease in the total attenuation coefficient around 35%. Although, in some cases, the reduction in the coefficient reached up to 90%.

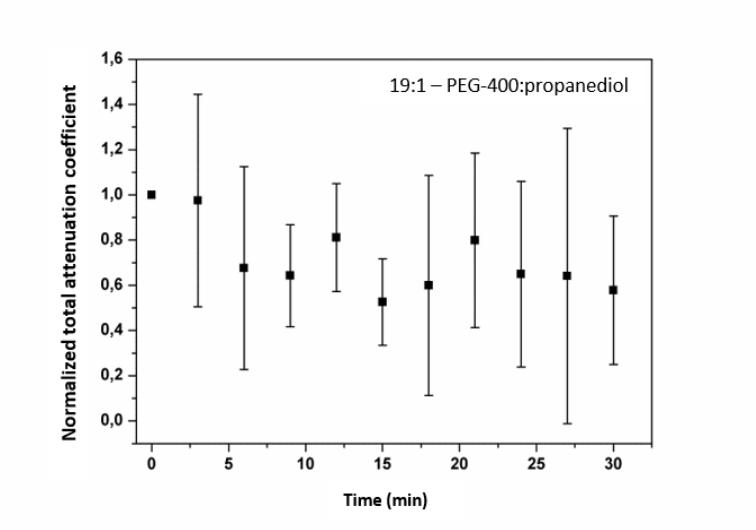

Figure 3.5 - Melanoma total attenuation coefficient before and after topical application of PEG-400 and 1,2 propanediol mix (19:1).

Source: By the author.

It was observed that glycerol 70% showed an average increase of the total attenuation coefficient of 308% when comparing both optical clearing solutions. However, the PEG-400 and 1,2 propanediol mix showed an average decrease of 35%, indicating the potential of OCA to change light distribution in the biological tissue. Based on these results, the white-light DRS measurements, as well as the PDT experiments were performed using only PEG-400 and 1,2 propanediol mix solution as the OCA.

The white-light DRS measurements are shown in Figure 3.6. The first measurements were taken immediately after the OCA topical application to reduce variations in optical coupling of the probe and tissue surface. For the normal skin (Figure 3-6A&B), the DRS signal varied ±20% for the entire spectra over the time investigated. In the case of melanoma, DRS showed a significant variation, reaching a decrease of 95% of the signal 45 minutes after the topical application of OCA. Sixty minutes after the application, the hemoglobin signal is observed, indicating that the OCA reached deeper vascularized layers of skin. In Figure 3.6D, one can see that the OCA has a slightly greater effect at shorter wavelengths. Since there is a gradient of concentration of OCA into the tissue with topical application, the clearing particularly affects the short wavelengths that have smaller penetration in tissue. Longer application times are required to clear deeper layers of the skin. Also, due to the presence of a rich vascular network, deeper layers of skin can rapidly attempt to

hydrate the tissue and re-establish the natural skin hydration values. Higher clearing effect may be obtained if the OCA was applied combined to physicomechanical diffusion enhancers as microneedles, temperature, ultrasound, and others.(83)

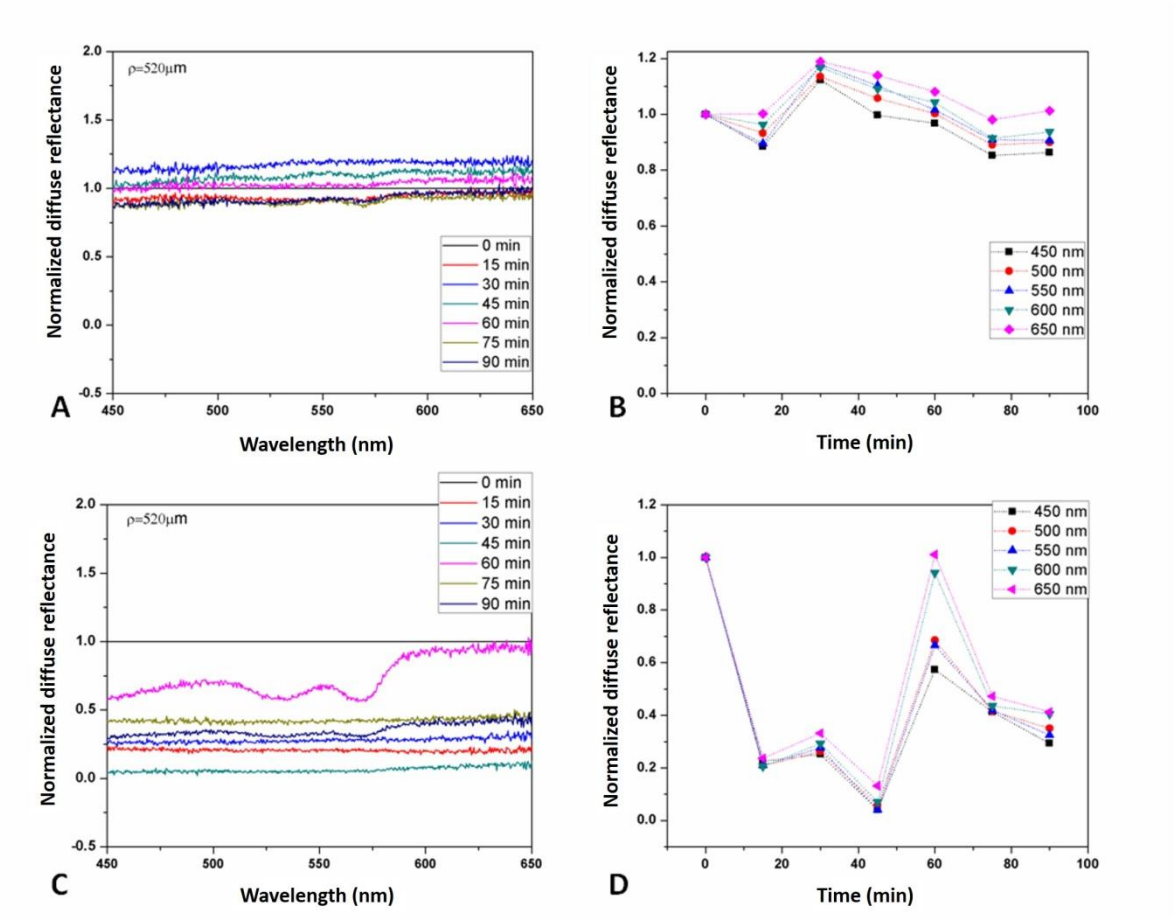

Figure 3.6 - Normalized diffuse reflectance spectroscopy and DRS as a function of time for normal skin (A) and melanoma (C). The first measurement was taken immediately after the topical application of PEG-400 and 1,2 propanediol mix to prevent probe-tissue coupling.

Source: By the author.

3.3.2 OCT imaging

A photograph of a pigmented tumor and the corresponding OCT B-scans are shown in Figure 3.7.

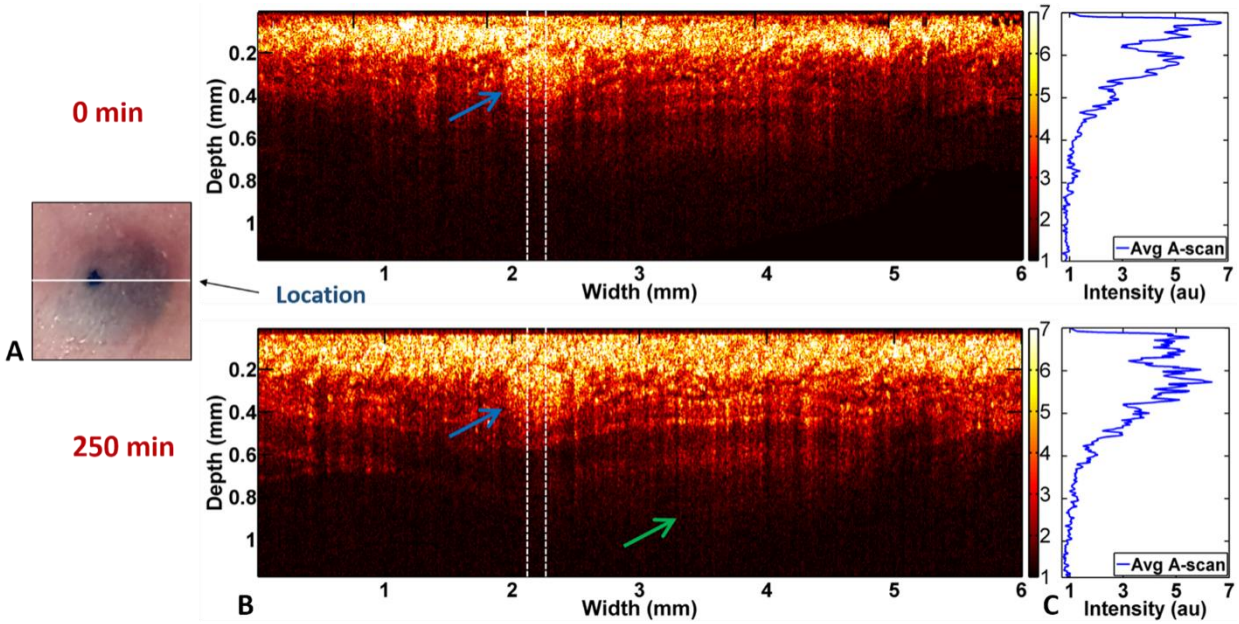

Figure 3.7 - B-mode OCT imaging of optical clearing in melanoma in vivo. (a) Photograph of the tumor at the skin surface. (b) Structural B-mode images at 0 (upper) and 250 min (lower) of topical application of OCA, taken through the dark spot seen in (a), which is indicated on the OCT images by the blue arrows. The increased OCT imaging depth (green arrow) due to the clearing is apparent. (c) Average intensity gradient with the depth of an area in B-scan (dot lines) before and after OCA application.

Source: By the author.

In the Figure 3.7A, one can see a darker dot and a larger blackish area that refers to pigmented melanoma in the most superficial layers and deeper layers of skin, respectively. In the upper OCT B-scan, it is possible to observe the superficial part of the melanoma (blue arrow) at a depth of ~400 µm, but no signal from the more deep tissue is detected. After the OCA application, the deeper part of the tumor becomes visible, improving the imaging of the entire tumor at a depth of ~750 µm. In C, it is possible to observe first the higher intensity signal on the skin surface and after the OCA application, the signal intensity shifts for deeper layers. It means that the superficial layers are becoming transparent and then images from deeper layers can be acquired.

The α/β ratio represents the average signal brightness in each ROI.(83) Comparing an area in the B-scan before and after OCA application for both, superficial normal skin and melanoma; one can see a decrease in the α/β ratio (Figure 3.8-A). In the beginning, the signal acquired comes mainly from the skin surface, then the OCA is applied, and the signal decreased, that is, the skin becomes

transparent. On the other hand, in the melanoma (deeper layer when compared to normal skin), the α/β ratio increases, that is, the light penetration into the tumor is increasing and making the tumor visible (Figure 3.8-B).

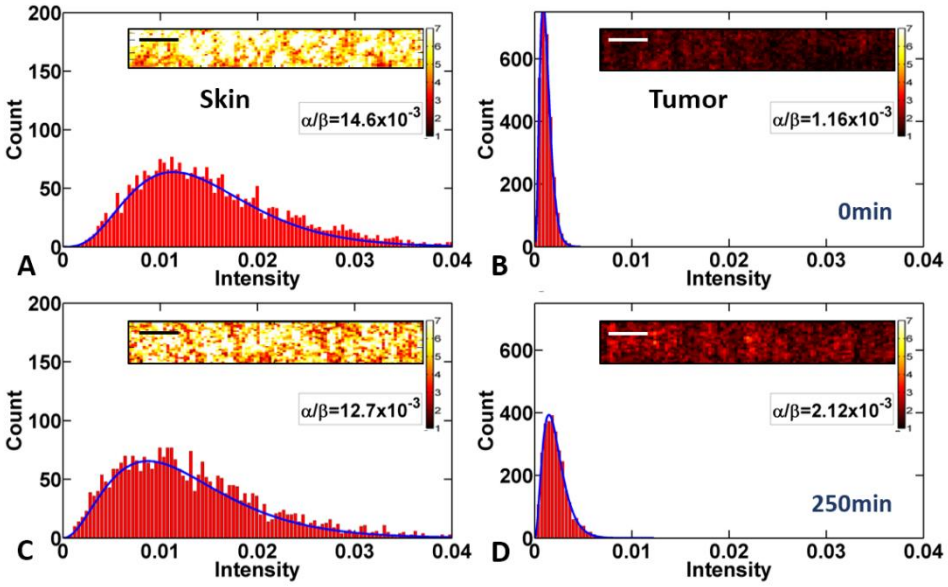

Figure 3.8 - OCT image pixel intensity distributions, fitted with Gamma distribution function. (A) Skin and (B) Tumor ROI pixel intensity distributions right after OCA topical application. (C) Skin and (D) Tumor ROI pixel intensity distributions 250 minutes after the massage and OCA topical application. Insets in each subfigure show the analyzed ROIs with scale equal to 100 µm.

Source: By the author

Speckle variance analysis provided tissue microvasculature images immediately after and with 120 and 250 min of OCA topical application (Figure 3.9). At time 0, OCT could image the vessels from the superficial skin and tumor layers, as also observed in the structural B-mode images. After 120 min application of the clearing agent, larger and deeper disorganized vessels became more visible, and this improves further at the 250 min time point.

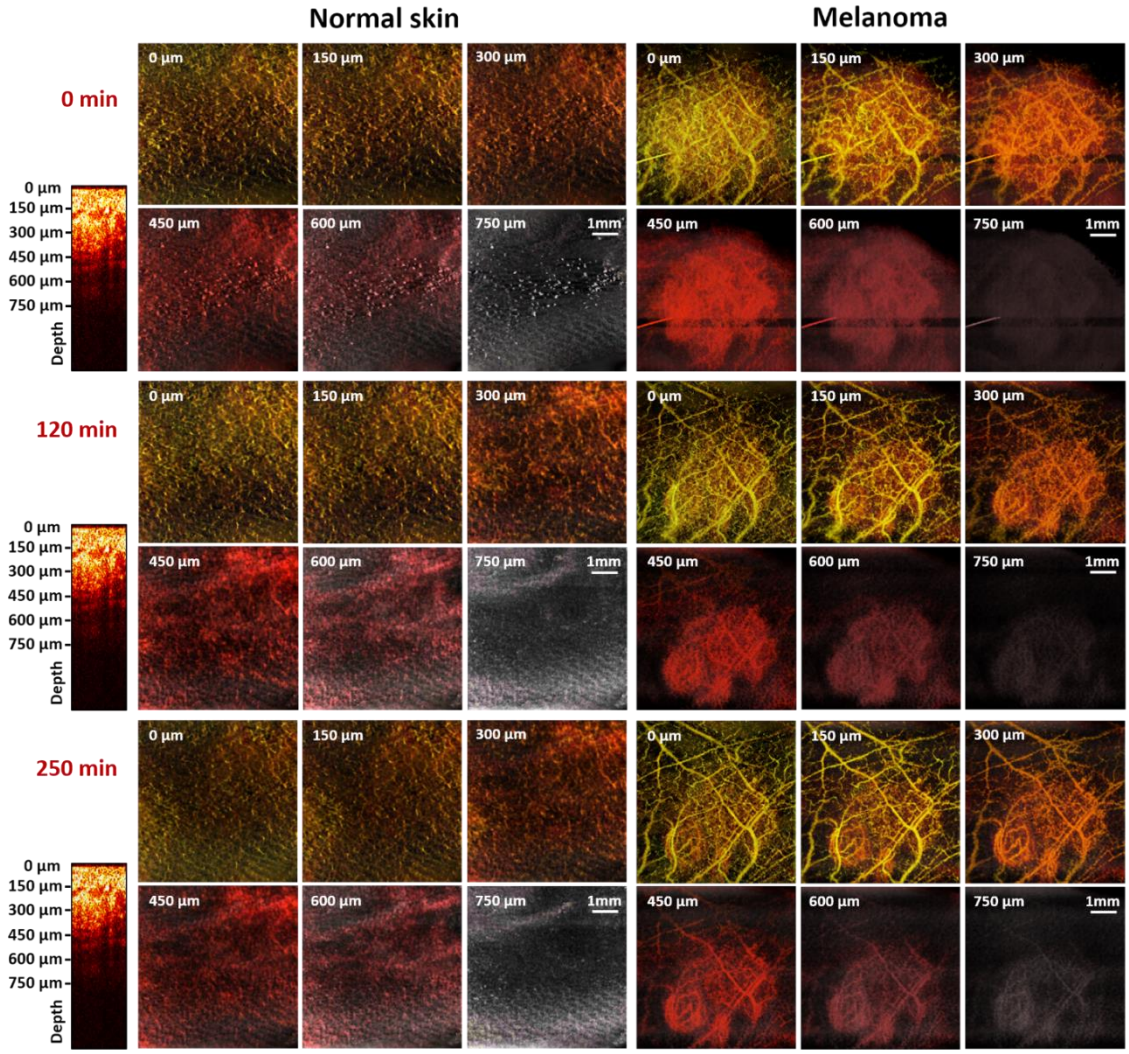

Figure 3.9 - *En-Face* projections for 0, 120 and 250 min after topical application of clearing agent. For each time, it can be observed vessels for different depth from 0 to 750 µm. At time 0, small vessels from the skin top layers are more visible. The high light scattering in skin limits light penetration and spatial resolution in depth. For this reason, it is possible to visualize vessels localized at up to 300 µm in depth. Hundred and twenty min after OCA application the top layers became transparent, improving the visualization of vessels up to 450 µm in depth. At this time, it is possible to observe larger and more disorganized vessels characteristics of the tumor. Two hundred and fifty min after OCA application, vessels up to 750 µm in depth became visible.

Source: By the author.

Near-infrared OCT improved the light penetration in melanoma, and it could provide information about the microvascular density present at up to 300 µm in depth. Although, when the image was performed using OCA, it was possible to observe not only an improvement in light penetration reaching around 750 µm in depth but also in the apparent image resolution.

Melanin has a high absorption in the entire visible spectrum, but besides that, melanin granules have also scattering properties. In a melanin scattering study using finite-difference-time-domain method for individual cells, Sergeev et al.(99) estimated melanin scattering coefficient at 830 nm and determined that it was three to five times higher for the pigmented cells than to the non-pigmented ones.(99)

Several studies used OCAs in matching the tissue refractive index to reduce its scattering and improve light penetration in depth. Shan et al.(62) investigated the use of OCA in skin diseases *in vitro* for OCT imaging. Liquid paraffin glycerol mix was used as an optical clearing agent for fibroma, pigmented nevus, seborrheic keratosis, and others. OCA showed efficiency for some diseases but did not clear pigmented nevus that, according to the authors, this may be related to the lesion architecture that difficult the OCA permeation in the dermis.(62) That is, OCA effect is related to the tissue morphology.

Our results obtained with DRS measurements and OCT imaging agree that PEG-400 and 1,2-propanediol mix resulted in a partial clearing of melanoma and improved light penetration in depth. In the DRS, only around 20% of the variation in signal was observed for normal skin, but for melanoma, 95% in the signal decrease was achieved. Also, the hemoglobin signal detected during the measurements indicates that the light penetrated deep enough to reach the vascularized layers of skin. These results agree with Shan et al. that described the difference on clearing obtained for different tissues.(62). Melanoma has a high growth rate and because of that, a disorganized morphology. This characteristic may be related to the higher clearing on melanoma observed when compared to normal skin.

OCT showed that OCA improved light penetration in depth providing information about melanoma microvasculature network, valuable information regarding tumor diagnosis and staging. In summary, DRS and OCT results showed that it is possible to change melanoma optical properties and improve light penetration in depth, improving optical diagnosis and potentially optical treatment response.

3.3.3 Photosensitizer kinetics

The PDZ kinetics obtained using LIFS is shown in Figure 3.10. One can see that the highest concentration of the photosensitizer in the lesion was obtained between one and three hours after its intravenous administration. Besides the fast concentration in the tumor, PDZ was eliminated from the organism in the first 24 hours after the injection, reducing the animal photosensitivity period. However, a minimum tumor selectivity was seen. Kinetics for the same photosensitizer was carried out by Shirmanova and collaborators (100) in a cervical carcinoma model using transillumination imaging. They reported that the dye kinetics was dose-dependent, that is, differences in the kinetics was observed regarding the administered dose. For 5, 10 and 25 mg/kg, the maximum signal was detected one hour, between three and six hours and between two and seven hours after the PS administration. Moreover, 24 hours after, the signal intensity was significantly lower due to organism clearance.(100) These results agree with those obtained in our study for both, photosensitizer accumulation and clearance.

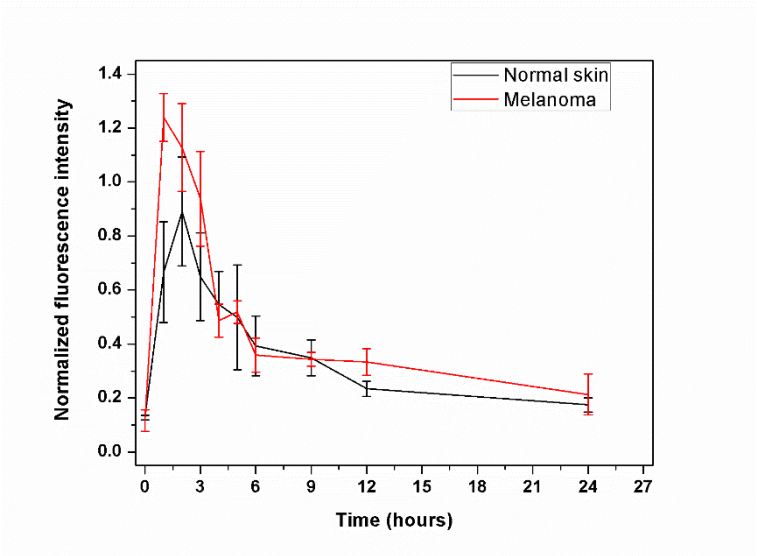

Figure 3.10 - Normalized PDZ fluorescence intensity as a function of time for normal skin (black) and melanoma (red).

Source: By the author.

For the photosensitizer chemical extraction, a previous absorption calibration curve was determined for melanoma and normal skin to be able later to quantify the amount of photosensitizer in the tissue as a function of time (Fig. 3-11).

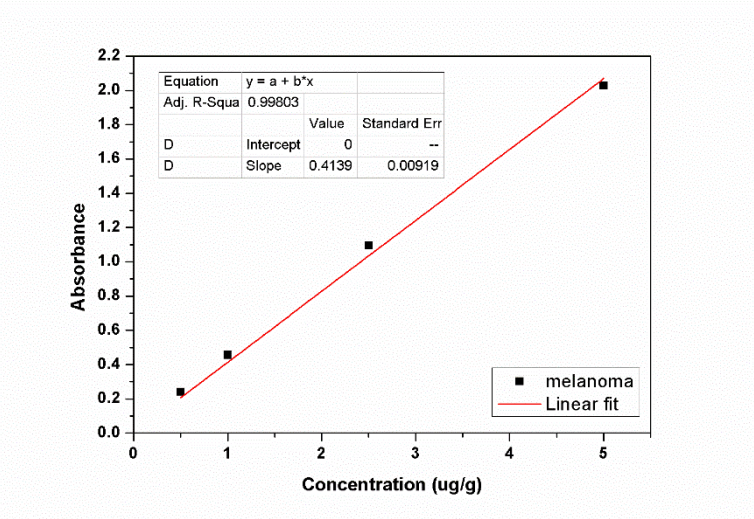

Figure 3.11 - An example of a calibration curve obtained for melanoma.

Source: By the author.

Based on the calibration curve, the photosensitizer was quantified for both, normal skin and melanoma for three timepoints, 30, 60, 120, 180, 360 and 720 minutes. The calibration curve was performed as a function of µg/mL of the extracted tissue as described by Peng et al. (Figure 3-12).(94)

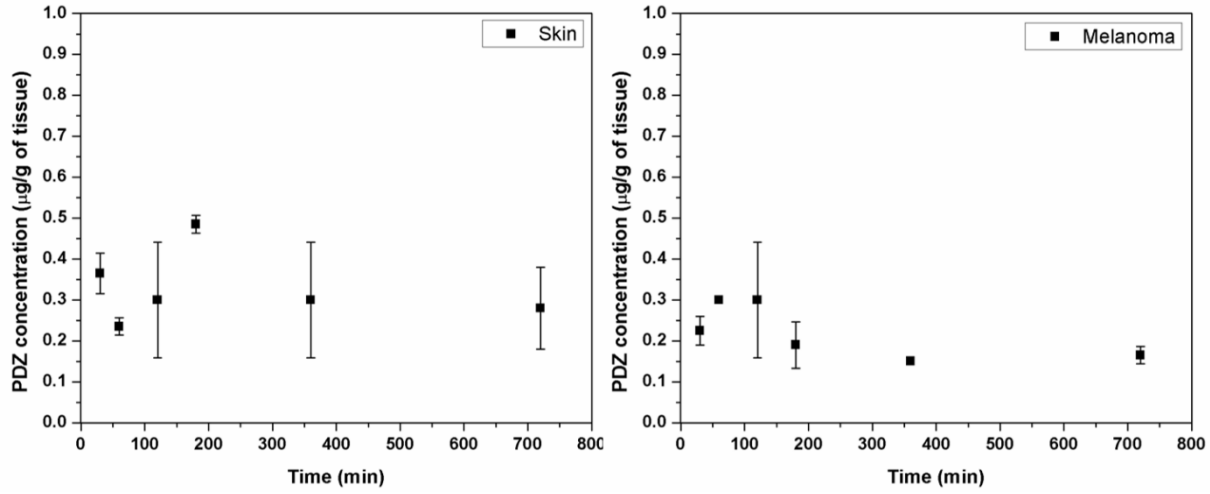

Figure 3.12 - Graphs of the PDZ concentration in µg per g of extracted tissue as a function of time for skin and melanoma. No tumor selectivity was observed, once the amount of dye extracted was similar between normal skin and melanoma.

Source: By the author.

The results obtained for the photosensitizer chemical extraction agree with those from the LIFS. For the skin, it was observed that 30 minutes after the dye administration, around 0.35 µg of PDZ per g of tissue and this value did not have a significant change for the timepoints investigated. Similar results were observed for melanoma that around 0.3 µg of PDZ per g of tissue was detected. These values are consistent with other studies involving photosensitizer uptake quantification. Biolo and collaborators(53) quantified the uptake of Si(IV)-naphtalocyanine incorporated into DPPC liposomes and Cremophor EL micelles in the same melanoma model. After administration intravenously of 0.5, 1 and 2 mg/kg of the photosensitizer into Cremophor EL micelles, the concentration detected in the melanoma were 0.57, 1.45 and 1.74 µg/g of tissue, respectively while for the DPPC liposomes the values were 0.46, 0.78 and 1.26 µg/g of tissue.(53) They also did not observe a significant difference between melanoma and normal skin. These results agree with those obtained in our study. Besides the non-selectivity behavior of PDZ, a substantial amount of photosensitizer was extracted from the tumor between 60 and 120 minutes after the dye administration. These results agree with those from LIFS that showed the highest amount of PDZ in the tumor between one and three hours after administration. Then, the PDT experiments were carried out using one-hour light-drug interval.

3.3.4 Assessment of PDT response

PDT inflammatory response was observed in the first 48 hours after the treatment for all groups treated. The necrosis process took place during 72 hours after the PDT session. For the OCA+PDT groups, in some cases the animals presented a motor limitation of the treated paw in the first days, that was recovered at the end of the evaluation period (10 days). An example of OCA+PDT response for non-pigmented tumor is shown in Figure 3.13. In A, an inflammation process is observed by erythema and slight edema at the treated site two days after the treatment. Followed by the beginning of the necrosis process, four days after the PDT session in (B) and the necrosis establishment eight days after treatment in (C).

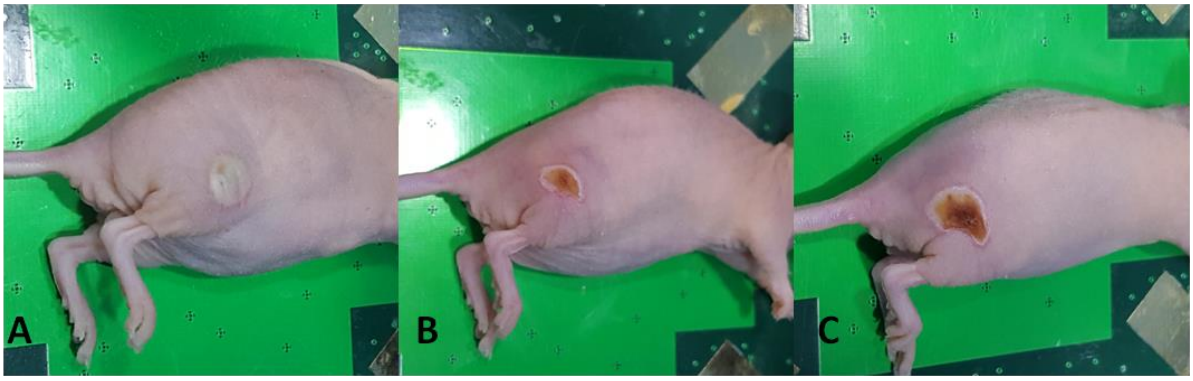

Figure 3.13 - Photographs of a non-pigmented tumor at two, four and eight days after PDT combined with OCA treatment, respectively. One can see the inflammation process in (A) followed by the necrosis in (B&C).

Source: By the author

For the pigmented groups, the inflammation, as well as the necrosis, observed varied accordingly to the photosensitizer used, but in all the cases, the necrosis was more evident for the PDT associated with OCA groups. An example of the PDZ-PDT response is shown in Figure 3.14. The pigmented tumor before treatment can be seen in Figure 3.14A. Four days later, an inflammation process with a necrotic core was established (Figure 3.14B), but eight days later, a significant tumor growth around this core was observed (Figure 3.14C).

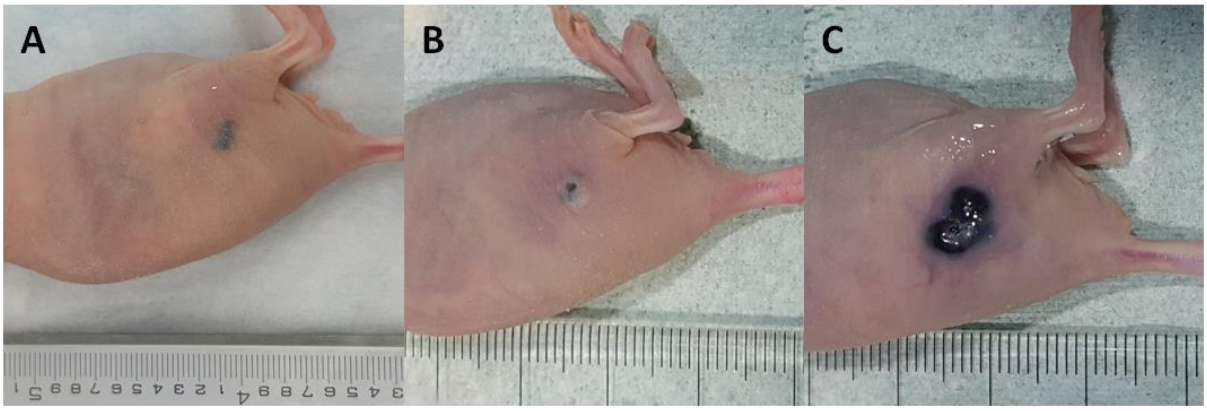

Figure 3.14 - Photographs of the murine pigmented tumor, before, four days and eight days after a single-agent PDT.

Source: By the author.

The inflammation and necrotic processes observed for the dual-agent PDT without OCA were more severe than the ones found for the single-agent PDT with or without OCA (Figure 3.15). The tumor before treatment, the inflammation process, and necrotic tissue can be seen in Figure 3.15A, B, and C, respectively.

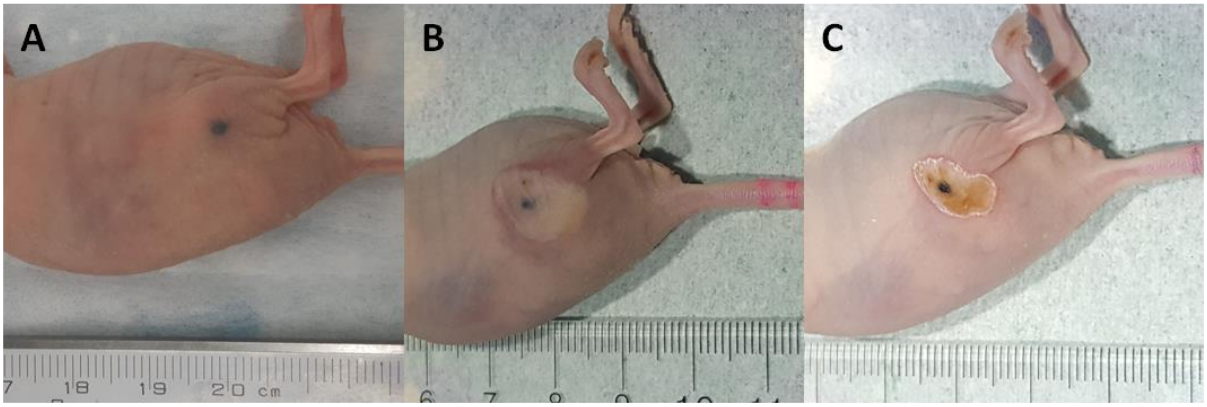

Figure 3.15 - Photographs of pigmented tumors treated with dual-agent PDT. (A) Before, (B) 4 days after and (C) 8 days after the treatment.

Source: By the author.

For the dual-agent mediated PDT associated with OCA, a more substantial inflammation, and necrosis process took place when compared with the same group without OCA (Figure 3.16). Both, the inflammation process and necrosis areas were

larger than the laser beam, probably due to the light scattering within the tissue and the vascular damage caused by VIS-mediated PDT.

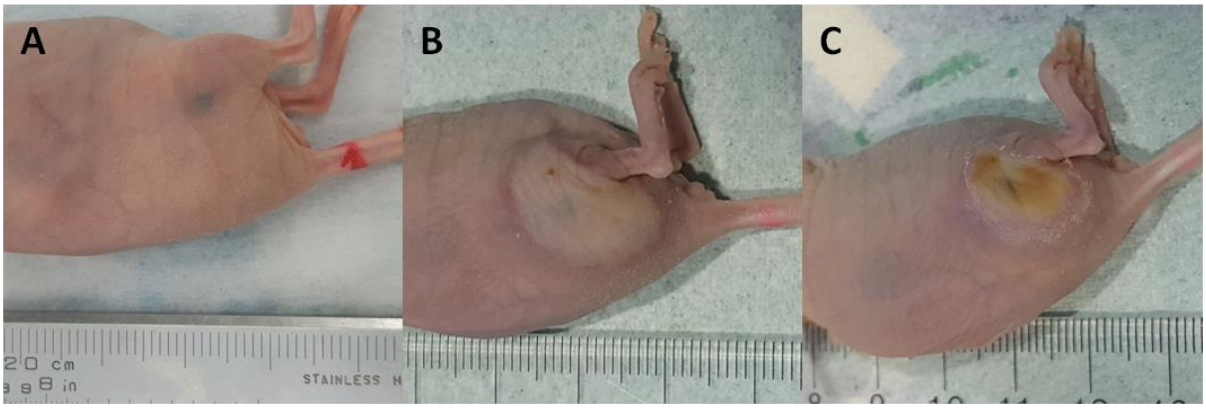

Figure 3.16 - Photographs of pigmented tumors treated with dual-agent mediated PDT combined with PEG-400 and 1,2 propanediol mix before and four and eight days after treatment.

Source: By the Author.

Following the humane endpoints established in this study, mainly tumor ulceration and tumor size over 1 cm, some animals from the pigmented groups were sacrificed before the end of the investigation period (10 days). Table 3.2 summarizes the number of animals sacrificed per day.

Table 3.2 - Summary of the number of animals from the pigmented groups sacrificed per day.

Day/ treatment groups (pigmented melanoma)	**0**	**2**	**4**	**6**	**8**	**10**
Control	0	0	2	1	-	-
PDZ-PDT	0	0	0	1	2	-
OCA+PDZ-PDT	0	0	0	0	0	3
VIS-PDT	0	0	0	3	-	-
OCA+VIS-PDT	0	0	0	0	0	3
PDZ-PDT+VIS-PDT	0	0	0	0	0	5
OCA+(PDZ-PDT+VIS-PDT)	0	0	0	0	0	5

Source: By the author.

The tumors volume as a function of time after treatment for each group is shown in Figure 3.17.

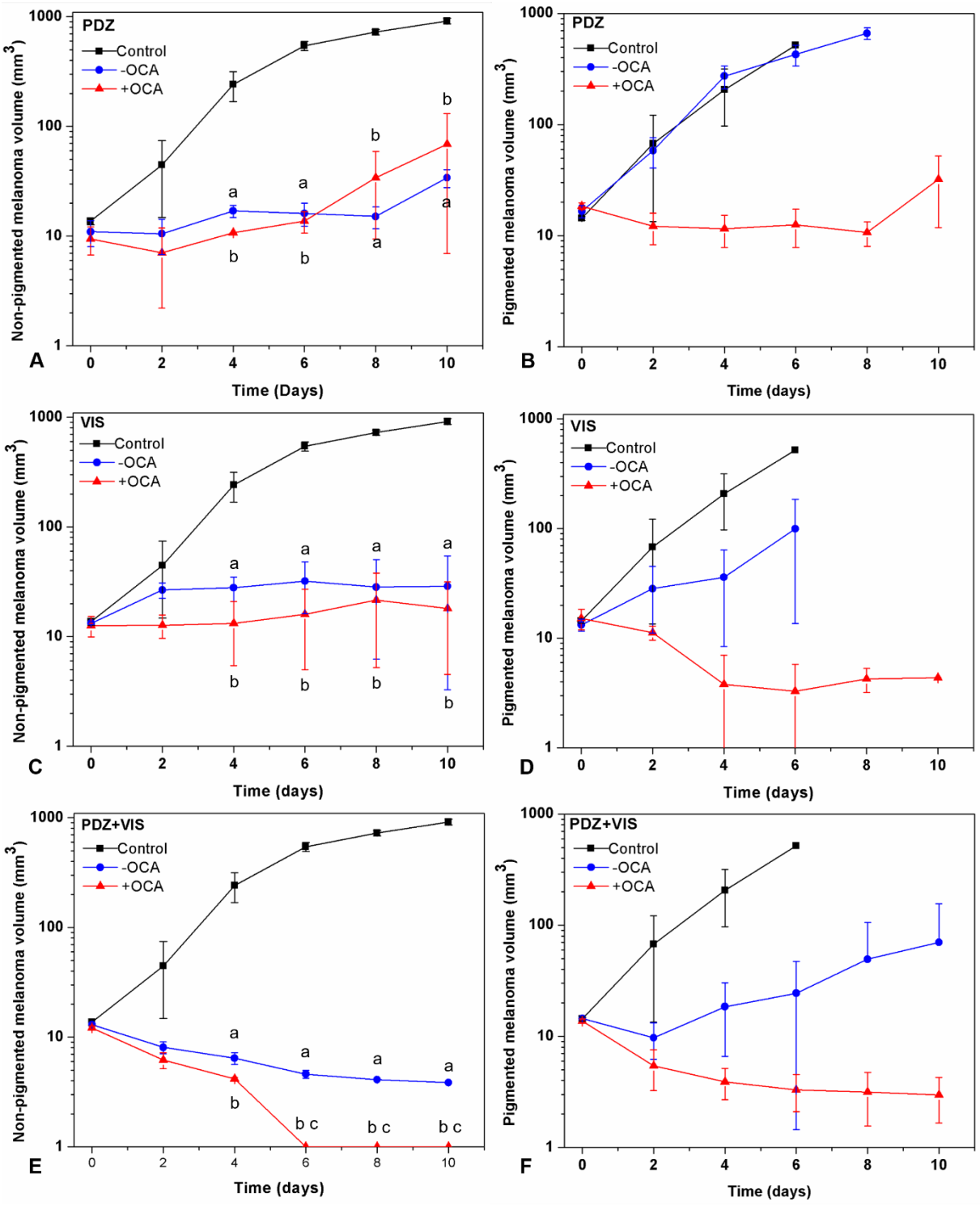

Figure 3.17 - Melanoma volume measured by photoacoustic and ultrasound imaging following treatment on Day 0 for both non-pigmented (A,C,E) and pigmented (B,D,F) tumors. Black lines refer to control groups; blue to groups treated with PDT without optical clearing and red lines to groups treated with PDT and optical clearing. The photosensitizer used in each graph is shown on the top of the corresponding graph. Each point corresponds to the mean volume ± standard deviation (N=3 for a single-agent PDT (A-D) and 5 for the groups treated with dual-agent PDT (E&F). For the non-pigmented groups, 'a' refers to statistical significance between PDT without OCA and control group; 'b' between PDT with OCA and control group; 'c' between PDT and PDT+OCA, for $p<0.0001$.

Source: By the author.

Following the humane endpoints (ulcerated tumor, animal weight loss, uncontrolled pain, or lesion size over 1cm in diameter), the animals with pigmented tumors from the control and VIS-PDT groups were sacrificed at day 6. As during the evaluation period some animals from the pigmented groups were sacrificed, statistical analysis was only performed for the non-pigmented groups.

In the non-pigmented groups PDZ-PDT and OCA+PDZ-PDT (Figure 3.17A), no difference was observed between the treated groups, although these groups showed a tumor volume reduction when compared to the control group. In the pigmented group (Figure 3.17B), the OCA enhanced the PDT effect when the PDZ was used, and no difference was observed between traditional PDT and control group.

In Figures 3.17C and 3.17D, one can observe the effect of VIS-mediated PDT combined or not to OCA for non-pigmented and pigmented tumors, respectively. It was slightly more efficient than PDZ-mediated PDT for both melanoma subtypes. Also, the OCA increased the PDT response for the pigmented tumor as it was observed for the group OCA+PDZ-PDT.

The best results were achieved when the dual-agent PDT was performed. In the non-pigmented groups (Figure 3.17E), the PDT with both photosensitizers could reduce the tumor volume and, when the optical clearing was added, no tumor was detected at the 4^{th} day after the treatment. Similar results were obtained for the pigmented groups with the dual photosensitization (Figure 3.17F). The use of both photosensitizers with the OCA application not only controlled the tumor growth as it was able to decrease the tumor volume and no regrowth was observed at the end of 10 days.

The photoacoustic and ultrasound imaging techniques provide in vivo measurements of the tumor, although it does not provide information about the tumor viability, and so the histology was performed using H&E and immunohistochemically stained for S100 protein expression.

3.3.5 Histology analysis

All the tumors were processed and stained with H&E and immunochemistry for S100 protein expression. This protein is characteristic of melanoma cells and is also

expressed in the murine melanoma model. S100 is involved in the cell signal transduction and associated with several activities such as cell cycle progression, proliferation, differentiation and apoptosis and control of enzyme activities of the cell(101). The S100 expression is staining in red, and it is negative in case of necrotic or absence of tumor cells.

Figures 3.18A&B and 3.18C&D revealed the histology of the non-pigmented group control stained with H&E and S100, respectively. It shows a dermal tumor proliferation with round and oval cells with nuclei at the periphery with cell invasion in the superficial layers and expansible nodule. The S100 staining (in red) shows the presence of tumor cells spread throughout the tumor, characteristic of the murine melanoma model. It can be seen that in the necrotic site, no S100 staining is observed as expected.

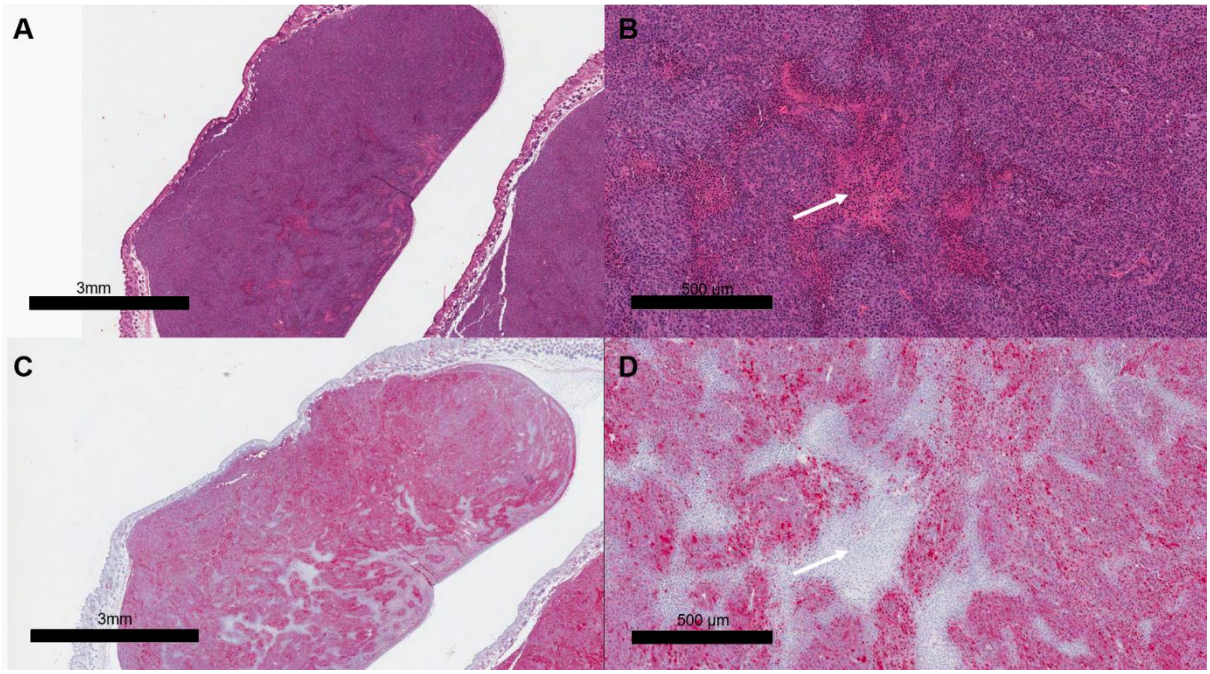

Figure 3.18 - HE and S100 staining slides of the non-pigmented melanoma A&B and C&D, respectively. Arrows indicate a necrotic site seen in both stainings.

Source: By the author.

The groups treated with PDZ-mediated PDT showed a signaficative reduction in the tumor volume and thickness (Figure 3.19). However, in both cases, without (Figure 3.19A-D) and with (Figure 3.19E-G) OCA topical application, the remaining

tumors still express S100 indicating that a tumor regrowth would possibly be later observed. The topical application of OCA did not improve the treatment response, and it might relate to the fact that the light penetration into small non-pigmented does not limit the treatment response, so the OCA did not affect the response. The complete tumor remission was not achieved probably due to melanoma resistance to PDT that involves not only melanin absorption as the antioxidant effect of this pigment; sequestration of PS inside the melanosomes, defects in apoptotic pathways and efflux of PS by the ATP-binding cassette as described by Huang and collaborators.(16) Also, a regenerated skin is observed in the tumor, and it induces a misinterpretation of the treatment response, lacking a further proper patient management, and then increasing the risk of tumor invasion and metastasis.

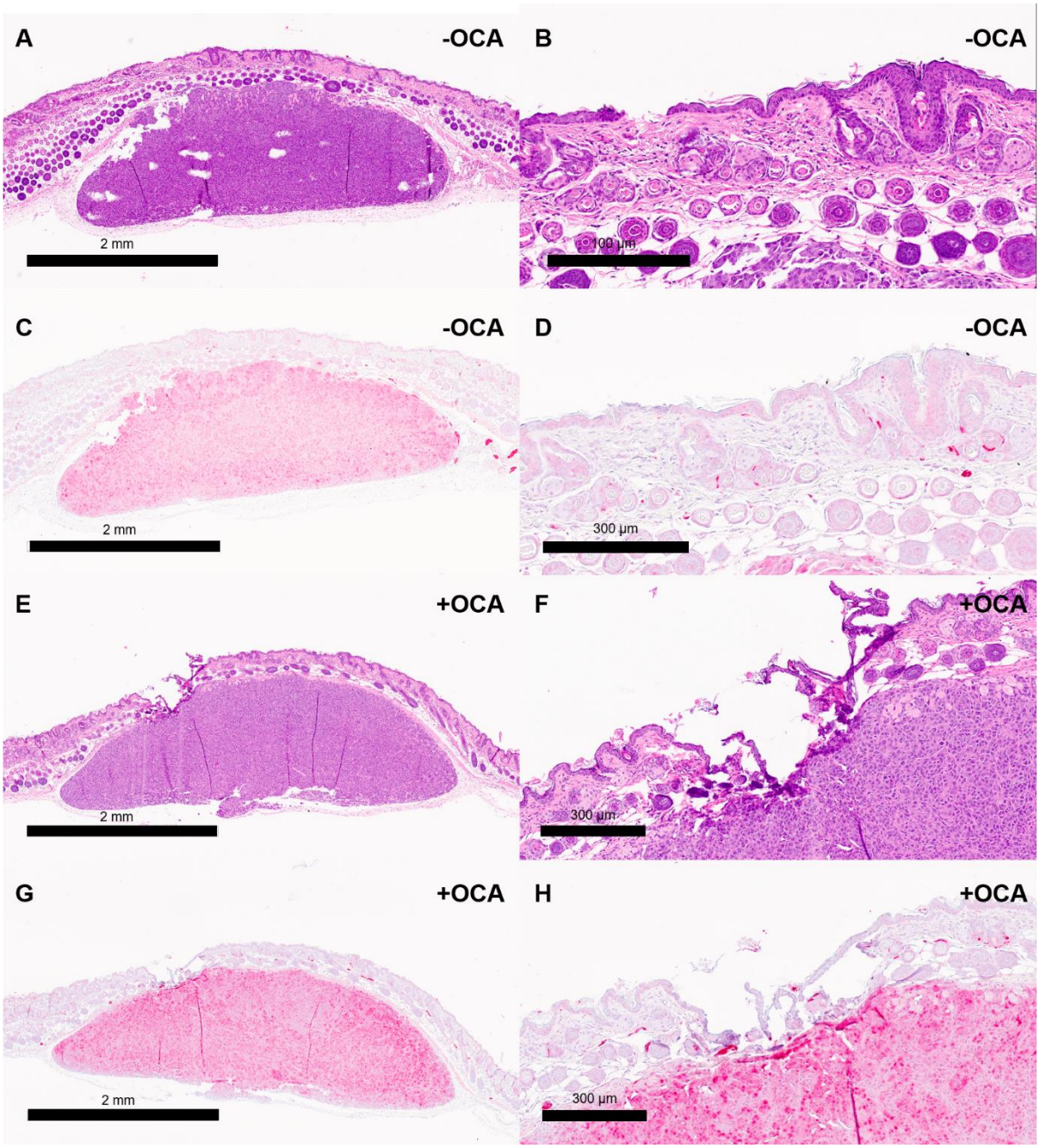

Figure 3.19 - Representative histology slides of groups treated with PDZ-mediated PDT, without (A-D) and with (E-H) topical application of OCA. S100 is expressed in both cases indicating the presence of melanoma cells.

Source: By the author.

Figures 3-20(A-D) and 3-20(E-H) refer to the non-pigmented groups VIS-PDT and OCA+VIS-PDT, respectively. In both cases, the tumors are entirely necrotic, proven by both H&E and S100 staining. In this case, the topical OCA application did not improve tumor response as it was observed for PDZ-mediated PDT.

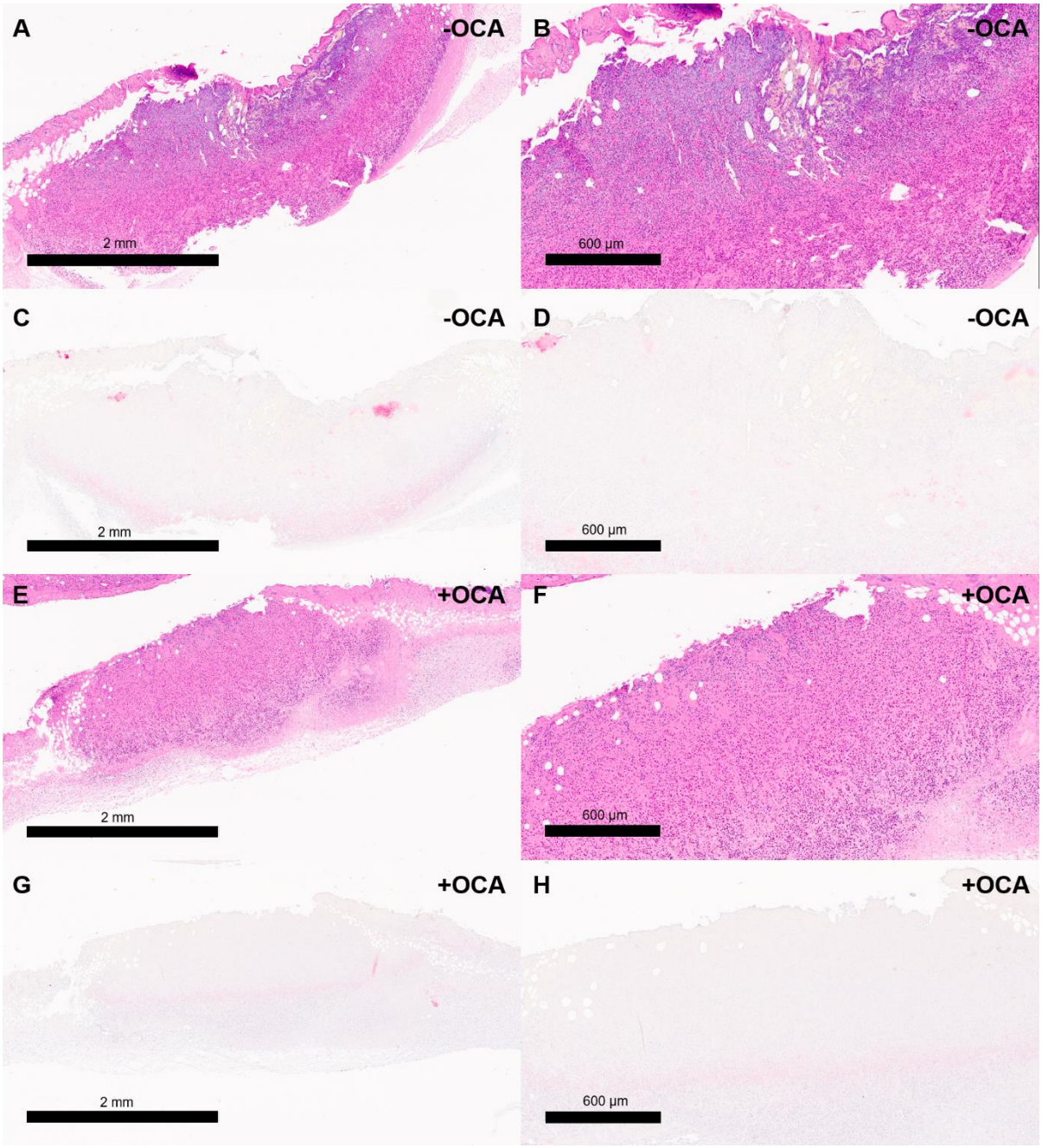

Figure 3.20 - H&E and S100 staining slides from the non-pigmented groups VIS-PDT (A-D) and OCA+VIS-PDT (E-H). Both tumors are entirely necrotic and negative for S100, indicating the complete tumor response to the treatment.

Source: By the author.

The results obtained for the dual-agent PDT groups are shown in Figure 3.21. No difference in the S100 expression was observed between the PDZ-PDT+VIS-PDT and OCA+(PDZ-PDT+VIS-PDT) groups. Although, the H&E revealed that the necrotic tumor is still observed PDZ-PDT+VIS-PDT while in the OCA+(PDZ-

PDT+VIS-PDT) group, the healing process is in an advanced stage, once one cannot see any remaining tumor.

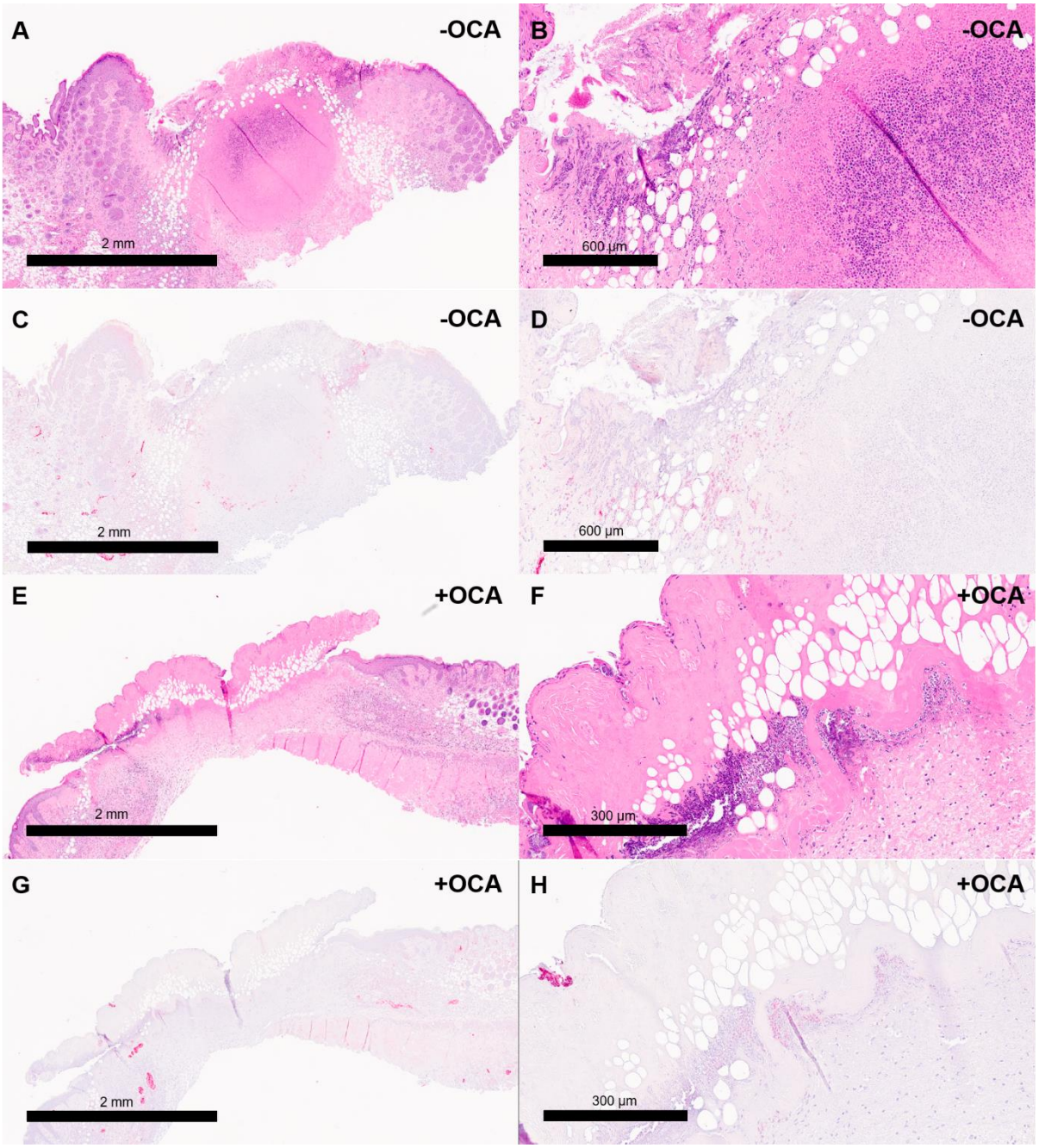

Figure 3.21 - Histology slides from the dual-agent PDT groups, without (PDZ-PDT+VIS-PDT) and with (OCA+(PDZ-PDT+VIS-PDT)) OCA topical application. The tumors are in different healing stages. In the PDZ-PDT+VIS-PDT group, the tumor is necrotic and negative for S100 while in the OCA-(PDZ-PDT+VIS-PDT) no tumor can be seen in the slides, indicating a more advanced tissue recovery stage.

Source: By the author.

Figure 3.22 shows melanoma from the pigmented control group. Besides the cells characteristic, melanin is also observed within the entire the tumor. A large necrotic core is also seen in the tumor core and is showed by arrows in both H&E (Fig 3.22A&B) and S100 (Fig 3.22C&D) staining.

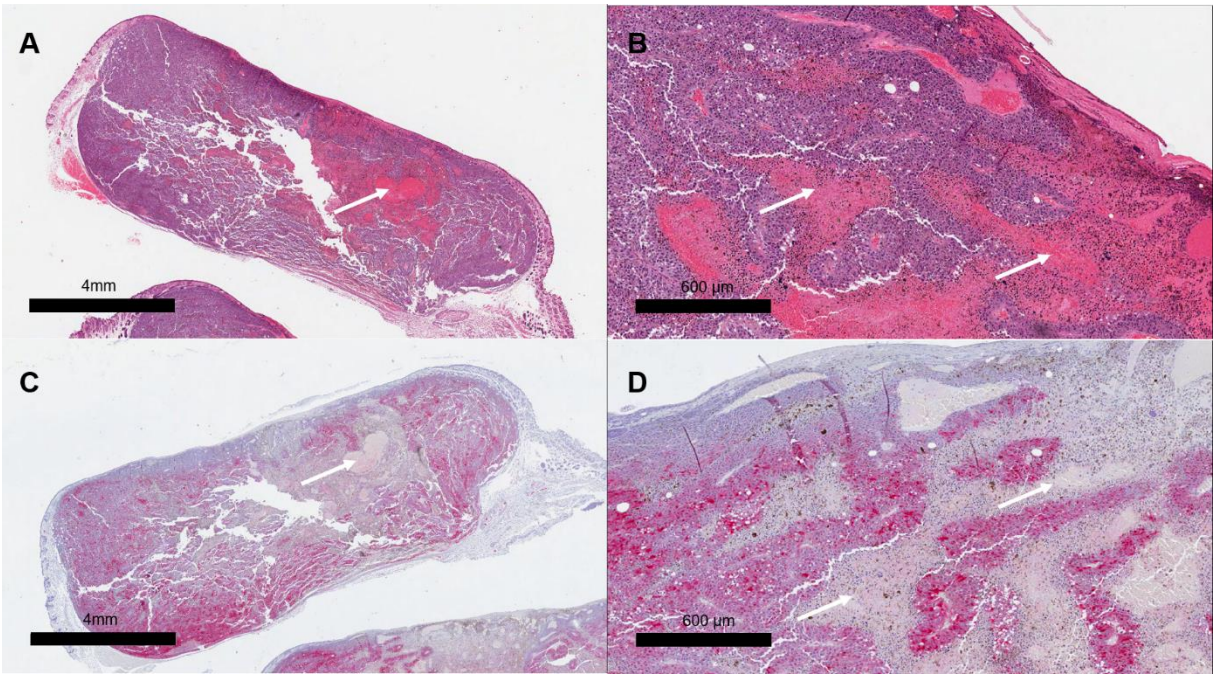

Figure 3.22 – Pigmented tumor of the control group. Arrows indicate necrosis in the tumor core (A&B). One can see S100 staining in reddish (C&D) expressed in the entire tumor, except by the necrotic sites indicated by the arrows.

Source: By the author.

Figure 3.23A&B represents the tumors treated only with PDZ-mediated PDT (group PDZ-PDT). The histology reveals a large superficial necrotic area surrounded by tumor with a significant expression of S100 protein. The histology from the group OCA+PDZ-PDT is shown in Figure 3.23C&D. The OCA improved the light penetration into the tumor and so, the PDT response. It is seen a more homogeneous response, related to the improved light distribution in the tumor. Also, a thinner tumor was observed compared to the group PDT-PDZ, although, still expressing S100 protein.

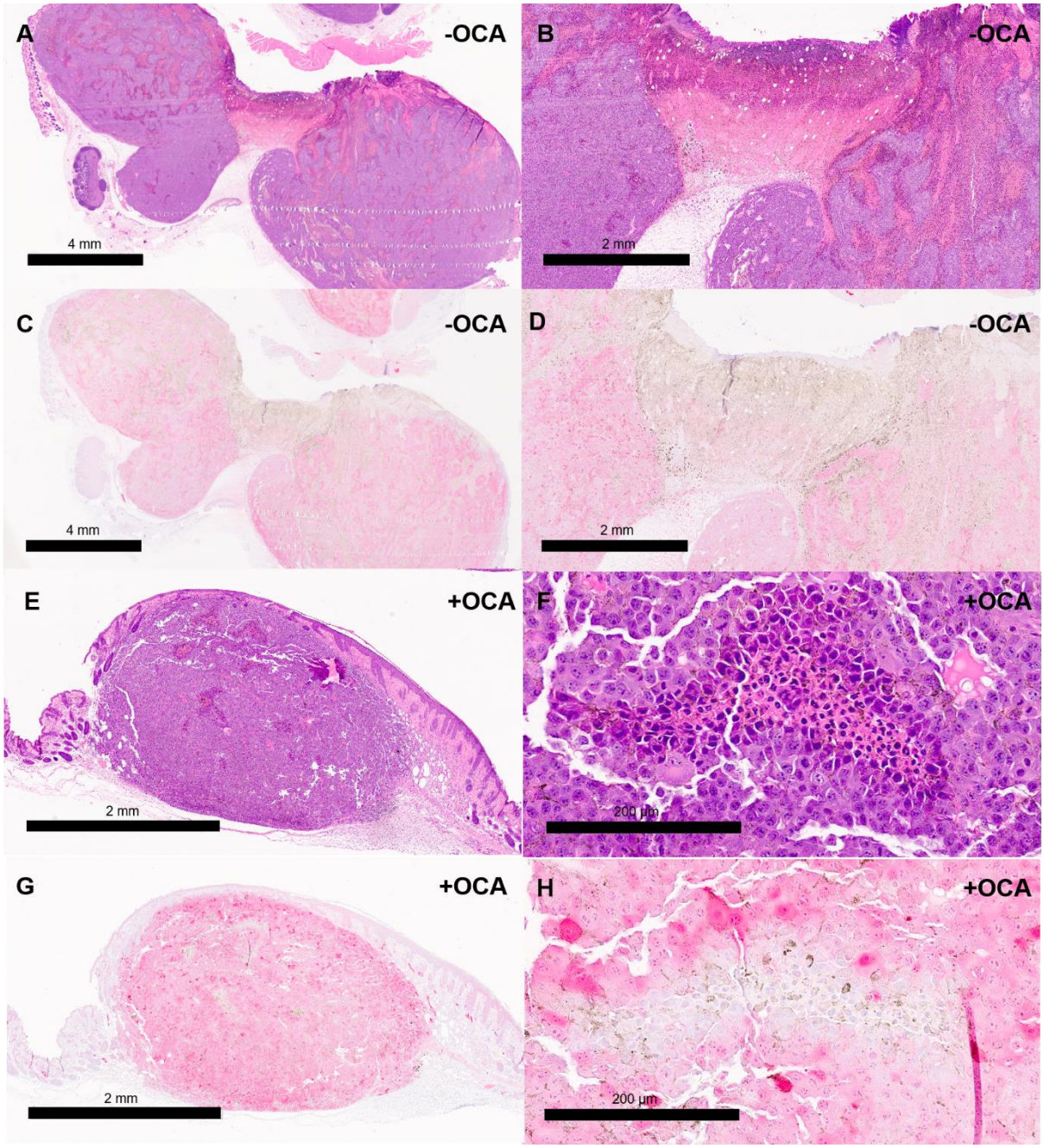

Figure 3.23 - H&E and S100 slides of pigmented melanomas from PDZ-mediated PDT. PDZ-PDT slides (A-D) showed large necrotic area on the tumor surface with surrounding tumor expressing S100. In the OCA+PDZ-PDT groups, the slides present necrotic sites in the lesion, not only on the surface. However, there is still S100 expression.

Source: By the author.

The group VIS-PDT (Fig. 3.24A-D) shows a large necrotic area at the surface of the tumor, although one can observe viable tumor around and underneath this area, still expressing S100 protein. It indicates that PDT effect was limited by the light penetration in the tumor, once the damage was superficial and was not present in the

entire lesion. Also, it is observed vascular damage and loss of epithelia with the reorganization of the collagen fibers in the superficial layers, characteristic of PDT treatment for cutaneous lesions.

Figure 3.24E-H show tumors from the group OCA+VIS-PDT stained with H&E (Fig. 3.24E&F) and for S100 expression (Fig. 3.24G&H). A thinner tumor is observed when compared to the VIS-PDT group, indicating the potential of the OCA on improving light penetration in melanoma. Vascular damage was also observed, mainly at the tumor margins. Although, the presence of S100 protein indicates that the tumor is still viable and regrowth would certainly be detected in the future.

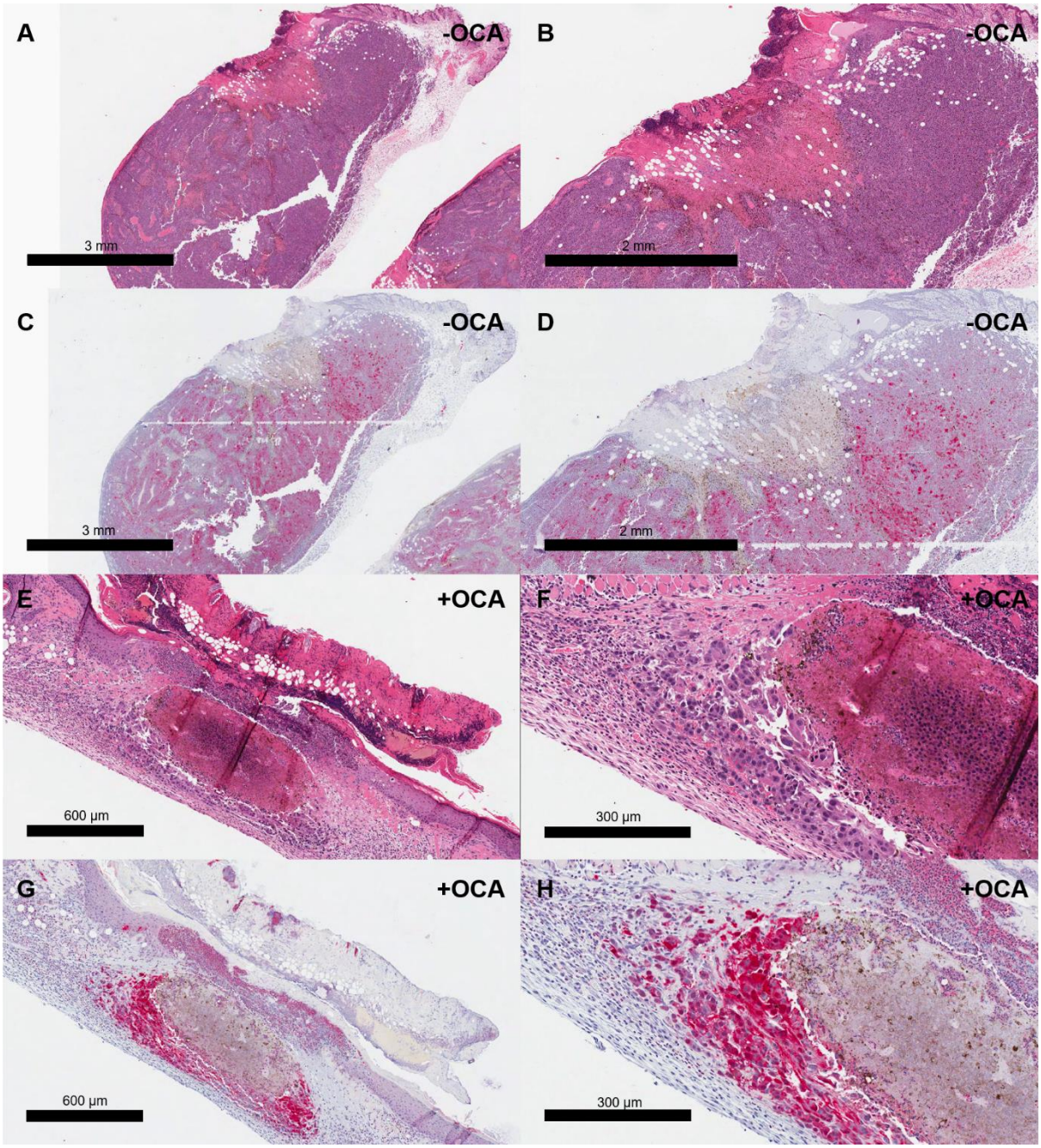

Figure 3.24 - Histology slides from the pigmented tumors treated with VIS-mediated PDT, without and with OCA application. Although the PDT with the OCA induced necrosis in the entire tumor, S100 protein is expressed on the tumors borders, indicating still the presence of melanoma cells.

Source: By the author.

Images of the histology slides from the pigmented tumors treated with the dual-agent PDT are shown in Figure 3.25. Fragile tumor core can be observed in the group PDZ-PDT+VIS-PDT. Besides that, the skin surface recovered from the treatment and no tumor is seen on this site. Although, as there is still tumor in deeper

layers of the skin, the healed superficial layers may induce to a misinterpretation that the tumor was eradicated.

The OCA+(PDZ-PDT+VIS-PDT) group achieved the best result for the pigmented tumors (Figure 3.25). One can still observe some injuries on the skin surface due to the treatment, but no viable tumor is observed, which is confirmed by the absence of S100 protein expression. In this case, a complete response was achieved.

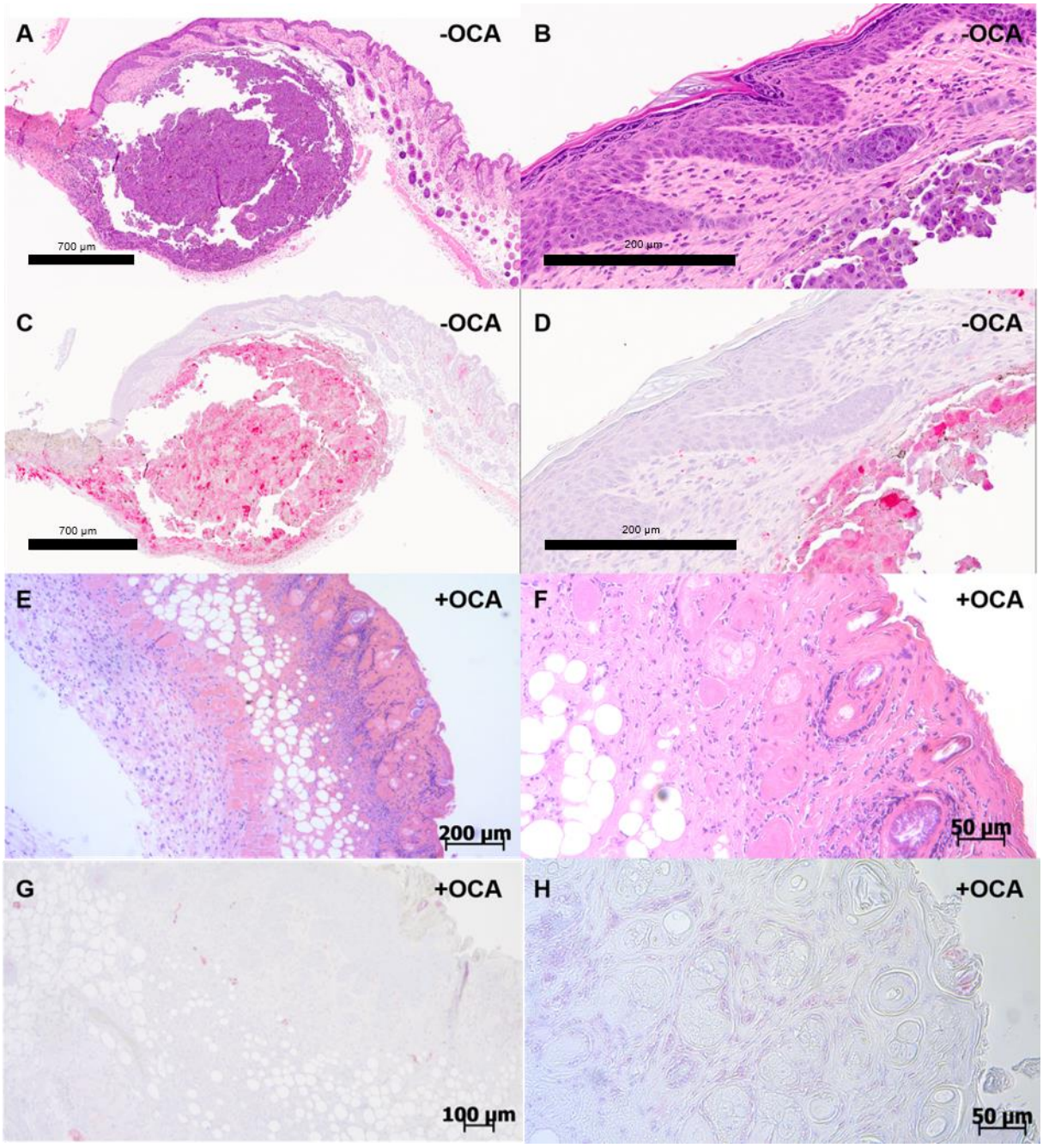

Figure 3.25 - H&E and S100 staining slides of the pigmented dual-agent PDT. (A-D) PDZ-PDT+VIS-PDT group shows a healed skin surface with a tumor expressing S100 underlying it. The additional of OCA (E-H) increased the PDT response, and no tumor is observed.

Source: By the author.

3.3.6 S100 expression quantification

The S100 protein is observed as a reddish stain in the histological slides, and it was used to quantify its expression in the tumor using the software MATLAB®. The software estimates the number of pixels of the entire tumor and the ones selected in

the threshold as positives for S100 expression. This number is related to the amount of S100 expression in the tumor is showed as a percentage value Figure 3.26. As the S100 protein is expressed only by the melanoma cells, it means that the positive staining is related to the presence of melanoma cells and in the case of negative staining, either the tissue is necrotic or, no melanoma cells are present there, meaning that a complete response was observed after the treatment.

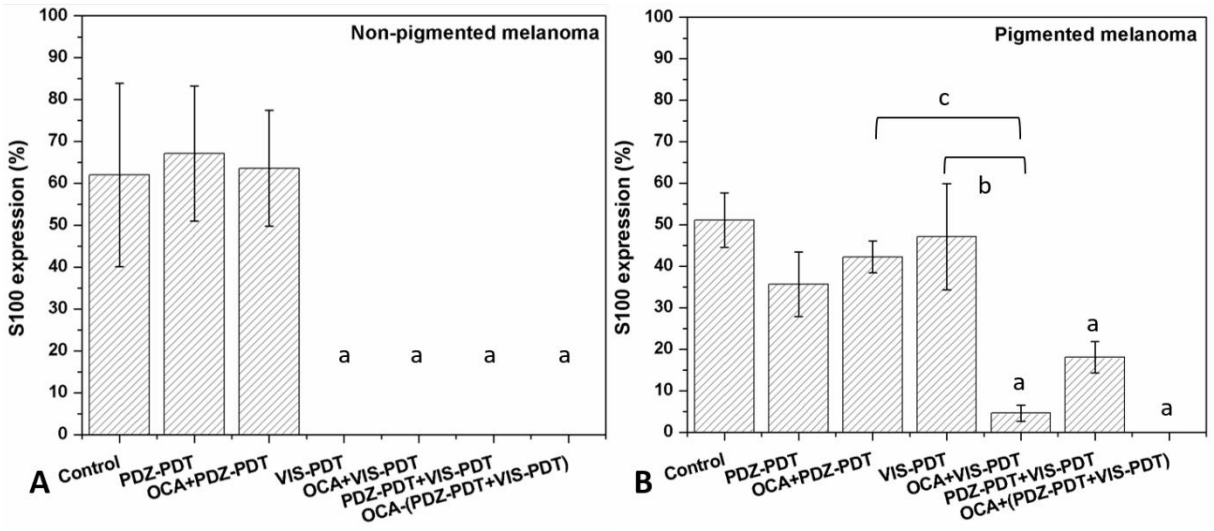

Figure 3.26 - Quantification of S100 expression in non-pigmented and pigmented tumors for the different PDT protocols. In both graphs, the small letters a, b, c, and d means statistical difference when compared to the control group and between the treated groups indicates in the figure, respectively.

Source: By the author.

For the non-pigmented groups, statistical significance was observed for all Visudyne, and dual-agent mediated PDT groups (VIS-PDT; OCA+VIS-PDT; PDZ-PDT+VIS-PDT; OCA+(PDZ-PDT+VIS-PDT), $p<0.0001$) when compared to the control and PDZ groups. Comparing both photosensitizers, with and without OCA, VIS-mediated PDT was more efficient at controlling tumor growth, and no S100 protein expression was observed in these groups. Also, OCA topical application did not improve the PDT response on non-pigmented melanomas. As the thickness of the tumor was between 0.7 to 0.9 mm, the tissue optical properties did not prevent the light penetration into the non-pigmented tumors, and then no effect of the OCA was observed. Besides that, these results are important to demonstrate that the topical application of OCA does not interfere negatively with the PDT treatment response.

Table 3.3 - Statistical analysis of the S100 expression in non-pigmented melanomas.

S100 expression – non-pigmented melanoma						
	PDZ-PDT	**OCA+PDZ-PDT**	**VIS-PDT**	**OCA+VIS-PDT**	**PDZ-PDT+VIS-PDT**	**OCA+(PDZ-PDT+VIS-PDT)**
Control	No	No	Yes p<0.0001	Yes p<0.0001	Yes p<0.0001	Yes p<0.0001
PDZ-PDT		No	Yes p<0.0001	Yes p<0.0001	Yes p<0.0001	Yes p<0.0001
OCA+PDZ-PDT			Yes p<0.0001	Yes p<0.0001	Yes p<0.0001	Yes p<0.0001
VIS-PDT				No	No	No
OCA+VIS-PDT					No	No
PDZ-PDT+VIS-PDT						No

Source: By the author.

Pigmented tumors response to PDT using single-photosensitizer without the OCA application (PDZ-PDT and VIS-PDT) was not significantly different to the control group. Besides the importance of exploring different treatment targets, light penetration into pigmented melanoma still makes optical therapeutics unsuitable. The use of OCA to improve light penetration into pigmented melanoma showed an enhancement of around 90% of the treatment response for the VIS-mediated PDT. Once melanoma is an aggressive tumor with high proliferation rates, the need for large amounts of nutrients implicates on the development of a rich vascular network. This characteristic explains the fact that Visudyne, a vascular-target photosensitizer was more efficient to control tumor growth than the cell-target dye - Photodithazine. In this case, after the changes in the melanoma optical properties, the tumor target resulted in a significant difference in the treatment response.

The dual-agent PDT decreased the S100 expression in around 60% and 50% when compared to the control and single-agent PDT groups (PDZ-PDT and VIS-PDT), respectively. The addition of OCA improved the dual-agent PDT response, and with a single PDT session, no S100 protein was detected in the immunohistochemistry assay, indicating necrotic tissue or absence of melanoma cells.

Table 3.4 - Summary of the statistical analysis of the S100 expression in pigmented melanomas.

S100 expression – pigmented melanoma						
	PDZ-PDT	**OCA+PDZ-PDT**	**VIS-PDT**	**OCA+VIS-PDT**	**PDZ-PDT+VIS-PDT**	**OCA+(PDZ-PDT+VIS-PDT)**
Control	No	No	No	Yes p<0.0001	Yes p=0.0035	Yes p<0.0001
PDZ-PDT		No	No	Yes p=0.0059	No	Yes p<0.0001
OCA+PDZ-PDT			No	Yes p=0005	No	Yes p<0.0001
VIS-PDT				Yes p<0.0001	Yes p=0.0117	Yes p<0.0001
OCA+VIS-PDT					No	No
PDZ-PDT+VIS-PDT						No

Source: By the author.

3.3.7 Tumor thickness assessment

The tumor thickness was measured in triplicate in each slide using the software ImageScope®, in the thickest site of the tumor expressing S100. Results for non-pigmented and pigmented melanomas are shown in Fig. 3.27A and 3.27B, respectively.

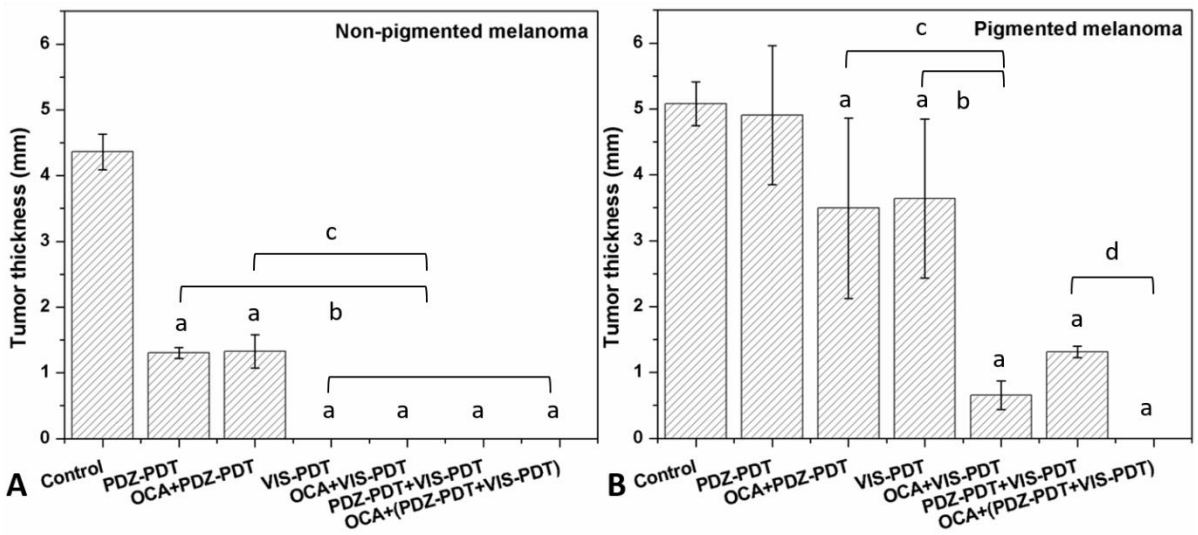

Figure 3.27 - Non-pigmented and pigmented tumors thickness at the end of the evaluation period. (a) refers to the significant difference to control group; b, c, and d, refers to statistical significance to the respective treatment groups.

Source: By the author.

The non-pigmented PDZ-PDT group showed high S100 protein expression, however, after the treatment, a flattened on the tumor volume was observed. This effect can be confirmed by the tumor thickness at the end of the evaluation period, around 75% thinner than the control group. As in the S100 expression, the OCA did not significantly improve the PDT response on non-pigmented tumors, once light penetration into the tissue is not an issue for the non-pigmented melanoma. Agreeing with the S100 assay, the best result was achieved by the VIS-PDT, OCA+VIS-PDT, PDZ-PDT+VIS-PDT, and OCA+(PDZ-PDT+VIS-PDT) groups. These groups were statistically significant when compared to both, control and PDZ-mediated PDT (with and without OCA application – Table 3.5).

Table 3.5 - Statistics summary for the non-pigmented melanoma thickness.

Tumor thickness – non-pigmented melanoma						
	PDZ-PDT	**OCA+PDZ-PDT**	**VIS-PDT**	**OCA+VIS-PDT**	**PDZ-PDT+VIS-PDT**	**OCA+(PDZ-PDT+VIS-PDT)**
Control	Yes p<0.0001	Yes p<0.0001	Yes p<0.0001	Yes p<0.0001	Yes p<0.0001	Yes p<0.0001
PDZ-PDT		No	Yes p=0.0158	Yes p=0.0158	Yes p=0.0158	Yes p=0.0158
OCA+PDZ-PDT			Yes p=0.0128	Yes p=0.0128	Yes p=0.0128	Yes p=0.0128
VIS-PDT				No	No	No
OCA+VIS-PDT					No	No
PDZ-PDT+VIS-PDT						No

Source: By the author.

The topical application of OCA improved PDT response significantly on pigmented melanoma in all protocols investigated OCA+PDZ-PDT; OCA+VIS-PDT; OCA+(VIS-PDT+PDZ-PDT) when compared to control group (Figure 3-27B and Table 3.6). OCA+VIS-PDT group reduced the pigmented melanoma thickness in 90% and 70% in comparison to control and PDZ-mediated PDT. However, the best result was achieved by the dual-agent PDT combined with OCA, as it was observed for the S100 expression assay. A complete response was observed for all the animals in this group.

Table 3.6 - Summary of statistical analysis of the pigmented tumor thickness.

Tumor thickness – pigmented melanoma						
	PDZ-PDT	**PDZ-(PDT+OCA)**	**VIS-PDT**	**VIS-(PDT+OCA)**	**(PDZ+VIS)-PDT**	**(PDZ+VIS)-(PDT+OCA)**
Control	No	Yes p=0.0015	Yes p=0.0065	Yes p<0.0001	Yes p<0.0001	Yes p<0.0001
PDZ-PDT		Yes p=0.0085	Yes p=0.0314	Yes p<0.0001	Yes p<0.0001	Yes p<0.0001
PDZ-(PDT+OCA)			No	Yes p<0.0001	Yes p<0.0001	Yes p<0.0001
VIS-PDT				Yes p<0.0001	Yes p<0.0001	Yes p<0.0001
VIS-(PDT+OCA)					No	No
(PDZ+VIS)-PDT						Yes p=0.0209

Source: By the author.

3.3.8 Determination of melanoma-specific growth rate (SGR) and doubling time (DT)

The specific growth rate and doubling time were estimated by the tumor volumes acquired using the photoacoustic and ultrasound imaging. The values are presented in Table 3.7.

The non-pigmented and pigmented tumors showed similar SGR and DT values. Both PDZ-PDT and OCA+PDZ-PDT groups for the non-pigmented melanoma showed a decrease on the SGR of around 80% and a DT increase of 8 days. As in the S100 staining, no tumor was found in the non-pigmented VIS-mediated groups, the SGR and DT could not be calculated for these groups.

The pigmented PDZ-PDT group did not show any difference when compared to the control group. This result agrees with those observed in the tumor volume measurements and the H&E and S100 histology. VIS-mediated PDT without OCA application reduced the SGR in approximately 50% and doubled the DT. The dual-photosensitizer PDT decreased the SGR by 90% and reached a DT of 10 days. The addition of OCA in both OCA+PDZ-PDT and OCA+VIS-PDT pigmented groups showed negative SGR; it means that during the investigation period, the tumor volume decreased, demonstrating the PDT efficiency.

The SGR and DT are parameters highly used to evaluate tumor growth as its response to different treatments. In this study, the values obtained for non-pigmented and pigmented groups agree with the results observed in the volume measurement, histology, S100 expression, and tumor thickness that indicated the OCA potential on improving the light penetration into the tumor and the PDT response.

Table 3.7 - Melanoma-specific growth rate and doubling time.

	Non-pigmented				Pigmented			
	SGR (mm^3/day)		DT (day)		SGR (mm^3/day)		DT (day)	
	Ave	SD	Ave	SD	Ave	SD	Ave	SD
Control	0.55	0.15	1.34	0.35	0.68	0.09	1.03	0.13
PDZ-PDT	0.09	0.04	9.90	6.38	0.62	0.08	1.12	0.15
OCA+PDZ-PDT	0.13	0.09	9.71	10.10	-0.04	0.09	-1.40	12.32
VIS-PDT	N/A				0.32	0.07	2.22	0.49
OCA+VIS-PDT	N/A				-0.25	0.10	-3.12	1.36
PDZ-PDT+VIS-PDT	N/A				0.07	0.02	10.15	1.94
OCA+(PDZ-PDT+VIS-PDT)	N/A				N/A			

N/A: not applicable

Source: By the author.

Several approaches have been used to improve PDT response on melanoma, including the development of new drugs with absorption at longer wavelengths,(17) use of quantum dots to generate light inside the tumor to excite the photosensitizers (upconversion mechanisms); multiple PDT sessions; and melanin bleaching using blue light,(56) high-peak pulsed laser(54) or chemical agents.(57,102) To the date, no PDT protocol has presented enough efficacy for a complete treatment of cutaneous melanoma, still being considered an experimental procedure.(21)

Optical clearing agents have been used mainly to improve imaging resolution for optical diagnosis. This improvement in the light distribution can also be used to increase optical treatments response for solid or pigmented tumors. The OCA effect on melanoma was measured by diffuse reflectance spectroscopy and OCT imaging. In both cases, it was observed that OCA could decrease DRS signal up to 95% and double the depth of the OCT imaging.

The DRS variation before and after OCA application was higher for melanoma than normal skin. As the tissue dehydration induced by the OCA changes the collagen fibers alignment, it is expected to achieve increased clearing on tumors once the fast development results in a more disorganized tissue. Besides the improvement on the light penetration into the tumor, the spectroscopy measurements revealed that melanoma became optically more homogenous after OCA application that is highly favorable for optical therapeutics, especially for PDT. Also, the use of OCA improved OCT imaging of pigmented melanoma vascular network, that is related to tumor staging and prognosis. To our knowledge, that was the first report of a non-invasive *in vivo* optical technique that can image melanoma microvessel network(83) and might represent an improvement in tumor staging and patient prognosis. Moreover, microvasculature imaging can also be used to monitor tumor response to different treatments.

To investigate if the increase in the light penetration into melanoma induced by OCA could be translated to an improvement of PDT response, OCA+PDT combination was evaluated using two photosensitizers in both, non-pigmented and pigmented model.

In this study, two photosensitizers were investigated a vascular-target and a mainly cellular-target, Visudyne, and Photodithazine, respectively. For the non-pigmented tumor, PDZ-mediated PDT reduced the tumor thickness in around 75%, SGR in 90% and the DT increased in 8 days when compared to control group. However, the tumor still expresses S100 protein, indicating that a tumor growth would be observed. No significant difference was observed with the addition of OCA, probably due to the non-pigmented tumor optical characteristics did not prevent the light penetration into the entire tumor. The tumor was not eliminated probably due to the melanoma resistance to PDT also described by Huang and collaborators.(16)

The PDT treatment using the vascular-target photosensitizer, Visudyne, was more efficient in treating non-pigmented melanoma than Photodithazine. In this case, no viable tumor was observed after a single PDT session, that was confirmed by the absence of S100 protein expression. As seen in the PDZ-mediated treatment groups, OCA did not improve non-pigmented tumors response. The dual-agent PDT, combining both vascular and cellular-target PDT also eliminate the tumor without or with OCA topical application. In summary, for non-pigmented melanoma, vascular-

target PDT showed promising results, combining or not with cellular-target photosensitizer or OCA.

For the pigmented tumors, PDZ-PDT did not show any statistical difference to the control group. This result is mainly related to the light absorption by the tumor surface, that is, even with a small damage on the surface layers, the tumor quickly recovers its growth, and this is the principal reason that PDT for melanoma is still restricted to experimental research. The addition of OCA increased tumor response, reducing average thickness in around 30%, SGR and DT values are negative that represents tumor volume reduction during the investigated period, but as S100 is still expressed in the entire tumor, its regrowth is expected for longer evaluation periods.

As it was observed for the non-pigmented tumors, VIS-mediated PDT was also more efficient for pigmented tumors than PDZ-mediated PDT. Histology from VIS-PDT group showed flattened tumors, 30% less thick than the control group. A 50% of the SGR and double DT was also observed, but S100 is still expressed in the entire tumor. The addition of OCA improved the pigmented melanoma response significantly. A decrease of 90% and 85% were achieved for S100 expression and tumor thickness, respectively. As it was observed for the OCA+PDZ-PDT group, SGR and DT values became negative, once during the investigation period, no significant regrowth was observed.

The dual-agent PDT, targeting vessels, and cells showed promising results for pigmented melanoma. Reduction of 40, 80, and 90% was observed for S100 expression, tumor thickness, and SGR, respectively, that are related to an adequate tumor control. In this case, multiple PDT session might be able to eliminate the tumor if positive rate between tumor death and tumor growth is present. However, the best results were achieved by the dual-agent PDT combined with OCA. No tumor was observed at the end of the evaluation period, confirmed by the negative S100 staining.

Melanoma is an aggressive type of cancer, and its resistance to PDT had already been described(16). In this study, an OCA was used to overcome melanoma optical interference and improve the treatment response in depth. Besides that, a dual-target PDT was chosen to overcome the PS sequestration by the melanosomes that can neutralize the free radicals generated during PDT. The combination of approaches could eliminate pigmented tumors in a single PDT session and may be an alternative to overcome melanoma resistance

The conventional treatment for melanoma is still the surgery, however this technique still has some disadvantages: limited safety margin depending on the anatomic site involved that increases the recurrence probability; in case that flaps are needed, as in the face (one of the leading sites of melanoma), the recovery is quite long and in some cases multiple surgeries are needed; anaesthesia is required; and the successful rate relies on the skill level of the clinician. Photodynamic therapy for skin cancers is a non-invasive technique, not limited by anatomical sites involved with quick recovery and excellent aesthetic results. As it is not a complicated technique, it can be performed in ambulatory, without anesthesia. PDT is already established for non-melanoma skin cancer and can become an attractive alternative for melanoma.

3.4 CONCLUSIONS

In this study, we investigated if OCA could change melanoma optical properties and improve light penetration into the tumor. DRS and OCT imaging were used to assess the effect of OCA on pigmented tumors. DRS signal showed a significant signal decrease of around 95% compared to a ±20% variation observed for normal skin. OCT combined to OCA doubled the depth of imaging when compared to the conventional technique. Moreover, due to increase in the light penetration into the tumor, we could image the tumor microvasculature network that is related to melanoma staging and patient prognosis. The procedure is simple, does not result in an increased measurement time, and the OCAs are safe, resulting in a feasible technique for clinical implementation.

The use of OCA associated to PDT did not significantly improve the treatment response of non-pigmented tumors, probably because the light penetration into the tumor is not limited in this case. On the other hand, the OCA association improved the pigmented melanoma response in all protocols investigated. The best results were achieved for the dual-agent PDT combined to OCA. The dual-agent targeted both, vessels and tumor cells, improving the melanoma response. This strategy involving changes in the tissue optical properties and targeting both cell and vessels seems to be essential to overcome melanoma resistance to PDT.

CHAPTER 4 TWO-PHOTON EXCITATION PHOTODYNAMIC THERAPY ON PIGMENTED AND NON-PIGMENTED MELANOMA CELLS

4.1 OBJECTIVE

This study aims to investigate the effect of TPE *in vitro* on synthetic melanin solution and PDT for pigmented and non-pigmented melanoma cells.

4.2 MATERIALS AND METHODS

4.2.1 Melanin characterization

Synthetic melanin was purchased from Sigma-Aldrich and diluted in DMSO to a final concentration of 1 uM (considering the molar mass of 318.28 g/mol). To investigate whether melanin could present 2-photon absorption (TPA), melanin linear absorption and the quadratic dependence between melanin fluorescence and laser power were investigated.

For the linear absorption assay, melanin solution was placed in a temperature-controlled water bath at 70°C, and the absorption spectrum was collected every 30 minutes for 210 minutes in a spectrometer (Cary UV-VIS 50, Varian®).

The quadratic dependence between the fluorescence intensity and the laser power was carried out in a laser scanning confocal microscope LSM780 Zeiss® (Carl Zeiss Jena GmbH, Jena, Germany) and a femtosecond pulsed laser at 865 nm (Chameleon) was used to excite melanin. The fluorescence collection was performed in the range of 500 to 600 nm. For this assay, it was considered:

$$I_{f(2p)} \sim \left(P_{average(2p)}\right)^2 \tag{4.1}$$

$I_{f(2p)}$ is the fluorescence intensity for TPE and $P_{average}$ is the laser average power, then

$$log\left(I_{f(2p)}\right) \sim 2log\left(P_{average\ (2p)}\right) \tag{4.2}$$

The angular coefficient should be around 2 to confirm the quadratic relation between fluorescence intensity and laser power.

4.2.2 Cell culture

The human cell lines (C32 and G361) and the pigmented murine melanoma cells were obtained from American Type Culture Collection (ATCC), and the non-pigmented murine melanoma (B78H1) was kindly donated by Dr. Pier-Luigi Lollini, University of Bologna, Italy. The C32 human non-pigmented melanoma was grown in MEM, the G361 was cultured in McCoy's modified 5A, and both murine melanoma cells were cultured in DMEM. All cell medias were supplemented with 10% fetal bovine serum (FBS) and penicillin-streptomycin at 37 °C and 5% CO_2.

4.2.3 Two-photon excitation photodynamic therapy (TPE-PDT)

For the TPE experiments, the peak power,(74) peak energy E,(74) average irradiance,(76) and peak irradiance(76) were calculated accordingly by the following equations:

$$P_{(peak)} = \frac{P_{(average)}}{\tau f} \tag{4.3}$$

Where P (average) is the power measured after the objective, τ is the pulse duration at the sample, and f the pulse repetition frequency. The peak energy was then determined as:

$$E_{(peak)} = P_{(peak)}\tau \tag{4.4}$$

The average irradiance was calculated by:

$$I_{(average)} = \frac{\pi P_{(average)}}{2}\left(\frac{\eta}{\lambda}\right)^2 (1-\cos\alpha)(3+\cos\alpha) \tag{4.5}$$

Where I is the intensity; η is the refractive index of the medium; λ the wavelength and α the semi-aperture angle of the objective that can be calculated by:

$$\alpha = \sin^{-1}\left(\frac{NA}{\eta}\right) \tag{4.6}$$

Where NA is the lens numerical aperture.

Assuming a Gaussian pulse shape, the peak irradiance is then determined:

$$I_{(peak)} = \left(\frac{ln2}{\pi}\right)^{1/2} \frac{2}{\tau f} I_{(average)} \quad (4.7)$$

4.2.3.1 LIVE/DEAD assay

One million cells (G361 or C32) were cultured in Petri dishes for 24 hours before PDT experiment. After the attachment of the cells, a glass pipette was used to mark the Petri dishes and use as a reference for the treatment (Figure 4.1A). A benzoporphyrin derivative (Visudyne, QLC Inc.) was added 3 hours prior illumination in a concentration of 2.5 µM. After the light-drug interval, the Petri dishes were placed under a laser scanning confocal microscope LSM 710 Zeiss® (Carl Zeiss Jena GmbH, Jena, Germany) for the irradiation. It was used a Titanium-Sapphire laser (Chameleon, Coherent) tunable from 720 to 960 nm, with 300 fs pulse duration at the sample and 90 MHz repetition rate and a 20x water-immersion objective with a numerical aperture of 1.0 were used. The laser was set up at 865 nm, and the average power varied from 0.2 to 5 mW over a 512 x 512-pixel area of 424 x 424 um and pixel dwell time of 1.58 µm (power peak: 8-185 W; energy (peak): 2 – 56 pJ; I (average): 9.3 x 10^4 - 2.4 x 10^6 W/cm^2; I (peak): 3.2 x 10^9 - 8.4 x 10^{10} W/cm^2; fluence: 4.6 x 10^5 – 1.2 x 10^7 J/cm^2). Twelve slices were irradiated, with a step size of 2 µm, to deposit PDT treatment throughout the entire cell culture.

After PDT, the cells were incubated with LIVE/DEAD fluorescence marker (LifeTechnologies – Invitrogen®), followed by imaging in the same microscope with excitation at 442 and 515 nm and image acquisition using two channels: between 460 and 500 nm for live cells and between 540 and 610 nm for dead cells. Besides the marks done in the Petri dishes, the treated area could also be defined by the photosensitizer bleaching (Figure 4.1B).

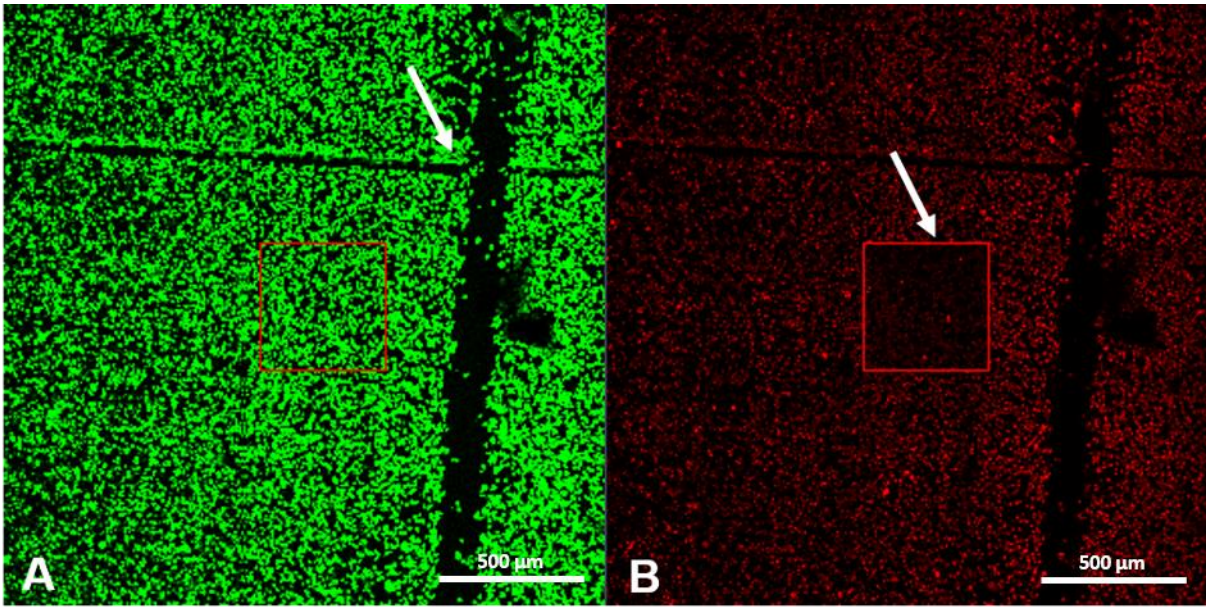

Figure 4.1 – Cells cultured in Petri dishes for the TPE-PDT. White arrows indicate an example of the glass pipettes marks that were used as references for the TPE-PDT treatment (A) and a bleaching site observed after the irradiation (B).

Source: By the author.

4.2.3.2 Real-time cell morphology evaluation

One million cells were cultured in the Petri dishes as described in the section above. Then, Visudyne (2.5 µM) was added following the same protocol for the LIVE/DEAD assay and placed under the microscope for the irradiation. It was used an inverted laser scanning confocal microscope LSM 780 Zeiss® (Carl Zeiss Jena GmbH, Jena, Germany) and a Titanium-Sapphire laser (Chameleon, Coherent®) tunable from 720 to 960 nm, with 300 fs pulse duration at the sample and 90 MHz repetition rate, and a 20x objective with numerical aperture of 0.8, average power of 12 mW over a 1024 x 1024-pixel area of 210 x 210 µm and a pixel dwell time of 1.58 µs (average power: 12 mW; peak power: ~445 W; energy (peak): 100 pJ; average irradiance: 2.6×10^6 W/cm^2; peak irradiance: 9.0×10^{10} W/cm^2). The reflected light was used to acquire images of the cell morphology during the TPE-PDT. The cells were considered dead when cell shrinkage and blebs were observed around the cell and counted manually to determine the treatment efficiency.

4.2.3.2.1 Two-photon photobleaching kinetics

The images from the time series acquired during the “real-time cell morphology” assay were used to compute the photosensitizer photobleaching rate spatially, that is the photobleaching rate calculated for each pixel of the image, using the software MATLAB® R2015a (Mathworks, USA). The image processing was performed as described by Lencione and collaborators(103). In summary, after selecting the ROI and determining the threshold, a bi-exponential decay function was used to fit the data collected.

$$I_{ij}(t) = A_{ij} + B_{ij}e^{\left(-t/\tau_{ij(1)}\right)} + C_{ij}e^{\left(-t/\tau_{ij(2)}\right)} \quad (4.8)$$

Where *ij*, *t*, *A*, *B*, and *C*, refer to the pixel position, time, offset parameter, and amplitudes, respectively. $\tau_{ij(1)}$ and $\tau_{ij(2)}$ are the photobleaching lifetime per pixel.
Then, the average lifetime per pixel can be calculated as:

$$\langle\tau\rangle_{ij} = \frac{B_{ij}{\tau_{ij(1)}}^2 + D_{ij}{\tau_{ij(2)}}^2}{B_{ij}\tau_{ij(1)} + B_{ij}\tau_{ij(2)}} \quad (4.9)$$

And the image average lifetime:

$$\langle\tau\rangle_{image} = \frac{\sum_{i,j=1}^{N}\langle\tau\rangle_{ij}}{N} \quad (4.10)$$

N is the number of pixels with higher fluorescence intensity than the background.

4.2.4 Transmission Electron Microscopy (TEM)

The cells were cultured as described above and irradiate following the TPE-PDT protocol in the absence of photosensitizer. The cells were then fixed with formalin 2% and sent to Electron Microscopy Lab – Medicine School, the University of Sao Paulo for processing. The images were performed in a Jeol JEM – 100 CXII microscope. With this assay, we aimed to investigate if the TPE induces any damage to the melanosomes organelles that might cause an improvement in the pigmented cell killing.

4.3 RESULTS

4.3.1 Melanin characterization

Melanin in DMSO solution has a broad absorption spectrum from UV to NIR, originated from highly conjugated structures (Figure 4.2A). The increase in the temperature broke down the larger molecules of melanin into smaller ones, shifting the absorption spectrum for shorter wavelengths (Figure 4.2A). It is possible to observe that, at 70º Celsius, the absorbance decreased at 800-1100 nm and increased at 355 nm as a function of time. These small molecules absorb mainly the shorter wavelengths, explaining the reason that even with a linear absorption at 865 nm, melanin also presents TPA at this wavelength. It can also be confirmed by the quadratic dependence between the melanin fluorescence intensity and the laser power (Figure 4.2B). The angular coefficient is ~1.8, indicating the TPA at 865 nm.

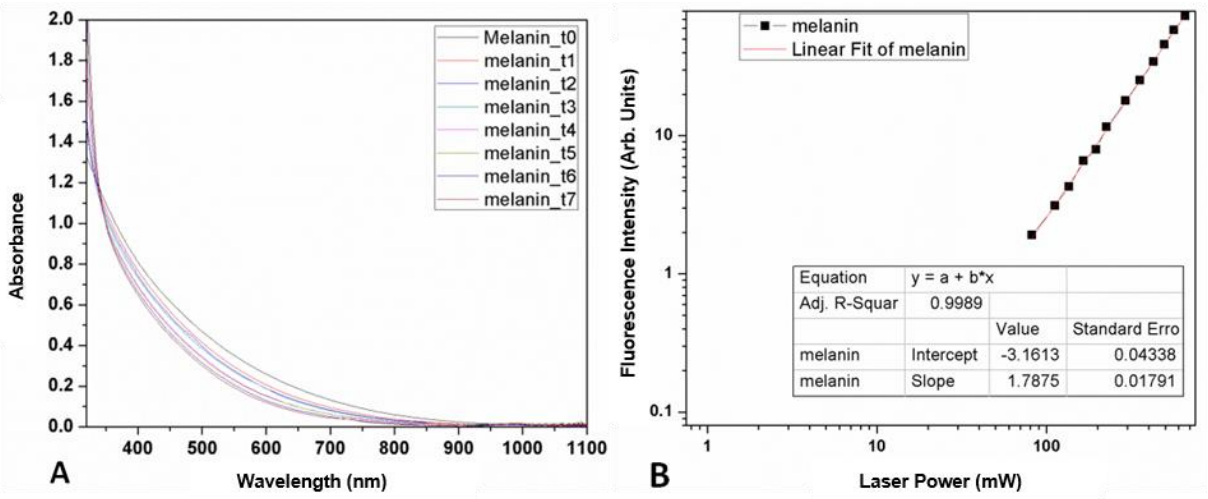

Figure 4.2 - (A) Measurements of melanin absorbance spectra every 15 minutes immersed in water at 70 Celsius degree for 105 minutes. (B) Melanin fluorescence quadratic dependence to laser power, proving the melanin capacity of absorbing 2-photon.

Source: By the author.

4.3.2 Two-photon excitation photodynamic therapy (TPE-PDT)

4.3.2.1 LIVE/DEAD assay

Melanin is an absorber, but it is also an antioxidant pigment which makes optic treatments a challenge. Then, the effect of TPE-PDT was investigated in both non-

pigmented and pigmented cells. In Figure 4.3, one can observe the apoptosis induced by TPE-PDT in pigmented cells.

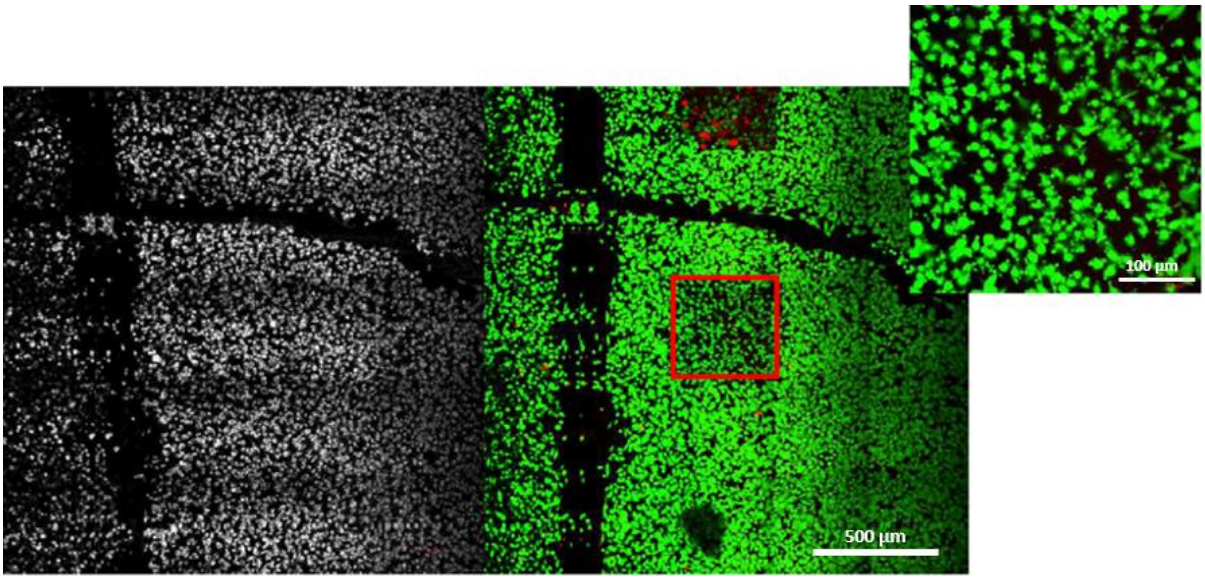

Figure 4.3 - Fluorescence image of melanoma cells before (A) and after TPE-PDT (B). In detail (C), one can see cell morphology changes characteristic of apoptosis.

Source: By the author.

The cell viability determined by the LIVE/DEAD assay is shown in Figure 4.4.

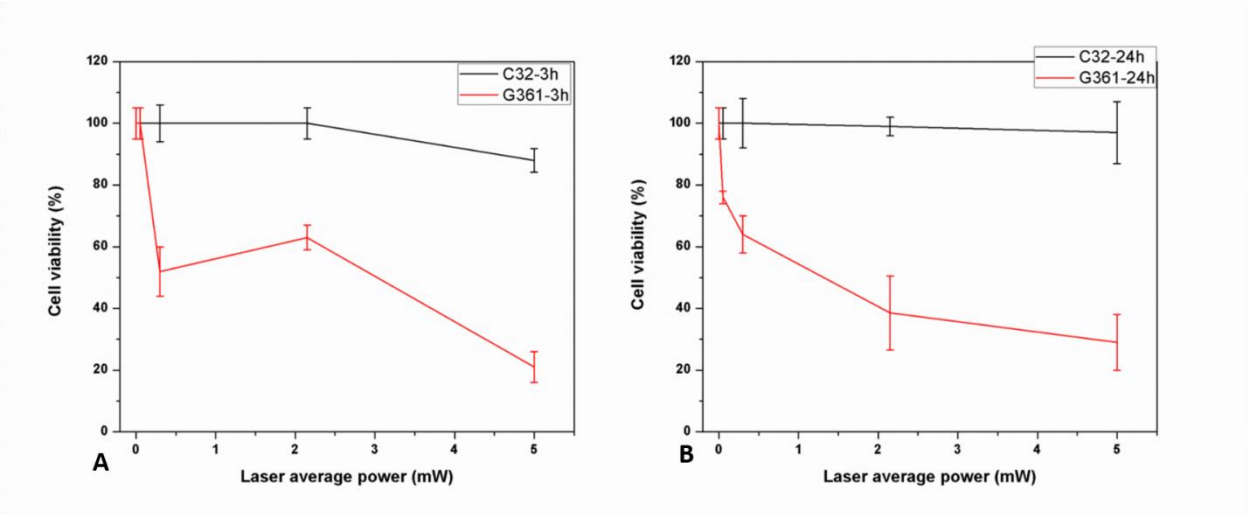

Figure 4.4 - Non-pigmented and pigmented human melanoma cells viability after 2-photon photodynamic therapy as a function of laser power. Light-drug interval of 3 (A) and 24 hours (B).

Source: By the author.

For both light-drug intervals (3 and 24 hours), the pigmented cells were more susceptible to the TPE-PDT. It was necessary ~ 1.2 x 107 J/cm^2 to induce apoptosis in 70-75% and 10-15% of the pigmented and non-pigmented cells, respectively. To evaluate the cell morphology changing during the TPE-PDT, a real-time investigation was performed.

4.3.2.1 Real-time cell morphology evaluation

To quantify the cellular death during TPE-PDT, cell morphology evaluation was carried out. The cell was considered dead when cell shrinkage and blebs were observed. Figure 4.5 and 4.6 shows the non-pigmented cells during the 2-photon irradiation only and TPE-PDT, respectively. Each image took 1.6 second, and a fluence at the sample was 4.2 x 10^6 J/cm^2 per scan.

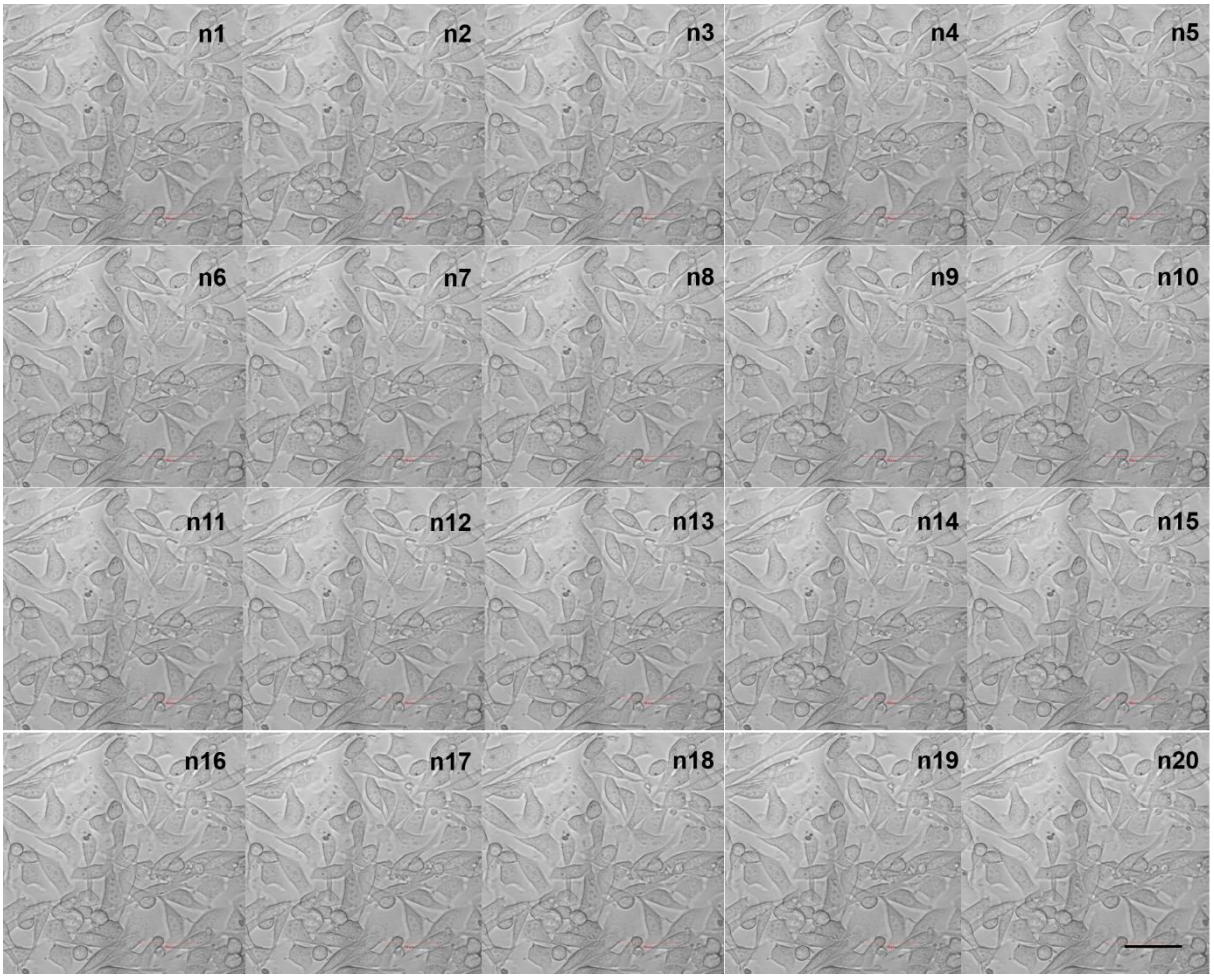

Figure 4.5 – Bright-field time-series of non-pigmented cells irradiated following the TPE protocol. No significant changes in cell morphology were observed. The images are 210 x 210 µm, and the scale bar is 50 µm.

Source: By the author.

The non-pigmented cell irradiation in the absence of photosensitizer does not induce cell damage. For the TPE-PDT morphology changes, mainly cell retraction was observed only in a few cells demonstrating that TPE-PDT was not effective on non-pigmented cell killing for the parameters investigated (Figure 4.6).

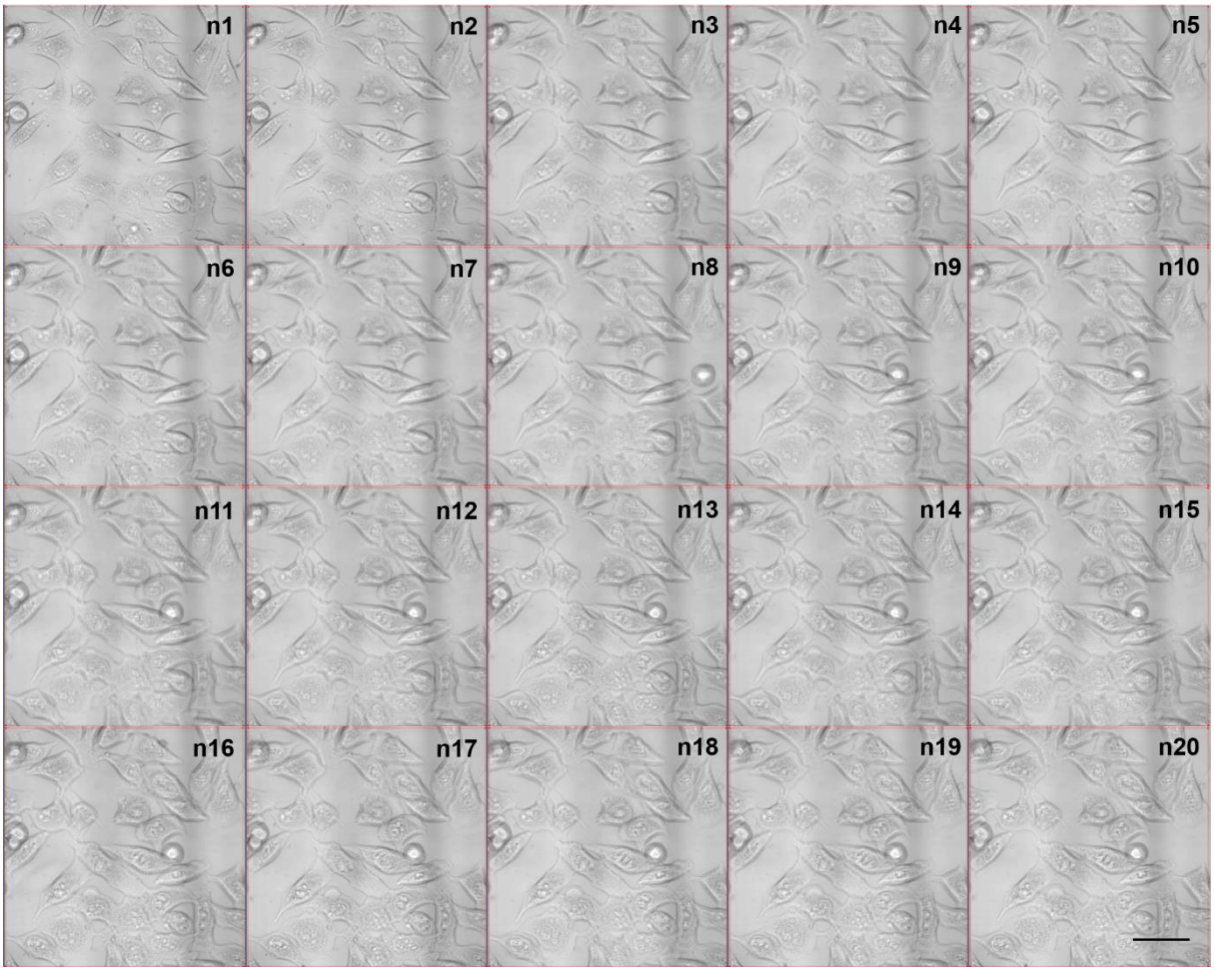

Figure 4.6 - Bright-field time series of non-pigmented melanoma cells during TPE-PDT. No significant changes in cell morphology were observed. The images are 210 x 210 µm, and the scale bar is 50 µm. Each image took 1.6 seconds, and one was taken immediately after the other.

Source: By the author.

The morphology of pigmented cells during the TPE, in the absence of photosensitizer, is shown in Figure 4.7. It is possible to observe a heterogeneous distribution of melanin inside the cells that agrees with natural melanin maturation process (104). Also, the 2-photon irradiation induced morphology changes in some

cells, mainly the most pigmented ones. It indicates that melanin may play a major role in the light absorption and the cell-damage induced.

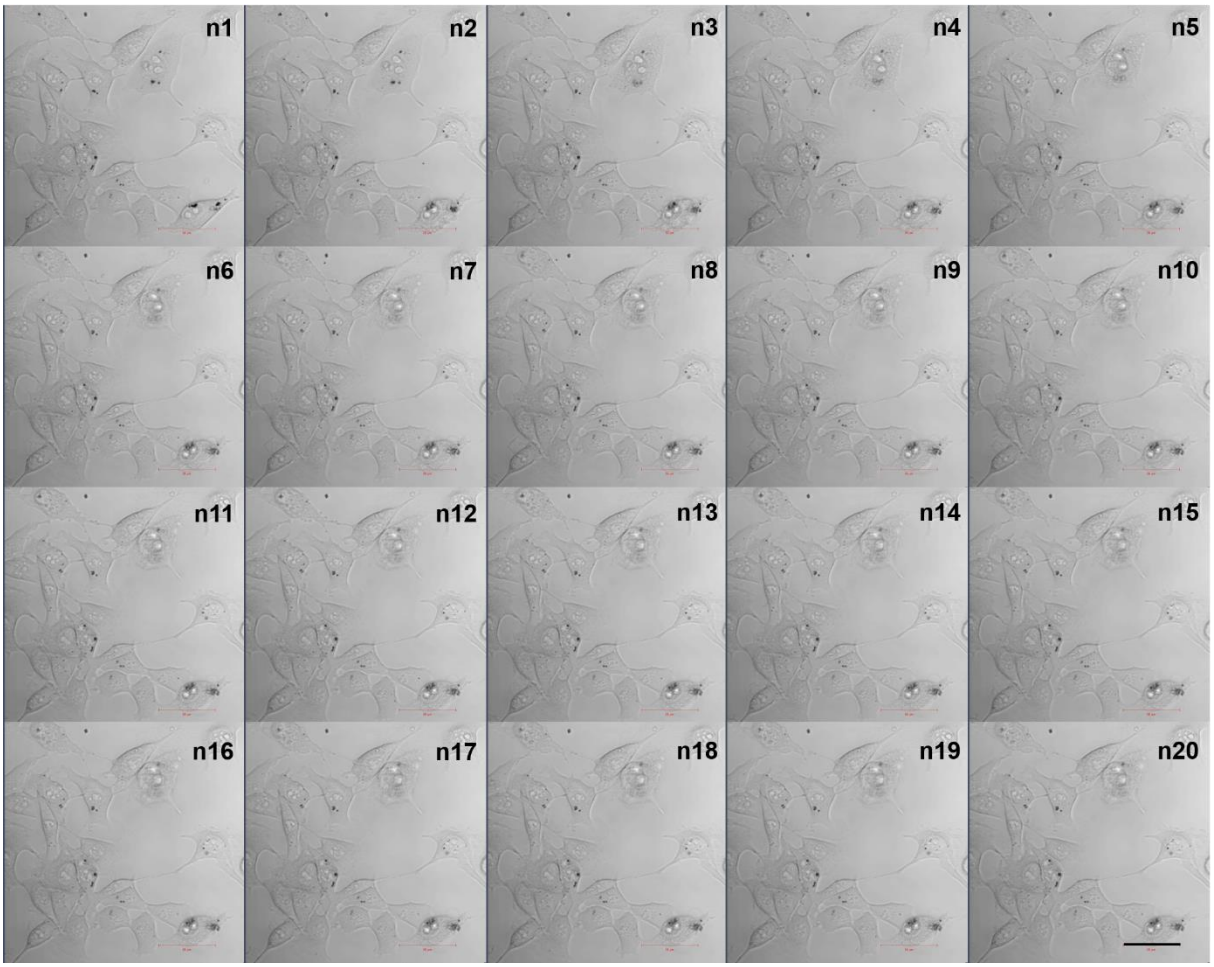

Figure 4.7 – Bright-field time-series of pigmented cells irradiated following the TPE protocol. No significant changes in cell morphology were observed. The images are 210 x 210 µm, and the scale bar is 50 µm. Each image took 1.6 seconds, and one was taken immediately after the other.

Source: By the author.

The TPE-PDT is shown in Figure 4.8. Immediately after the first scan (~4,2 x 10 J/cm^2), it is possible to observe cell shrinkage and membrane blebs in some cells and this effect progress significantly as a function of the fluence or scans. The blebs are probably related to the apoptosis induced by the TPE-PDT.

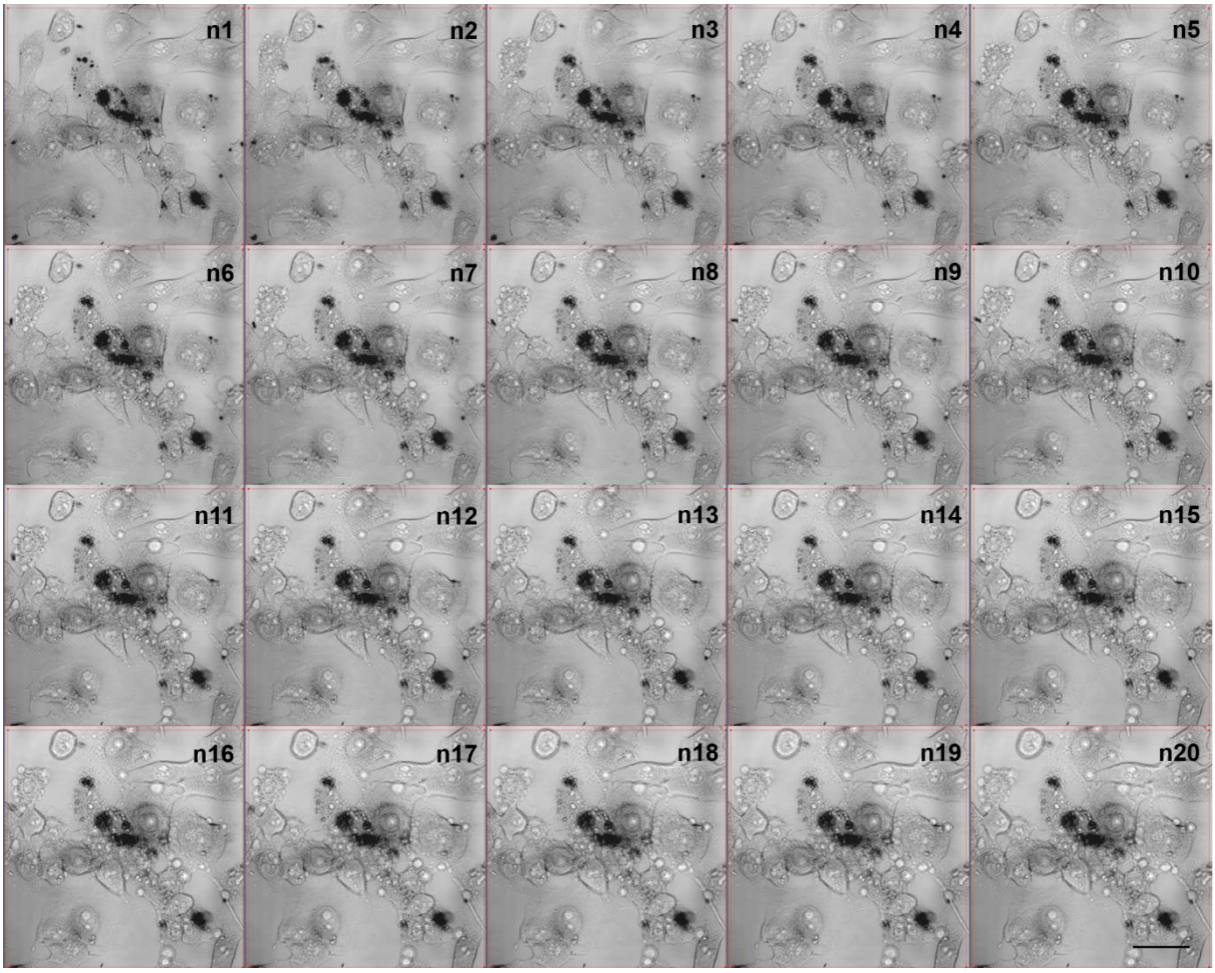

Figure 4.8 – Bright-field time series is showing the morphology changes in the pigmented cell during TPE-PDT evidenced by the cell shrinkage and blebs. The images are 210 x 210 µm, and the scale bar is 50 µm. Each image took 1.6 seconds, and one was taken immediately after the other.

Source: By the author.

The changes in the cell morphology, involving cell shrinkage and membrane blebs were also observed by Qiu and collaborators.(105) The fluorinated ruthenium (II)-mediated TPE-PDT assay was carried out in HeLa cells. They noted that the photosensitizer incubation time was related to the TPE-PDT and cell morphologic change.(105)

The cell death was then quantified manually, and the results are shown in Figure 4.9.

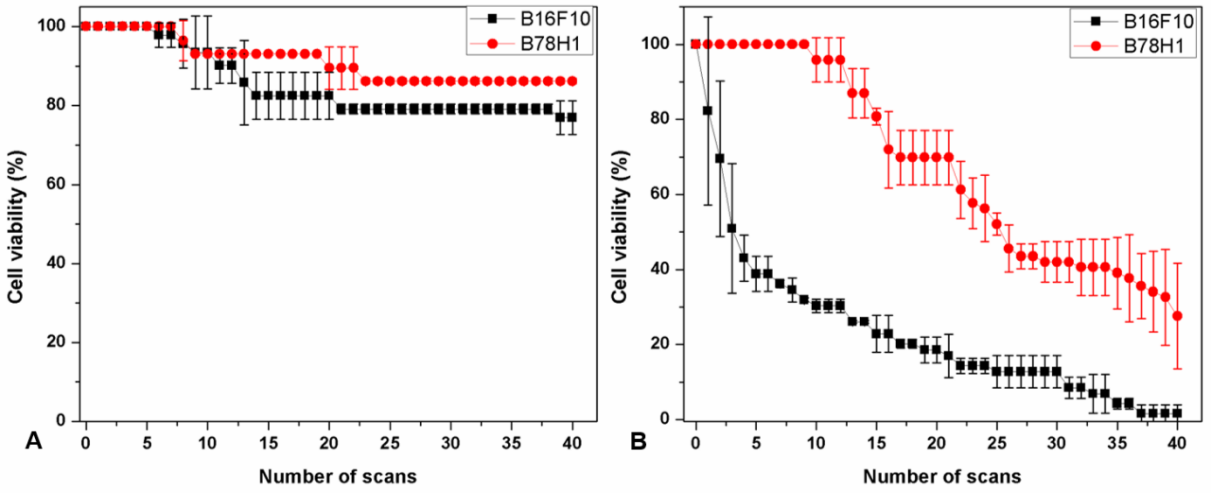

Figure 4.9 - Cell viability of pigmented (B16F10) and non-pigmented (B78H1) cells irradiated under the TPE protocol (A) and treated with VIS-mediated TPE-PDT (B).

Source: By the author.

The TPE, in the absence of photosensitizer decrease the cell viability in 15 and 20% at the end of 40 scans or 1.7 x 10^8 J/cm^2 for non-pigmented and pigmented cells, respectively. However, for the TPE-PDT, after ten scans (4.2 x 10^7 J/cm^2) the pigmented cells viability was reduced to 30% from its initial condition. At the same time, the non-pigmented cells viability was still around 95%. These results agree with the LIVE/DEAD assay that showed a decrease in the pigmented cell viability of 70 to 75% after 1.2 x 10^7 J/cm^2.

The B78H1 cells (non-pigmented) viability started to decrease after 10 scans (energy per scan 4.2 x 10^6 J/cm^2) or ~4.2 x 10^7 J/cm^2. After 40 scans, ~1.7 x 10^8 J/cm^2, the cell viability of the non-pigmented cells was reduced to 30% from the initial number of cells. That is, the non-pigmented cells needed four times more energy to reach 30% of cell viability when compared to the pigmented cells.

4.3.2.2 Determination of Visudyne photobleaching rate

To verify if the photosensitizer photobleaching rate was similar for non-pigmented and pigmented cells, fluorescence images were acquired during the TPE-PDT. A time series of the fluorescence images is shown in Figure 4.10.

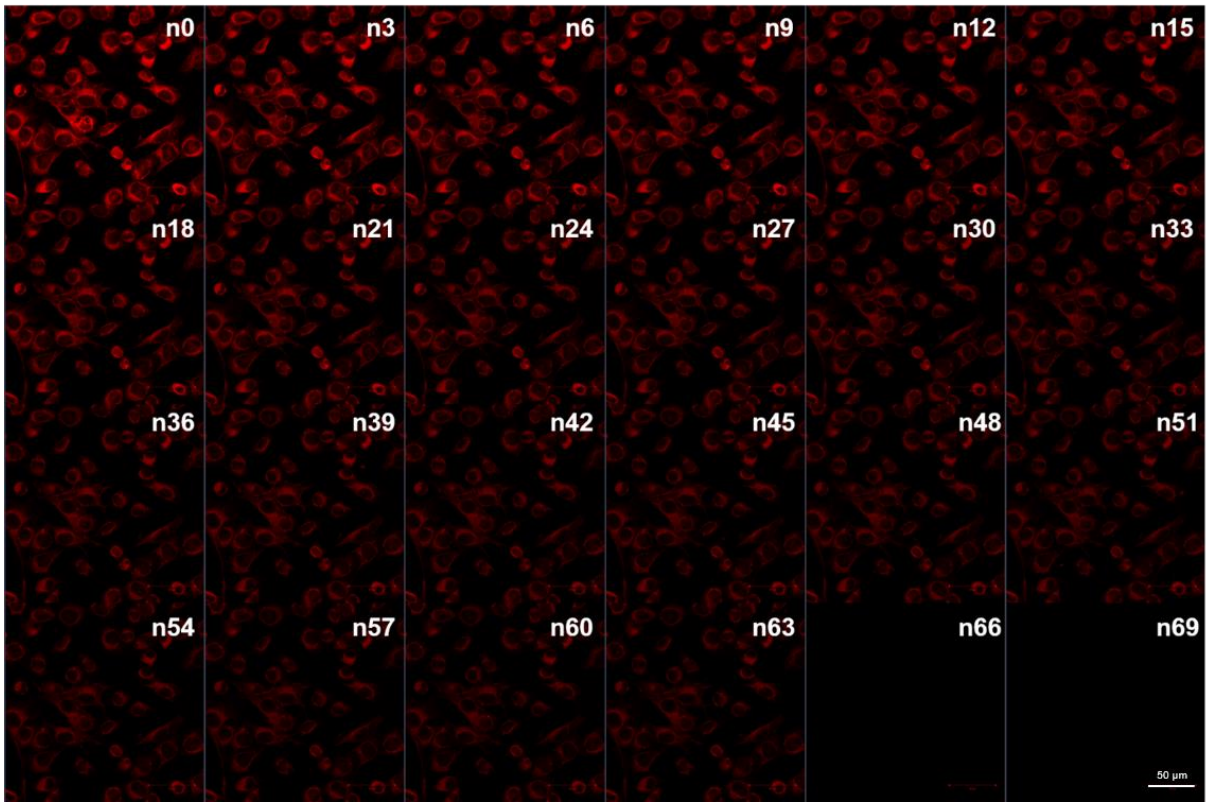

Figure 4.10 – Two-photon excited fluorescence time-series with excitation at 865 nm and collection from 650 to 700 nm, related to the VIS emission. The acquisition time was 1.6 sec per image. Scale bar: 50 µm.

Source: By the author.

The photobleaching rate was then calculated for every pixel of the fluorescence images, and a color-coded photobleaching lifetime imaging was generated for both, non-pigmented and pigmented cells as described by Lencione and collaborators(103) (Figures 4.11 and 4.12).

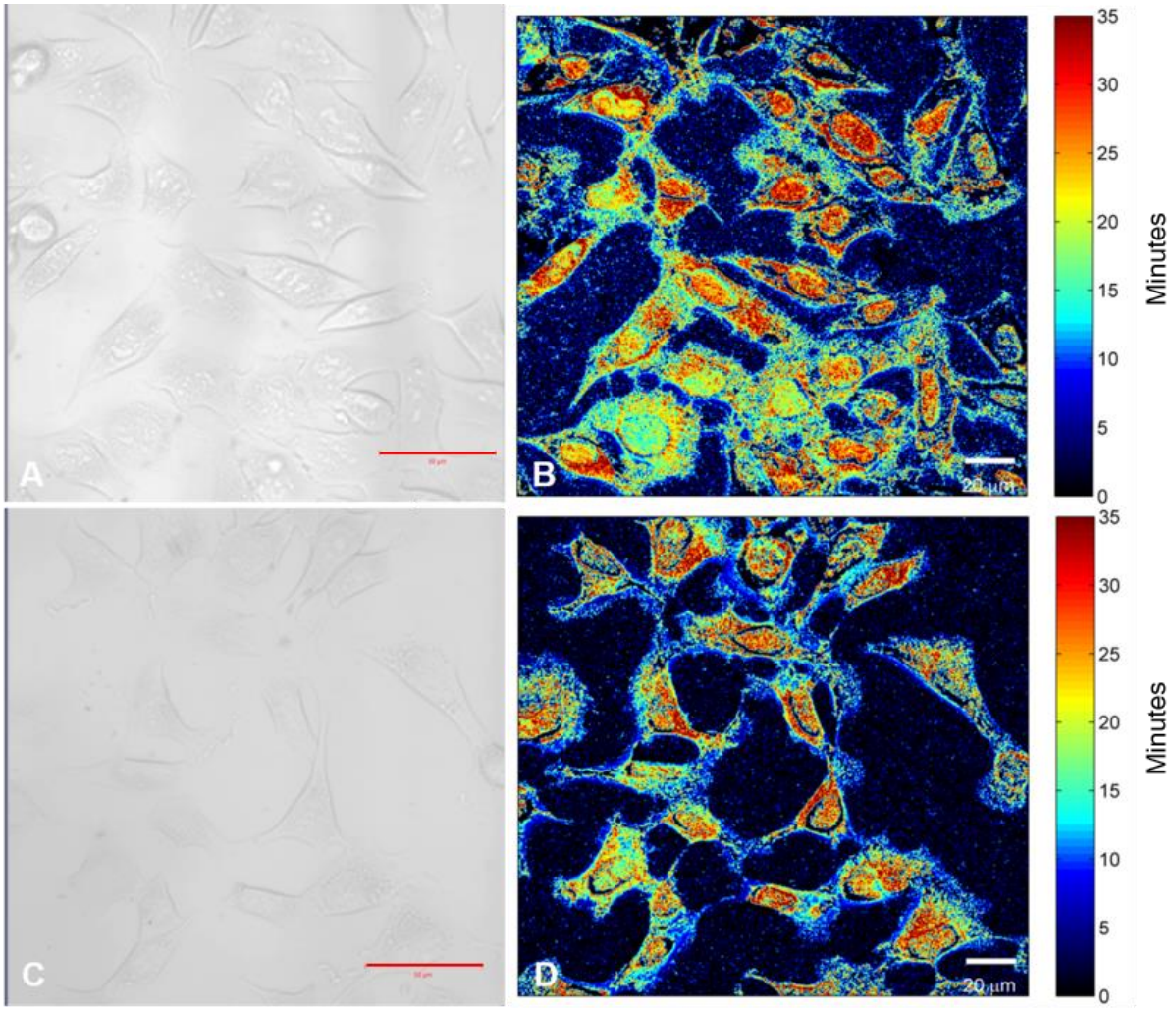

Figure 4.11 - Bright-field images (A&C) and its corresponding color-coded photobleaching lifetime imaging (B&D) of non-pigmented B78H1 cells. The average photobleaching lifetime computed was 25 ± 1 minutes. Scale bars: 50 µm (A&C) and 20 µm (B&D).

Source: By the author.

The color-coded photobleaching lifetime imaging of non-pigmented cells showed an increase in the lifetime for sites around the nuclei. The average lifetime computed was 25 ± 1 minutes. The color-coded images for the pigmented tumors are shown in Figure 4.12.

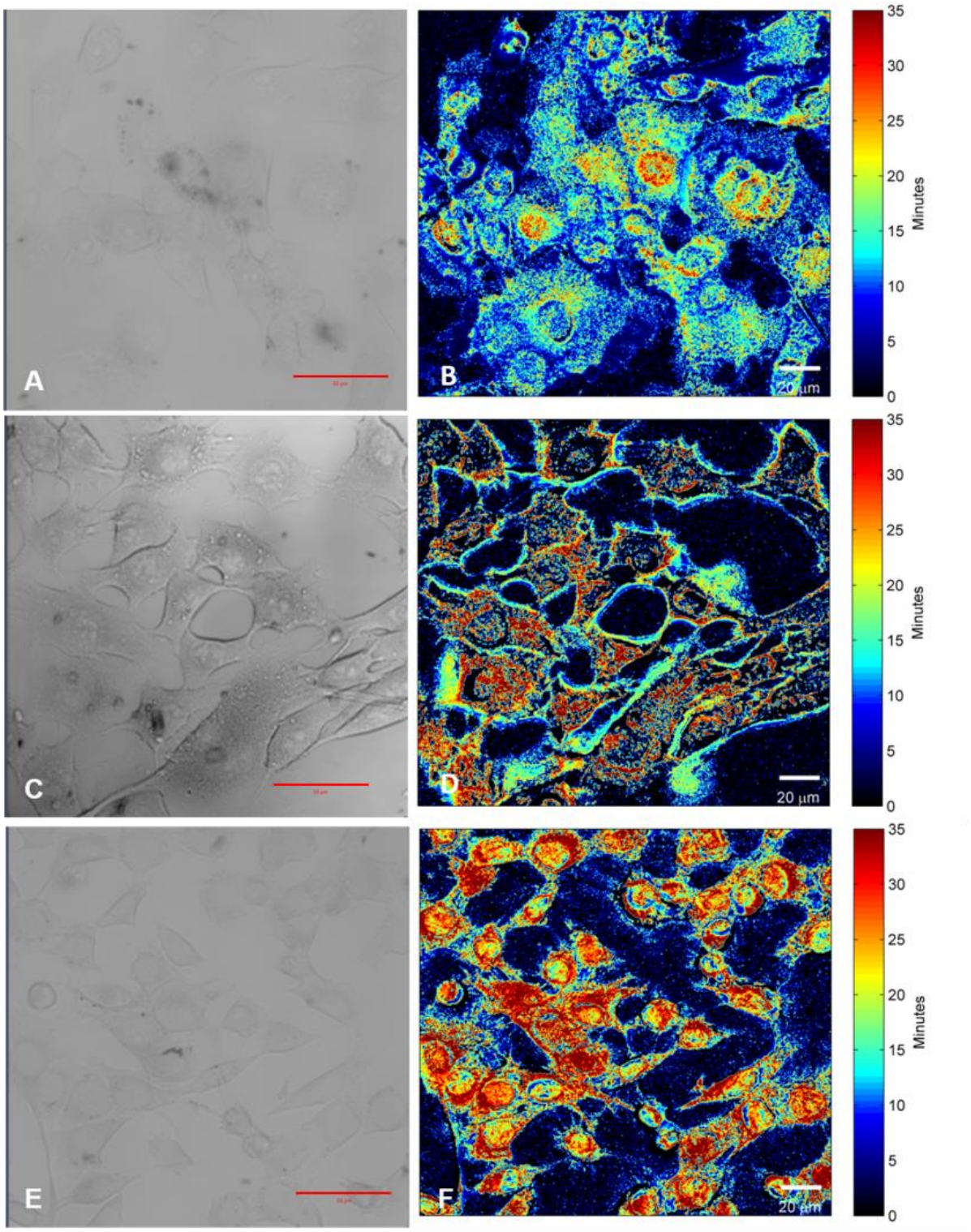

Figure 4.12 – Bright-field images (A, C, E) and its corresponding color-coded photobleaching lifetime imaging for pigmented cells. It can be seen a large variety of colors that means a significant variation on the bleaching lifetime (24 ± 8 minutes). Scale bars: 50 µm (A, C, E) and 20 µm (B, D, F).

Source: By the author.

The color-coded photobleaching lifetime images of the pigmented cells showed a considerable variation in the bleaching lifetime when compared to the non-pigmented cells. This fact might be related to the melanin TPA. Under TPE at 865 nm, melanin exhibits a weak green fluorescence, then in the case of melanin leakage in the cytoplasm, the melanin fluorescence could excite the photosensitizer, decreasing the bleaching lifetime. Besides that, melanin could also oxide the dye, and it also would induce a reduction in the bleaching rate. Both hypotheses could explain the variation on the bleaching lifetimes computed and moreover, the TPE-PDT response on pigmented cells observed in the LIVE/DEAD and real-time TPE-PDT assays. To determine the effect of TPE on the melanosome membrane, transmission electron microscopy was performed.

4.3.3 Transmission electron microscopy (TEM)

To investigate whether the melanin TPA could break the melanosomes' membrane, TEM was conducted in a control group and cells irradiated under the same conditions of the TPE-PDT but in the absence of photosensitizer.

The TEM image of the control group in different magnification is shown in Figure 4.13. Melanosomes are the most electron-dense structures (dark and round dots) distributed throughout the cell cytoplasm.

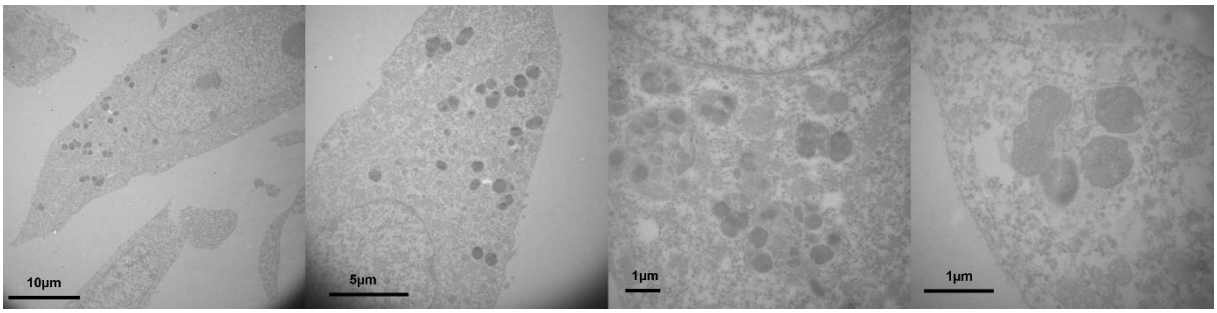

Figure 4.13 - Transmission electron microscopy images of the pigmented cells from the control group.

Source: By the author.

The TEM images of the cells irradiated under the TPE-PDT protocol in the absence of photosensitizer is showed in Figure 4.14. Changes in the

melanosome shape are observed in all the cells. Blebs can be seen around the melanosome indicating the organelle damage induced by the irradiation, mainly in the example showed in the first row of the Figure 4.14. Moreover, melanosomal membrane rupture can be seen, indicating the leakage of the melanin and its byproducts that could induce cell death, as reported in the literature.(104,106) The cell membrane and the other organelles show similar morphology as of the non-irradiated cells, indicating that no damage could be observed under the irradiated conditions and at the performed fixation time.

Wachter and collaborators(73) reported that the most of the energy absorbed by melanin is converted to heat by phonon-phonon coupling and that under specific irradiation conditions, the melanin could be converted to phototoxic products.(73) Baptista et al.(107) described the effect of UV (355 nm) and visible light (532 nm) radiation on epithelial cell lines with different melanin content. They reported that the cells with a lower amount of melanin were more susceptible to UVB irradiation when compared to highly pigmented cells, which is consistent with melanin photoprotection characteristic. On the other hand, for the visible irradiation, the most pigmented cells showed more phototoxicity than the cells with a low amount of melanin, indicating that the phototoxicity is related to the amount of melanin in the cell. Moreover, the visible irradiation induced the generation of singlet oxygen in the cells and it was increased in the highly pigmented cells, indicating that melanin plays an essential role in the singlet oxygen generation(107). The generation of free radicals including the singlet oxygen could also be related to the melanosome damage and more susceptibility of pigmented than non-pigmented cells to the TPE-PDT. These radicals can oxidize the melanosome membrane, inducing its rupture observed in the TEM images (Figure 4.14).

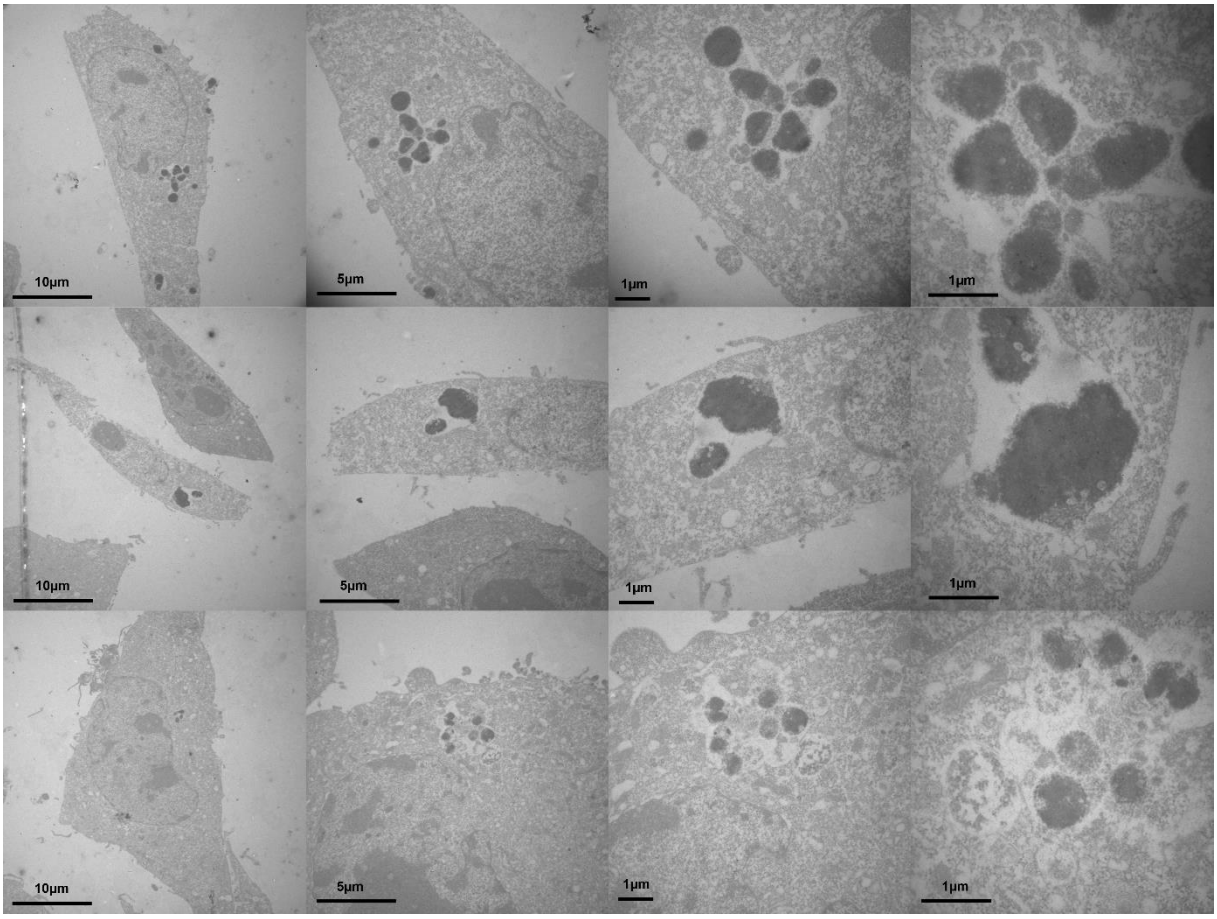

Figure 4.14 – Transmission electron microscopy images of pigmented melanoma cells irradiated with a femtosecond pulsed laser following the TPE-PDT protocol, but in the absence of photosensitizer. Different magnifications are shown per line to detail the effect of the irradiation on the melanosomes. One can see the melanosomes loss of shape, blebs and membrane rupture.

Source: By the author.

An investigation of the type of cell death of pigmented melanoma and non-melanoma cells revealed that pheophorbide-a mediated PDT induces cell death via different pathways. The non-pigmented cell died via autophagy and apoptosis processes, while the pigmented melanoma cell died only by apoptosis via a p38-mediated caspase-3 dependent apoptotic pathway.(108) A similar study was reported by Ji and collaborators.(109) They compared the type of cell death induced in a pigmented and non-pigmented melanoma cell lines using 5-ALA as a photosensitizer precursor. The non-pigmented and pigmented cells died by autophagy and apoptosis, respectively. Although it is not well detailed the reason that PDT induced cell killing by different pathways, some authors believe that it might be related to the presence of melanin or melanosomes.(109)

Kars and collaborators(110) evaluated the PDT effect on SKMel-30 cells using a femtosecond pulsed laser. Different from the studies described before, they found that the cells died by apoptosis and necrosis.(110) These results demonstrate that not only melanin or melanosomes but the type of photosensitizer and its localization inside the cell as well as the irradiation regiment might interfere in the cell death pathway.

Melanoma can vary from non-pigmented to highly pigmented tumors. The black and the reddish to yellow pigments are called eumelanin and pheomelanin, respectively. The amount of these pigments, as well as the tumor color, varies with the melanogenetic stage, cell genotype and with the environment.(104) Melanin is a pigment synthesized in the melanosomes through the tyrosinase hydroxylase activity that involves tyrosine (TYR) and tyrosinase-related proteins 1 and 2 (TYR1, TYR2) being converted to 3,4-dihydroxy-phenylalanine (DOPA) followed by the conversion into DOPAquinone by the DOPA oxidase activity.(106) During these processes two mainly toxic byproducts are produced: 5,6-dihydroxyindole and 5,6-dihydroxyindole-2-carbolic acid. Melanin biogenesis involves four stages: in the first two stages, no melanin is found in the organelle, and the stages three and four the synthesis of intermediates products starts to generate matrix favorable to melanin production.(104) For this reason, melanin is synthesized inside the melanosomes – a membrane protein-bound organelle that prevents the leakage of these toxic products to the cytoplasm.(106)

Davids & Kleeman suggested that melanosome-target PDT would be more efficient due to its synthesis and storage function. If the PS could penetrate the melanosome, the PDT damage in the membranes would cause a leakage of the cytotoxic intermediates produced during melanin synthesis into the cytoplasm, increasing the treatment response.(106) However, as these intermediates are generated during the late maturing stages 3 and 4, it would not be expected that the PDT effect would be increased in all the cells. Although, most melanomas present the late-stage melanosomes in its cytoplasm, which would still be attractive to PDT. Despite that, Davids & Kleeman (106) investigated the effect of hypericin-mediated PDT on non-pigmented and pigmented melanoma cells and concluded that even targeting the melanosomes, PDT was more efficient on killing the non-pigmented

cells than the pigmented one. They found that the melanin chemoresistance might be linked to PDT resistance too.(106)

On the other hand, in our study, the TPE-PDT was more efficient to pigmented than non-pigmented cells. A different photosensitizer was investigated but more relevant than that, a nonlinear irradiation regimen was used. Instead of choosing a melanosome-target photosensitizer, in our case, the light interacted with the melanosomes inducing the membrane breakage and phototoxic byproducts leakage to the cytoplasm. Melanin TPA and TPE-PDT had a synergic effect, increasing the pigmented cell killing when compared to the non-pigmented cell. Besides that, our hypothesis that with the membrane rupture, melanin was also released in the cytoplasm. Melanin can be excited at 865 nm and emit fluorescence at the green region. Then, this light emitted could be absorbed by the photosensitizer also favoring the TPE-PDT on pigmented cells. Although further investigations still need to be done to describe the whole process involving TPE-PDT on pigmented cells, we already have the TEM images showing the melanosomes rupture that indicates the leakage of the phototoxic byproducts in the cytoplasm.

4.4 CONCLUSIONS

This study is the first report of the use of TPE-PDT on both pigmented and non-pigmented melanoma cells. We demonstrated that melanin could absorb two-photon at 865 nm, causing the melanosomal membrane breakage and the release of melanin byproducts, causing toxicity to the cells. Then, during TPE-PDT we have an amplified effect on pigmented cells when compared to non-pigmented cells. This amplified effect may be related to the PDT effect by itself combined with the cytotoxic byproducts released into the cytoplasm. Besides initial results, they are promising on the development of safety protocols for the treatment of pigmented lesions that still has a poor response when treated with optical techniques.

CHAPTER 5 TWO-PHOTON EXCITATION PHOTODYNAMIC THERAPY FOR CONJUNCTIVAL MELANOMA TREATMENT

5.1 OBJECTIVE

This study aims to investigate the TPE-PDT for the treatment of a conjunctival pigmented murine melanoma model, using Visudyne as a photosensitizer. This study was conducted in collaboration with Dr. Yeni Yucel from the St. Michael´s Hospital/ Department of Ophthalmology and Visual Sciences, UofT.

5.2 MATERIALS AND METHODS

5.2.1 Conjunctival melanoma model

Three thousand B16F10 murine melanoma cells in 5uL of PBS were injected using a 30G Hamilton syringe into the left conjunctiva of 6-weeks nude athymic mice (n=3 per group - Figure 5.1). The animal was anesthetized using 5% of isoflurane and 2% for maintenance, and the cells injection was performed in a surgical suite to prevent contamination, using a surgical microscope to ensure the needle position in the conjunctiva. The tumor growth was followed by visual inspection under a microscope, and the treatment performed when the tumor reached between 350 and 600um in length. This animal protocol was approved by the UHN/Princess Margaret Cancer Centre Animal Committee (protocol 4001.4).

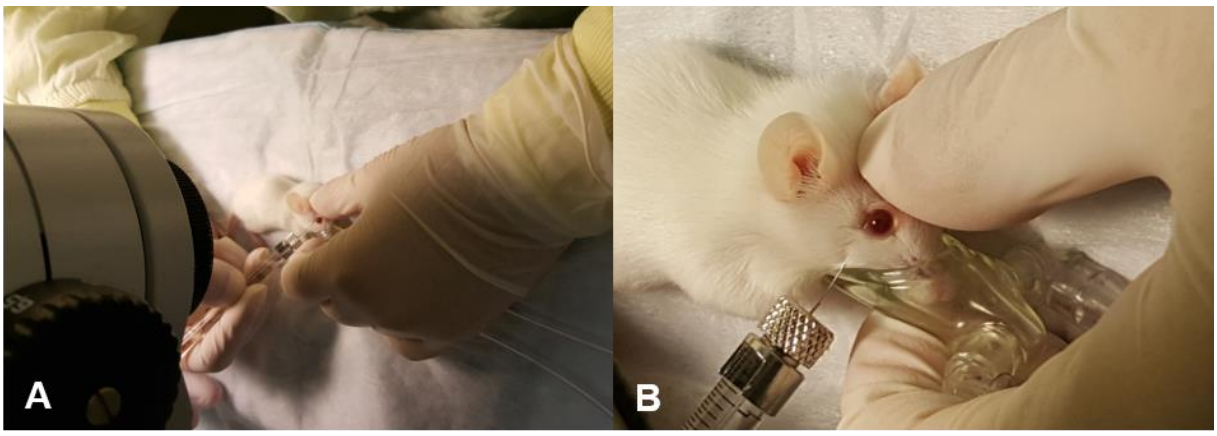

Figure 5.1 – Photographs of the melanoma cells injection into the mouse conjunctiva.

Source: By the author.

5.2.2 Two-photon excitation photodynamic therapy (TPE-PDT) protocol

The animal was anesthetized using 5% of isoflurane for induction and 2% for maintenance in a small mask that covered only the mouse nostrils (Figure 5.1B), allowing the eye exposition. Visudyne at a concentration of 44 mg/kg that contains 0.8 mg/kg of verteporfin was administered by intravenous injection into the tail vein 30 minutes before the irradiation. After the light-drug interval, the animal was positioned under the microscope on a home-made heating pad for the irradiation, following the same anesthetic protocol. It was used a femtosecond Titanium-Sapphire laser tunable from 700 to 1000 nm, emitting at 865 nm with 300 fs pulse duration at the sample and 90 MHz repetition rate. The average and peak power of 25 mW and 930 W, respectively. A 10x dry objective with a 0.45 numerical aperture and a 512 x 512-pixel area of 424 x 424 µm was used. A tumor scanning with a pixel dwell time of 6.30 µs, average laser irradiance of 2.2 x 10^6 W/cm^2, and peak irradiance of 7.7 x 10^{11} W/cm^2 was performed. Tumors were scanned up to 800 µm (267 scans) in depth with a 3 µm step between scans. Reflectance imaging at 635 nm was used to determine the tumor position as well as to plan the Z-scan irradiation avoiding photosensitizer bleaching before the PDT. The animals were sacrificed by cervical dislocation under general anesthesia at two-time points, 24 and 48 hours after treatment.

5.2.4 Histology

After the animals' sacrifice, the eyes were enucleated, embedded in paraffin and sectioned from anterior to posterior, every 50 um to ensure that the treatment site could be found in the histology. Then, the slides were stained with H&E and TUNEL (Terminal deoxynucleotidyl transferase-mediated dUTP Nick End Labelling) assay, an apoptosis biomarker.

5.3 RESULTS AND DISCUSSION

5.3.1 Two-photon excitation photodynamic therapy (TPE-PDT) protocol

A tumor photograph can be seen in Figure 5.2A. The conjunctival melanoma is the small dark dot on the superior edge of the eye, close to the eyelids. In Figure 5.2B, one can observe the animal position and lesion irradiation set up.

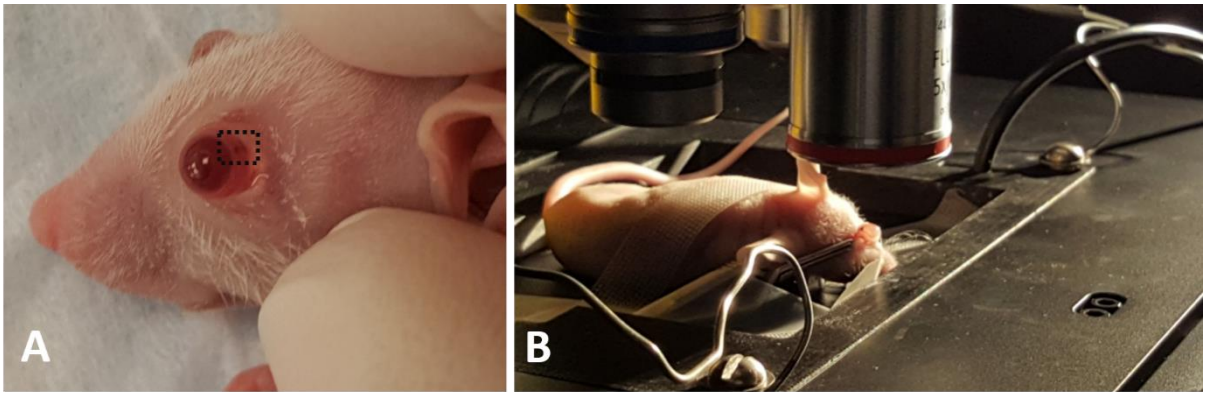

Figure 5.2 – Photographs of the conjunctival melanoma (B), highlighted by the dotted square and of the animal's positioning set up for the irradiation (B).

Source: By the author

Immediately after the photosensitizer administration, the animal positioning procedure started. Tear gel was applied to the eye to facilitate the melanoma exposure. Then, a tape was used to fix the eyelids as well as the animal's head to minimize bulk tissue motion due to, for example, breathing. Once the animal was positioned, bright-field (Figure 5.3A) and reflectance images (Figure 5.3B&C) were performed to determine the treatment volume site.

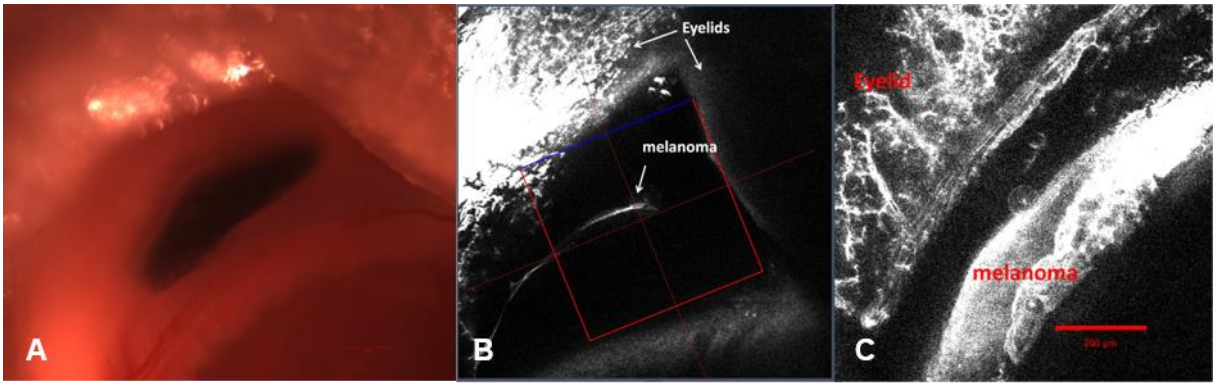

Figure 5.3 – Bright-field imaging of the conjunctival melanoma model (A) and reflectance images (B&D) used to determine the TPE-PDT site.

Source: By the author.

No side effects were observed in the mice eye or its behavior, probably due to the highly localized effect of the TPE-PDT that is a significant advantage of the TPE-PDT due to the relevance of the surrounding anatomic structures involved in this treatment.

5.3.2 Histology

In this study, two endpoints were investigated: 24 and 48 hours after the TPE-PDT. Figure 5.4 shows the bright-field image (Figure 5.4A) that was used to set up the irradiation site and the histology of the same animal stained with H&E (Figure 5.4B) and TUNEL – stained in yellowish (Figure 5.4C).

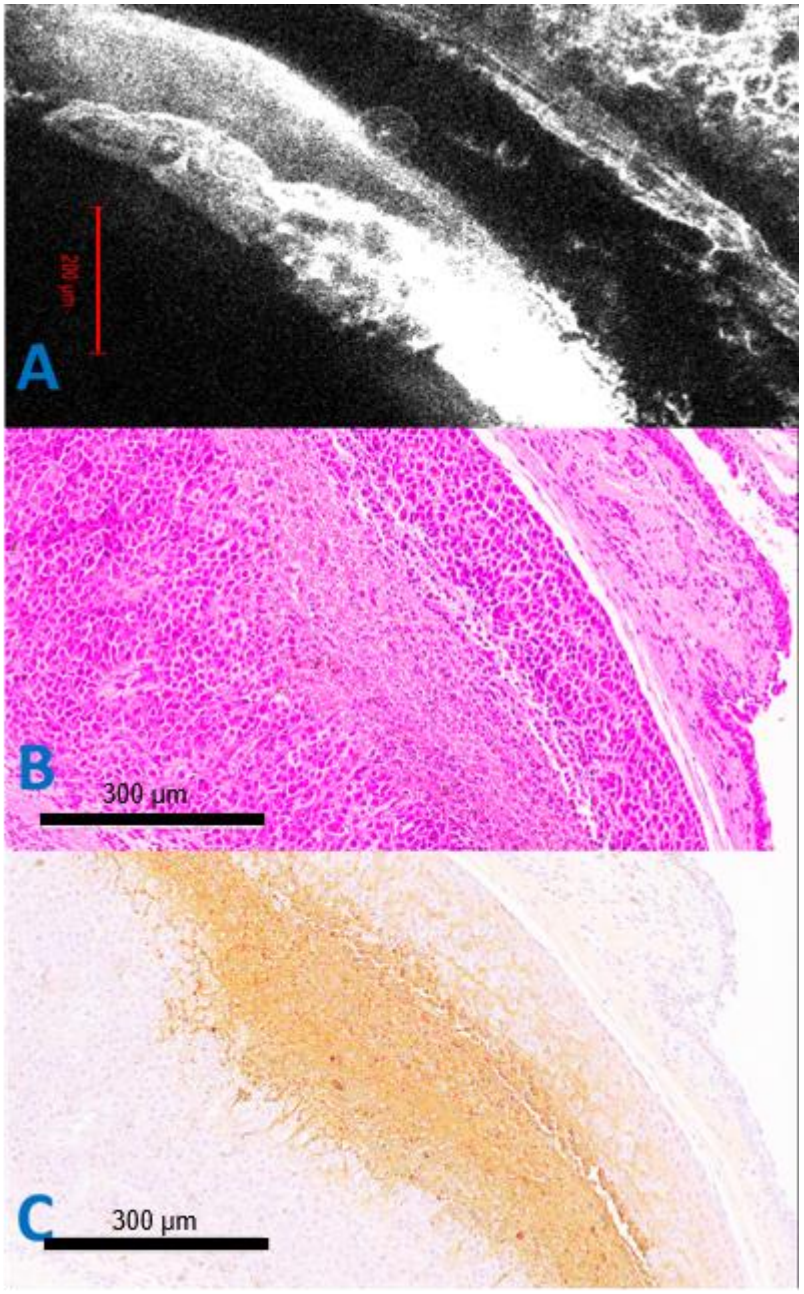

Figure 5.4 – (A) Reflectance image used to determine the treatment site and (B&C) histology of the eye 24 hours after the treatment, stained for H&E and apoptosis (TUNEL assay), respectively.

Source: By the author.

The TPA process occurs only in the focal volume when a high power pulsed laser can deliver a significant number of photons in a short time interval and microscopic volume. Due to these characteristics, the tissue damage in optical treatments involving TPE as in the TPE-PDT, is well localized, preventing injuries to the surrounding tissue as can be seen by the normal cell morphology, and absence

of tissue damage features in Figure 5.4. Besides the animal breathing that certainly affects the tumor positioning under the microscope and then the treatment volume, the tumor site set up for treatment seen in Figure 5.4A is similar to the area with apoptotic cells stained in yellowish observed in the histology (Fig. 5.4C).

Examples of the tissue slides after the treatment can be seen in Figures 5.5 and 5.6.

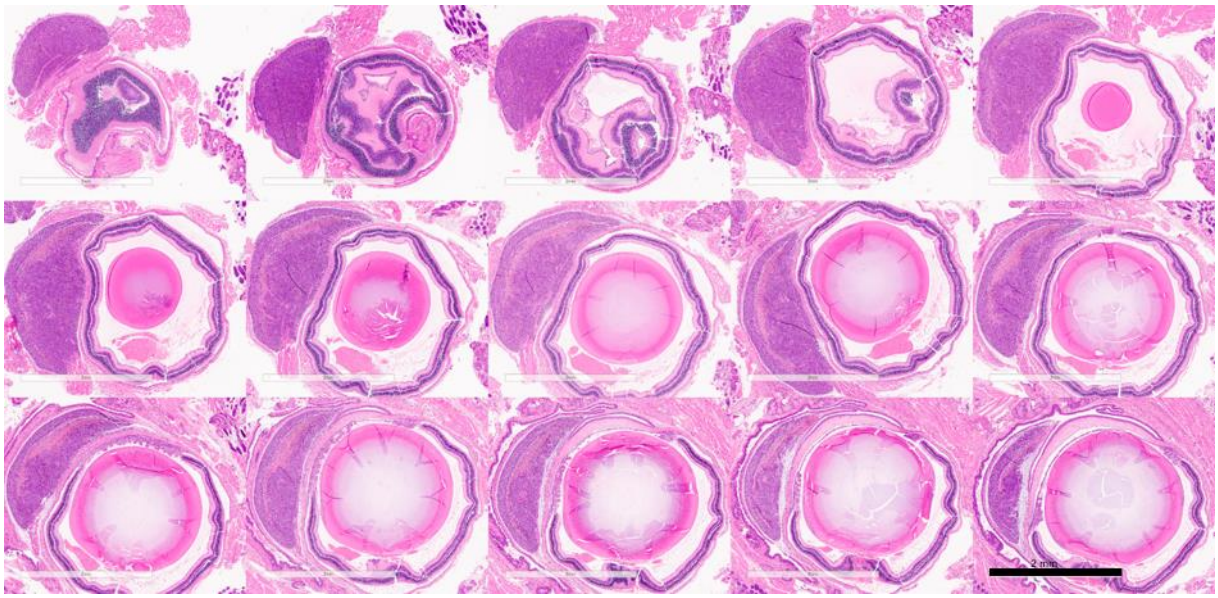

Figure 5.5 – Conjunctival melanoma slices stained with H&E. The step between each slice is around 50 µm, and the scale bar is 2 mm.

Source: By the author.

One can observe that the apoptotic site changes slightly between the histology cuts. It happens due to the tumor positioning during the irradiation that was performed angled about the anterior eye chamber, once the tumors were induced in the conjunctiva. This set up also do not provide quantitative data about the treatment thickness, but in robust estimative apoptotic cells were observed up to 700 µm in depth (Figure 5.6). The estimative of the treatment thickness was based on the histology cuts thickness plus the step size between consecutive cuts, that is, a 5 µm histology cut for each staining and 40 µm step size between consecutive cuts, the total step size of 50 µm was estimated. Further experiments in cutaneous melanoma using TPE-PDT will be performed to determine the maximum melanoma thickness that can be treated by this technique.

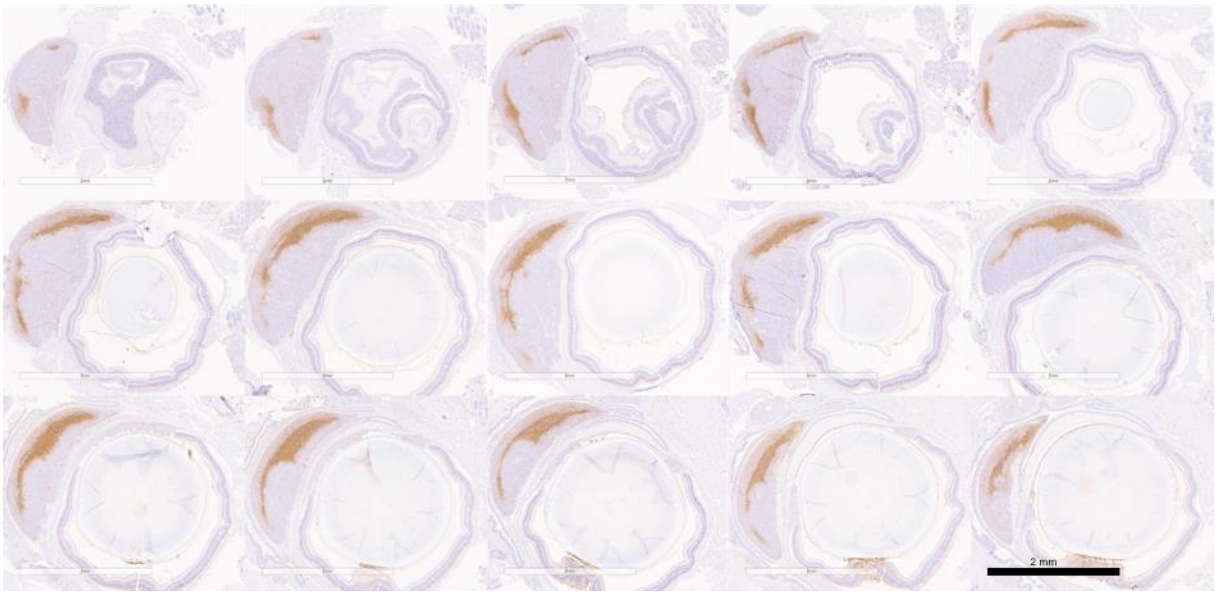

Figure 5.6 – Example of the TPE-PDT effect in different histology slices of a single eye staining for apoptosis in brownish (TUNEL assay). The distance between each slice is around 50µm, and the scale bar is 2 mm.

Source: By the author.

It was also investigated the TPE-PDT response for an entire tumor treatment. Unfortunately, as the tumors were too small, we could not find any technique that was able to measure this investigated tumor volume precisely. Then, the number of z-scans were personalized for each tumor (varying from 150 to 200 scans). The TPE-PDT results are shown in Figure 5.7. The tumor showed a fast growth, with melanin distributed throughout the entire tumor. Vascularization and necrotic sites are also observed.

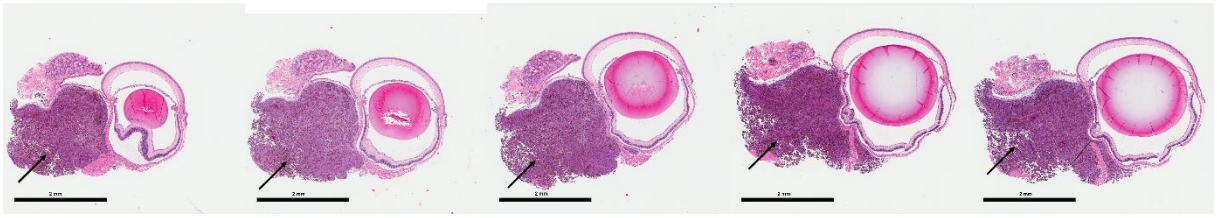

Figure 5.7 – Representative slides of murine conjunctival melanoma stained with H&E from the control group. Arrows indicate the tumor. Scale bar: 2 mm.

Source: By the author.

Moreover, it is not possible to compare the treatment groups regarding tumor volume, only qualitatively as presence or absence of melanoma. The light only and TPE-PDT groups results are shown in Figure 5.8.

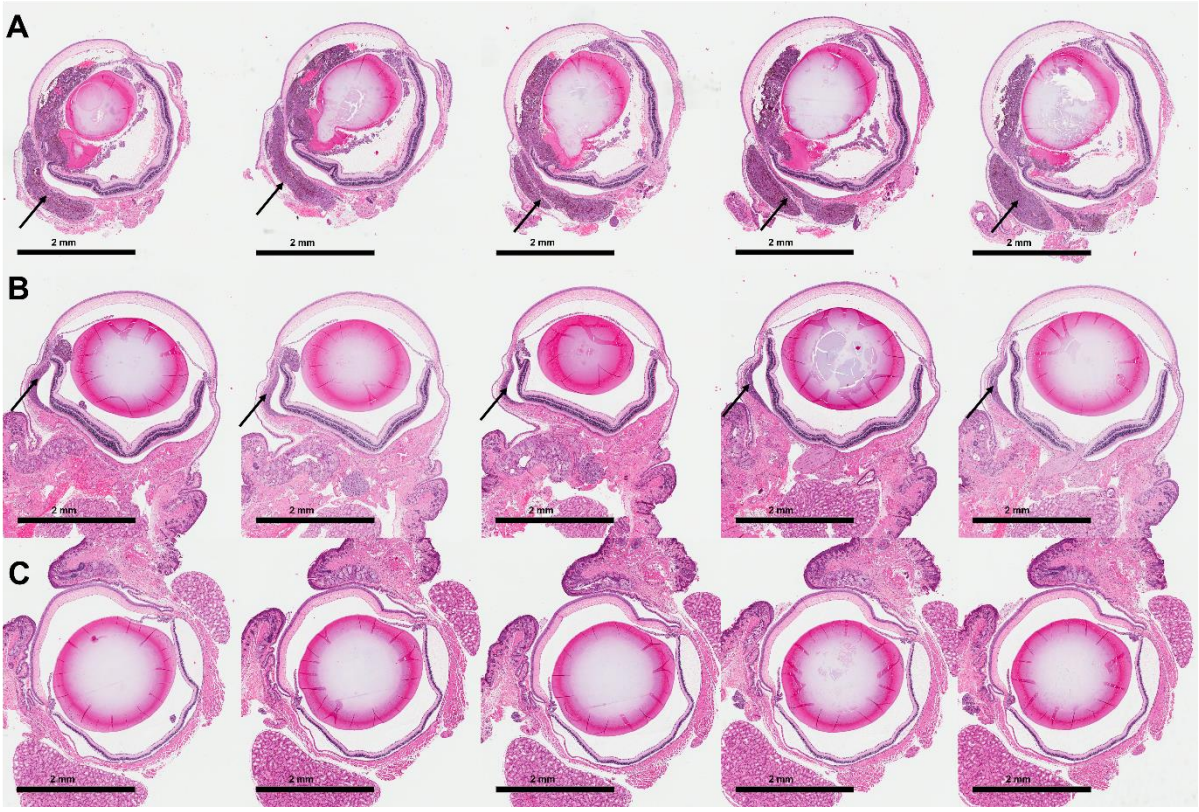

Figure 5.8 – Representative H&E slides of mouse eye with conjunctival melanoma treated only with light (A) and TPE-PDT with two concentrations of verteporfin: 0.5 mg/kg (B) and 0.8 mg/kg (C). Arrows indicate the conjunctival melanoma. Scale bar: 2 mm.

Source: By the author.

The light only group showed remaining tumor 48 hours after treatment. Besides that, no damage is observed in the H&E staining. The same result was observed for the group treated with TPE-PDT using verteporfin at 0.5 mg/kg. The best result was achieved for the TPE-PDT group treated with verteporfin at 0.8 mg/kg. No tumor was found in the histology, indicating that a complete response was achieved. Moreover, the surrounding tissue does not present any damage induced by the treatment, demonstrating the technique safety for this anatomical site.

Schmidt-Erfurth and collaborators(111) investigated a benzoporphyrin derivative monoacid (2 mg/kg) in non-pigmented Green hamster melanoma model. Tumors were treated when reached a height of 2 mm, measured by the

ultrasonography. After the photosensitizer administration, the irradiation was performed at 692 nm, 150 mW/cm^{2,} and 100 J/cm^2. The angiography and histology showed photothrombosis and complete tumor necrosis within 24 hours after the treatment. Superficial hemorrhage and minimal inflammatory reaction were observed, although these side effects were localized and reversible.(111) In a six weeks follow up, no tumor regrowth was seen. PDT studies were also carried out in a pigmented choroidal melanoma model in rabbits. A chloroaluminum sulfonated phthalocyanine (5 mg/kg) and a 675 nm laser were used for the treatment with a total fluence of 25 to 70 J/cm^2. The tumor was assessed by ophthalmoscopic and histology. Tumor arrest and regrowth, and severe side effects as subretinal hemorrhage, conjunctival chemosis, and serous retinal detachment were observed.(112) PDT for pigmented melanoma was also investigated in a rabbit model using the highly pigmented murine cell line B16F10. A liposomal benzoporphyrin derivative was used at a concentration of 2 mg/kg followed by irradiation at 690 nm and fluences from 40 to 150 J/cm^2. The tumors treated with 40 J/cm^2 showed tumor growth, but for higher fluences, tumor arrest was observed in all the cases.

Visudyne (liposomal benzoporphyrin derivative verteporfin) was approved for the treatment of age-related macular degeneration (AMD) by the Food and Drug Administration (FDA) agency in 2000. Moreover, in the last years, VIS-mediated PDT has been used in clinics for the treatment of many ocular vascular conditions such as choroidal neovascularization,(113) pathologic myopia,(114) and histoplasmosis syndrome.(115) Some studies involving ocular tumors as choroidal hemangioma,(116) retinoblastoma,(117) choroidal melanoma,(118) eyelid tumors, and conjunctival tumors has also been published.(119) Choroidal melanoma treatment using PDT has been successful in pre-clinical studies, although clinical studies remain to a small number of cases and with different results.(120)

Canal-Fontcuberta and collaborators(121) investigated the use of PDT for the treatment of pigmented choroidal melanomas in clinics. They found that combining PDT with bevacizumab could induce superficial vasculature closure but was not enough to induce tumor destruction.(121) A clinical study of small pigmented posterior pole choroidal melanoma was conducted in 15 patients. Three verteporfin-mediated PDT sessions were performed in each patient, achieving tumor control in 12 cases in a 15 months follow-up time. In three patients, PDT could not control or eradicate the tumor, so radiation therapy was performed with success. In all these

unsuccessful cases, the tumors were completely pigmented. Besides that, neither local or systemic side effect not metastatic disease was observed (122)

The TPE-PDT has the advantage to use longer wavelengths to excite the photosensitizers at its Soret band, it means, at its maximum absorption and still can penetrate the biological tissue due to the tissue optical transparency at these wavelengths. Hammer and collaborators(123) studied the laser induced breakdown (LIB) and minimal visible lesions (MVL) induced in monkey eyes by ultrashort pulse duration. The LIB was correlated to the MVL, including the plasma formation. They observed that the irradiance threshold has an inverse relationship with the pulse duration, then for hundreds of femtosecond pulses the irradiance threshold is around 10^{-12} W/cm^2, that is much lower than the irradiance used in our study (2.2×10^6 W/cm^2). This study also demonstrates that the femtosecond pulsed lasers are ideal for TPE.(123)

Wachter and collaborators(73) studied the effect of ultrafast lasers on an M3-melanoma model. They aimed to activate melanin and its precursors and convert them into phototoxic products, as the melanin precursors 5-S-cysteinyldopa (phaeomelanin) that photobind to DNA under irradiation at 300 nm. During the non-focused NIR irradiation, the tumor temperature increased between 15 and 25ºC and was kept for five minutes. Immediately after the irradiation, a blanching was observed. The best results were achieved with femtosecond pulses at 730 or 1047 nm and the poor response was seen at 800 nm. This was explained due to the low absorption of melanin precursors at the 400 nm range. Besides the tumor clearance observed 18 days after the treatment at 1047 nm, a secondary tumor growth was noted at the end of the evaluation period.(104) The use of melanin and its precursors to induce tumor damage under light activation showed promising results, although it is limited to the presence of these compounds inside the cell during the irradiation. These compounds are produced during the melanin maturation process and are not present in all stages of the synthesis. Then, the cells that still did not reach the maturation process, when these compounds are synthesized, would not be affected by the irradiation, and then, tumor regrowth would be observed. In our study, we proposed the use of TPE-PDT, using a focused 865 nm femtosecond pulsed laser with a high peak irradiance that may interact with melanin inducing the melanosomal membrane breakage and leakage of the the cytotoxic products producing during the melanin maturation process, as it was demonstrated in the *in*

vitro studies – Chapter 4. However, the treatment response would result from a synergic effect of TPE-PDT and the leakage of melanosomal cytotoxic products.

Although TPE-PDT has not been investigated in conjunctival melanoma model, it has been studied in some preclinical models for AMD. Samkoe and collaborators(124) reported the complete occlusion of blood vessels in the chick chorioallantoic membrane after VIS-mediated TPE-PDT. The average and peak irradiances were 3.3 x 10^6 W/cm^2 and 3.7 x 10^{11} W/cm^2, respectively. A total fluence of 1.1 x 10^8 J/cm^2 was used to induce complete occlusions of vessels with 15 µm in diameter.(124) The TPE-PDT for AMD has also been investigated in the vascular dorsal window chamber model. The authors evaluated the TPE-PDT effect on arteries of around 40 µm in diameter. The irradiation was performed at 920 nm, 39 mW in an area of 83x83 µm^2, and in a vertical stack mode that five images were taken, each 10 µm apart. Immediately after the treatment, the artery appeared thinner, and a segment was no longer visible. Moreover, no damage was observed in the surrounding vessels.(78)

As the probability of the TPE process depends on the molecule 2-photon cross-section and the quadratic of the laser intensity, the development of new sensitizers with large 2-photon cross-sections could improve the TPE-PDT response. Khurana and collaborators(125) investigated two photosensitizers, the commercial Visudyne with TPA cross-section of 50 GM and a synthetic porphyrin dimer developed for the TPE-PDT with a TPA cross-section of ~17,000 GM. To compare different PDT protocols, they established a parameter based on the product of drug concentration and fluence (drug-light product). They performed the treatment in a small area of 80 x 80 µm^2 on the selected blood vessel ~40 to 50 µm in diameter. A femtosecond pulsed laser emitting at 865 and 920 nm were used to excite Visudyne and the porphyrin-dimer, respectively and ~40 mW average power, 3.2 x 10^{10} W/cm^2 peak irradiance, 1.6 µs pixel dwell time, and fluence of 6.5 x 10^5 and 3.2 x10^5 J/cm^2 for Visudyne and porphyrin-dimer, respectively. They compared VIS-mediated PDT and -TPE-PDT and observed that the energy used for the TPE was more than three orders of magnitude when compared to the current PDT, mainly due to its low TPA absorption cross-section. Besides that, the porphyrin dimer has a 340-fold higher two-photon absorption cross-section when compared to Visudyne, although the drug-light product was only twenty times lower than the one obtained for Visudyne. This fact might be related to photosensitizer uptake or kinetics.(125)

Zou and collaborators(79) reported TPE-PDT on HepG2 (human liver cancer cell line) xenograft model using water-soluble Bis(arylidene)cycloalkanone photosensitizers with large TPA cross-section, ~885 GM. The tumors were irradiated at 800 nm and 6.3 W/cm^2 for 23 minutes, and their volume was monitored by measurements using calipers. They reported a hemorrhagic injury that inhibits the tumor size, improving the animals' survival significantly. Similar results were achieved in a study conducted by Qiu and collaborators.(105) The Fluorinated Ruthenium (II)-mediated TPE-PDT (PS cross-section 163 - 191 GM) was investigated in a HeLa tumor-bearing mice. It was used a femtosecond pulsed laser emitting at 800 nm, 1.18 W/cm^2 for 25 minutes. The tumors showed an apparent growth inhibition and no organ damage could be found.(105)

Starkey et al.(126) evaluated the depth efficacy of TPE-PDT in three murine xenograft models: human small cell lung cancer (NCI-H69), non-small cell lung cancer (A549), and breast cancer (MDA-MB-231). The synthetic tetrapyrrole-based photosensitizer (2-photon cross section ~ 1,500 to 2,000 GM) was intratumorally injected, and four hours later the irradiation at 800 nm in a 15 x 15 mm^4 area was performed. The average power at the sample, average irradiance, peak irradiance and the energy per pulse were 600 to 800 mW, 10 to 20 W/cm^2, 10 to 100 GW/cm^2, and 0.6 to 0.8 mJ, respectively. Most of the tumors showed initial regression followed by tumor regrowth, although effective PDT at 2 cm in depth was achieved.(126) A summary of the TPE-PDT parameters for different studies is presented in Table 5.1.

Table 5.1 – Summary of TPE-PDT parameters for different studies. *Refers to values calculated based on the data provided in the published studies.

Target and ref	PS	λ (nm)	σ_2 (GM)	Area (μm^2)	$P_{(average)}$ (mW)	$P_{(peak)}$ (W)	$I_{(average)}$ (W/cm^2)	$I_{(peak)}$ (W/cm^2)	Fluence (J/cm^2)
Vessels(124)	Visudyne	865	30				3.3×10^6	3.7×10^{11}	1.1×10^8
Arteries	Visudyne	920	30	83 x 83	39	1444*	9.3 x 10^5*		
Vessels(125)	Visudyne	865	30	80 x 80	40			3.2×10^{10}	6.5×10^5
Vessels(125)	Porphyrin-dimer	920	~17,000	80 x 80	40			3.2×10^{10}	3.2×10^5
Xenograft tumors(126)	Terapyrrole-based	800	~1,500 to 2,000	1500 x 1500	600 to 800		10 to 20	(10 to 100) x 10^9	12000 – 36000*
HeLa tumor model(105)	Fluorinated Ruthenium (II)	800	163 - 191				1.18		~1630*
Xenograft tumor(79)	Bis(arylidene) cycloalkanone	800	885				6.3		~8700*
Conjunctival Melanoma	Visudyne	865	30	424 x 424	25	930	2.2 x 10^6	7.7 x 10^{11}	5.6 x 10^8 - 7.5 x 10^8

Source: By the author.

The VIS-mediated TPE-PDT studies, in general, used an average and peak irradiance in the magnitude orders of 10^6 and 10^{11} W/cm^2. Due to the photosensitizer

small TPA cross-section, higher peak irradiances should be used to obtain the TPE process, once the probability of a molecule to absorb two photons relies on the molecule TPA cross-section and the laser peak irradiance as described by the equation 5.1.

$$P = \frac{\sigma_2 I^2}{2} \quad (5.1)$$

Starkey et al.(126) performed TPE-PDT using a synthetic dye with a TPA cross-section between 1500 to 2000 GM, that is 30 times higher than Visudyne cross-section, but to induce tumor damage, the peak irradiance was kept between 10^{10} to 10^{11}, similar to the one used in our study for conjunctival melanoma. Besides the photosensitizer TPA cross-section, the photosensitizer localization and uptake also influences on the TPE-PDT biological response as seen by Khurana and collaborators.(125) In our *in vitro* study, we noted that melanin TPA and the TPE-PDT had a synergic effect, improving the therapy response on pigmented cells. The same is probably happening in these pigmented tumors.

To our knowledge, this is the first study to report the use of TPE-PDT for conjunctival melanoma *in vivo* and to demonstrate that a single TPE-PDT session can treat the entire ocular pigmented melanoma.

5.4 CONCLUSIONS

The TPE-PDT showed promising results for the treatment of pigmented conjunctival melanoma. The localized effect of the TPE is an advantage for ocular treatments due to the critical anatomical sites involved. The TPE-PDT induced tumor apoptosis and prevent damages to the surrounding tissue, keeping the organ function. Besides that, small tumors are good candidates for the technique once as the irradiation is performed by laser scanning throughout the sample, the treatment of larger tumors would not be clinically feasible considering the long session time. Although, the scanning time can be optimized when using photosensitizers with larger 2-photon absorption cross-section. This is the first time that TPE-PDT was investigated in an *in vivo* conjunctival melanoma model and besides preliminary results, they demonstrated the technique effectiveness and may become an important approach for the treatment of ocular tumors.

CHAPTER 6 - GENERAL DISCUSSION AND FUTURE PERSPECTIVES

Melanoma is the deadliest type of skin cancer, and with significant rising in the number of cases. Conventional treatment techniques still do not present satisfactory success rate, diagnosis at early tumor stages is the most relevant factor for patient prognosis. In this scenario, development of high-resolution diagnostics and effective treatment protocols is crucial. In this study, we investigated the efficacy of the time-resolved fluorescence lifetime technique to distinguish cutaneous melanoma to normal skin in a murine model. This optical diagnostic technique was based on the excitation of free and protein-bound forms of NADH and FAD, cofactors present in aerobic and anaerobic metabolism, aiming to distinguish melanoma and normal skin due to its respiration pathway. Due to tumor fast development, its metabolism even when in the presence of oxygen is mainly anaerobic. This behavior is called glycolysis or Warburg effect. Although the number of ATP molecules produced by the glycolysis is smaller than the ATP production by the aerobic or oxidative phosphorylation pathway, the glycolysis process is much faster and then is preferable for tumor development. On the other hand, normal skin metabolism is based on the oxidative phosphorylation respiration pathway or Pasteur effect. NADH co-factor has two forms, free and protein-bound, that is related to a short and long fluorescence lifetime, respectively. Besides that, the protein-bound present in the mitochondria is linked to the oxidative phosphorylation or its free form found in the membrane and related to the glycolysis. Then, detecting these cofactors, we could differentiate tissues based on its respiration pathway. The time-resolved fluorescence lifetime for cutaneous melanoma detection, achieved 99.4% of sensitivity, 97.4% of specificity and 98.4% of accuracy. These results show the potential of the technique for real-time, non-invasive detection of cutaneous melanoma.

The studies involving cutaneous melanoma optical characterization showed heterogeneous tumor pigmentation, fast development of the lesion and morphological and optical heterogeneity, both intra- and intertumorally. These characteristics, especially the optical heterogeneity, qualify the use of this lesion as a model for photodynamic therapy due to the significant similarity presented with the clinical observations of human melanoma. The use of optical clearing agents – hyperosmotic agents that induce tissue dehydration and refractive index matching –

improved light distribution inside the tumor. The tumors became more optically homogeneous which is highly favorable for optical treatments. Besides that, glycerol 70% and PEG-400: 1,2 propanediol mix induced different changes in the total attenuation coefficient showing that OCAs could probably be used to modify tissue optical properties for each application. In our case, PEG-400 mix showed the best response improving the light penetration in depth. Moreover, the DRS measurements revealed that the PEG-400 mix could decrease its signal up to 95% and reach vascularized layers of skin. The OCT assay showed that the OCA application resulted in imaging of deeper tissue layer, an improvement about twice in deep. It was also possible to image the tumor microvasculature network which might be useful for the melanoma prognosis and staging.

Both PDZ kinetics experiments, laser-induced fluorescence spectroscopy, and chemical extraction, showed PDZ accumulation in the lesion mainly between 1 and 3 hours after its intravenous administration. No tumor selectivity was observed for the cutaneous melanoma. Despite this fact, PDZ is still considered a suitable photosensitizer due to its high efficiency of production of reactive oxygen species and, therefore, its high efficiency of photodynamic response.

The PDT assays were performed in both, pigmented and non-pigmented melanomas, using a vascular and a mainly cellular-target photosensitizer. As it was expected, non-pigmented tumors showed a better response for PDT, in general, when compared to the pigmented ones. Comparing the photosensitizers, the VIS-meditated PDT was more efficient in the treatment of non-pigmented tumors and in all investigated protocols, could induce necrosis in the entire tumor. Moreover, the histology staining for the S100 protein was negative, indicating a tumor eradication. The PDZ-mediated PDT could reduce tumor size, but the tumor was still expressing S100 at the end of the evaluation period. The combination of photosensitizers did not improve the treatment response; once the tumor elimination was already achieved by the VIS-mediated group. The addition of OCAs also did not affect the PDT response. As these tumors were non-pigmented from 600 to 800 μm in thickness, then the light penetration into the tumor is not a limitation of this technique. However, these results demonstrate that OCAs did not interfere negatively with the PDT.

For the pigmented tumors, the PDZ-PDT groups did not show any difference in the tumor growth or S100 expression for the control group. The VIS-mediated PDT

group showed tumor reduction in a first moment, but regrowth was observed at the end of the experiment. The combination of photosensitizers improved the PDT response, but the tumor was still expressing S100 at the end of ten days. These results indicate that, besides melanoma resistance to PDT, the light penetration into the tumor is still the most limiting factor. The addition of OCA improved the PDT response on all protocols investigated in this study, reducing tumor volume and inhibiting its growth. The tumor doubling time was of 1.03 and 1.12 days for the control and PDZ-PDT groups, respectively. With the addition of OCA, the doubling time of the OCA+PDZ-PDT group was reduced to -1.40. A reduction in the doubling time from 2.22 to -3.12 was also observed for the VIS-PDT and OCA+VIS-PDT groups, respectively. Comparing the groups OCA+PDZ-PDT and OCA+VIS-PDT with PDZ-PDT+VIS-PDT, it was observed that the addition of OCA was more efficient improving the treatment response than only the drug combination. The doubling time values for these groups were of -1.40, -3.12 and 10.15, respectively. This result highlight that the melanoma optical properties still are the main cause of melanoma resistance to PDT. The best result was achieved by the dual-agent PDT combined with the topical application of OCA. At the end of the evaluation period, no tumor was observed in the histology. Also, the immunohistochemistry staining was negative. These results suggest that a PDT protocol for melanoma should involve multiple-targets photosensitizer and changes in the tumor optical properties.

The TPE *in vitro* assay showed that melanin, a highly conjugated structure, has a broad absorption spectrum from UV to NIR. Although it presents a low absorption at 865 nm, melanin still has TPA at this wavelength. The increase in temperature of a melanin solution showed that the larger molecules are broken into smaller ones, and it shifts the absorption spectrum to smaller wavelengths. That is, in a mix of melanin molecules, the small ones can absorb two-photon, as was demonstrated by the quadratic dependence between melanin fluorescence intensity and laser power.

The TPE-PDT in cells showed a high efficiency in killing pigmented melanoma cells when compared to the non-pigmented ones, for both techniques: LIVE/DEAD and real-time morphology assays. The fluence necessary to kill 30% of the cells was three times higher for the non-pigmented cells than for the pigmented ones. To determine the reason for pigmented cells being more susceptible to the TPE-PDT,

the photobleaching rate was computed. One could observe that the pigmented cells showed a considerable variation in the photobleaching lifetime when compared to the non-pigmented cells that highlight the possible interference of melanin during the TPE-PDT. Therefore, TEM was performed in pigmented cells irradiated following the TPE-PDT protocol but in the absence of photosensitizer. It revealed that during the two-photon irradiation, the light interacts with melanin, inducing damage of the melanosomal membrane. Although it is not possible to confirm how this damage was induced, we hypothesize two main reasons: melanin absorbs the light and generates a local increase in the temperature leading to membrane rupture or after the light absorption, melanin produces radicals that oxidize the melanosomal membrane. Despite the mechanism, with the membrane rupture, the toxic melanin byproducts leakages to the cytoplasm, leading the cell to death. Then during the TPE-PDT, a synergic effect is observed.

The TPE-PDT in the conjunctival melanoma model induced apoptosis in the entire treatment site within 24 hours after the treatment. Besides that, no damage was observed in the surrounding tissue, preserving the function of the eye. When the TPE-PDT was performed in the entire tumor, the animals treated using the protocol with 0.8 mg/kg of verteporfin did not show viable melanoma cells at the end of 48 hours.

These results indicate that different strategies should be used to treat melanoma in different sites. The OCA application is a cheap, non-invasive and feasible strategy to be used in the clinics for the cutaneous melanoma lesions that are much bigger than conjunctival melanoma, for example. On the other hand, it is unsuitable for improving PDT response on conjunctival melanoma due to the eye sensibility to the OCA. However, TPE-PDT with its highly localized effect is crucial for conjunctival melanoma treatment.

The promising results achieved in this study highlighted the efficiency of OCA and TPE-PDT for cutaneous and conjunctival melanoma treatment. To improve our understanding and the response to the PDT protocols and to a potential translation of these technologies, further studies are needed. Some of the ideas for future studies are: (1) to investigate the OCA-PDT response in naturally occurring cutaneous melanoma, as in cats and dogs; (2) to investigate the use of OCA-PDT in pigmented

basal cell carcinoma; (3) to investigate whether or not the use of OCAs can improve diagnostic resolution of optical techniques; (4) to investigate *in vitro* and *in vivo* the mechanisms of TPE-PDT.

CHAPTER 7 – FINAL CONCLUSIONS

In the present study, we develop and investigate the efficacy of optical technologies for melanoma in animal models. The main conclusions are:

(1) Time-resolved fluorescence lifetime for cutaneous melanoma detection, achieved 99.4% of sensitivity, 97.4% of specificity and 98.4% of accuracy.

(2) PEG-400 mix as a topical optical clearing agent used with OCT resulted in imaging of deeper tissue layer, an improvement about twice in deep, providing information of the skin vascularization.

(3) OCA+PDT with a dual photosensitizer (PDZ and VIS) resulted in eradication of cutaneous melanoma with no viable melanoma cells after 10 days of treatment.

(4) TPE-PDT for conjunctival melanoma resulted in tumor eradication, no induced damage in the surrounding tissues and no viable melanoma cells after 48 hours of treatment.

REFERENCES

1 CHANG, A. E.; KARNELL, L. H.; MENCK, H. R. The National Cancer Data Base report on cutaneous and noncutaneous melanoma: a summary of 84,836 cases from the past decade. American College of Surgeons Commission on Cancer and the American Cancer Society. *Cancer*, v.83, n.8, p.1664–1678, 1998.

2 PINHEIRO, A. M; C. et al. Melanoma cutâneo: características clínicas, epidemiológicas e histopatológicas no Hospital Universitário de Brasília entre janeiro de 1994 e abril de 1999. *Anais Brasileiros de Dermatologia*, v. 78, n. 2, p. 179–186, 2003.

3 GARBE, C.; EIGENTLER, T. K. Diagnosis and treatment of cutaneous melanoma: state of the art 2006. *Melanoma Research*, v. 17, n. 2, p. 117–127, 2007.

4 LEITER, U. et al. Hazard rates for recurrent and secondary cutaneous melanoma: an analysis of 33,384 patients in the German Central Malignant Melanoma Registry. *Journal of the American Academy of Dermatology*, v. 66, n. 1, p. 37–45, 2012.

5 TARLAN, B.; KIRATLI H. Uveal melanoma: current trends in diagnosis and management. *Turkish Journal of Ophthalmology*, v. 46, n. 3, p. 123–137, 2016.

6 BLANCO, P. L. et al. Characterization of ocular and metastatic uveal melanoma in an animal model. *Investigative Ophthalmology and Visual Science*, v. 46, n. 12, p. 4376–82, 2005.

7 PAPASTEFANOU, V. P. et al. Uveal Melanoma, uveal melanoma. *Journal of Skin Cancer,* v. 2011, p. e573974, 2011. doi: 10.1155/2011/573974.

8 KOLLIAS, N.; ZONIOS, G.; STAMATAS, G. N. Fluorescence spectroscopy of skin. *Vibrational Spectroscopy*. v. 28, n. 1, p.17–23, 2002.

9 MARCHESINI, R. et al. Optical imaging and automated melanoma detection: questions and answers: *Melanoma Research*, v. 12, n. 3, p. 279–286, 2002.

10 SEIDENARI, S. Multiphoton laser tomography and fluorescence lifetime imaging of melanoma: morphologic features and quantitative data for sensitive and specific non-invasive diagnostics. *PLoS ONE*, v. 8, n. 7, p. e70682, 2013.

11 OCHSNER, M. Photophysical and photobiological processes in the photodynamic therapy of tumours. *Journal of Photochemistry and Photobiology B*, v. 39, n. 1, p.1–18, 1997.

12 SONGCA, S. P.; MBATHA, B. Solubilization of meso-tetraphenylporphyrin photosensitizers by substitution with fluorine and with 2,3-dihydroxy-1-propyloxy groups. *Journal of Pharmacy and Pharmacology*, v. 52, n. 11, p.1361–1367, 2000.

13 DOUGHERTY, T. J. et al. Photodynamic therapy. *Journal of the National Cancer Institute*, v. 90, n. 12, p.889–905, 1998.

14 DOLMANS, D. E. J. G. J.; FUKUMURA, D.; JAIN, R. K. Photodynamic therapy for cancer. *Nature Reviews Cancer*, v. 3, n. 5, p.380–387, 2003. doi: 10.1038/nrc1071.

15 RAMIREZ, D. P. et al. Experience and BCC subtypes as determinants of MAL-PDT response: preliminary results of a national Brazilian project. *Photodiagnosis and Photodynamic Therapy*, v. 11, n. 1, p. 22–26, 2014.

16 HUANG, Y-Y. et al. Melanoma resistance to photodynamic therapy: new insights. *Biological Chemistry*, v. 394, n. 2, p. 239–250, 2013.

17 MROZ, P. et al. Stable synthetic bacteriochlorins overcome the resistance of melanoma to photodynamic therapy. *FASEB Journal*, v. 24, n. 9, p. 3160–3170, 2010.

18 GENINA, E. A.; BASHKATOV, A. N.; TUCHIN, V. V. Tissue optical immersion clearing. *Expert Review of Medical Devices*, v. 7, n. 6, p. 825–842, 2010.

19 GENINA, E. A. et al. Optical clearing of skin under action of glycerol: Ex vivo and in vivo investigations. *Optics and Spectroscopy,* v. 109, n. 2, p.225–231, 2010.

20 LARIN, K. V. Optical clearing for OCT image enhancement and in-depth monitoring of molecular diffusion. *IEEE Journal of Selected Topics in Quantum Electronics*, v. 18, n. 3, p.1244–1259, 2012.

21 BALDEA, I.; FILIP, A. G. Photodynamic therapy in melanoma--an update. *Journal of Physiology and Pharmacology*, v. 63, n. 2, p.109–118, 2012.

22 IOANA, B. Melanocyte pygmentation–friend or foe on the route to melanoma. In: TANAKA, Y. (Ed.) *Breakthroughs in melanoma research*. InTech, 2011. doi: 10.5772/20157.

23 CLARK, W. H. et al. The histogenesis and biologic behavior of primary human malignant melanomas of the skin. *Cancer Research*, v. 29, n. 3, p. 705–27, 1969.

24 BRESLOW, A. Thickness, cross-sectional areas and depth of invasion in the prognosis of cutaneous melanoma. *Annals of Surgery*, v. 172, n. 5, p. 902–908, 1970.

25 ROBINSON et al. Regional lymphatic drainage in primary malignant melanoma of the trunk determined by colloidal gold scanning. *Surgical Forum*, v. 28, p. 147–148, 1977.

26 JOVANOVIC, P. et al. Ocular melanoma: an overview of the current status. *International Journal of Clinical and Experimental Pathology*, v. 6, n. 7, p. 1230–1244, 2013.

27 FINGER, P. T. Whole body PET/CT for initial staging of choroidal melanoma. *British Journal of Ophthalmology*, v. 89, n. 10, p. 1270–1274, 2005.

28 KARIMKHANI, C. et al. The global burden of melanoma: results from the Global Burden of Disease Study 2015. *British Journal of Dermatology*, v. 177, n. 1, p. 134–40, 2017.

29 MOGENSEN M, et al. Assessment of optical coherence tomography imaging in the diagnosis of non-melanoma skin cancer and benign lesions versus normal skin:

observer-blinded evaluation by dermatologists and pathologists. *Dermatologic Surgery*, v. 35, n. 6, p. 965–72, 2009.

30 BORISOVA E. Fluorescence detection improves malignant melanoma diagnosis. *SPIE Newsroom*, 2006. doi: 10.1117/2.120061.0470.

31 ZHU, C. et al. Diagnosis of breast cancer using fluorescence and diffuse reflectance spectroscopy: a Monte-Carlo-model-based approach. *Journal of Biomedical Optics,* v. 13, n. 3, p.034015, 2008.

32 SCHWARZ, R. A.; RICHARDS-KORTUM, R. R.; GILLENWATER, A. M. Fluorescence and reflectance spectroscopy for detection of oral dysplasia and cancer. In: WONG, B. J-F.; ILGNER, J. (Ed). *Biomedical optics in otorhinolaryngology*. New York: Springer, 2016. p. 431-449. doi: 10.1007/978-1-4939-1758-7_26

33 KONG, K. et al. Raman spectroscopy for medical diagnostics — from in-vitro biofluid assays to in-vivo cancer detection. *Advanced Drug Delivery Reviews*, v. 89, p.121–34, 2015.

34 GNIADECKA, M. et al. Melanoma diagnosis by raman spectroscopy and neural networks: structure alterations in proteins and lipids in intact cancer tissue. *Journal of Investigative Dermatology*, v. 122, n. 2, p. 443–449, 2004.

35 FARNETANI, F. et al. Skin cancer diagnosis with reflectance confocal microscopy: reproducibility of feature recognition and accuracy of diagnosis. *JAMA Dermatology,* v. 151, n. 10, p.1075, 2015.

36 RSTOM, S. A.; LIBÓRIO, L. S.; PASCHOAL, F. M. Reflectance confocal microscopy of cutaneous melanoma. correlation with dermoscopy and histopathology. *Anais Brasileiros de Dermatologia*, v. 90, n. 3, p. 411–414, 2015.

37 RICHARDS-KORTUM, R.; SEVICK-MURACA, E. Quantitative optical spectroscopy for tissue diagnosis. *Annual Review of Physical Chemistry*, v. 47, n. 1, p.555–606, 1996.

38 BORISOVA, E. G.; AVRAMOV, L. A. Laser system for optical biopsy and in-vivo study of the human skin. *Proceedings of the SPIE*, v. 4397, p. 405-409, 2001. doi: 10.1117/12.425175.

39 NA, R.; STENDER, I. M.; WULF, H. C. Can autofluorescence demarcate basal cell carcinoma from normal skin? a comparison with protoporphyrin IX fluorescence. *Acta Dermato-Venereologica*, v. 81, n. 4, p. 246–249, 2001.

40 BACHMANN, L. et al. Fluorescence spectroscopy of biological tissues—a review. *Applied Spectroscopy Reviews*, v. 41, n. 6, p.575–90, 2006.

41 PANJEHPOUR, M. et al. Laser-induced fluorescence spectroscopy for in vivo diagnosis of non-melanoma skin cancers. *Lasers in Surgery and Medicine*.v. 31, n. 5, p.367–373, 2012.

42 DE LEEUW, J. et al. Fluorescence detection and diagnosis of non-melanoma skin cancer at an early stage. *Lasers in Surgery and Medicine*, v. 41, n. 2, p. 96–103, 2009.

43 BEREZIN, M. Y.; ACHILEFU, S. Fluorescence lifetime measurements and biological imaging. *Chemical Reviews,* v. 110, n. 5, p. 2641–84, 2010.

44 MARCU, L. Fluorescence lifetime techniques in medical applications. *Annals of Biomedical Engineering*. v. 40, n. 2, p. 304–31, 2012.

45 WARBURG, O. On the origin of cancer cells. *Science*, v. 123, n. 3191, p. 309–314, 1956.

46 TADROUS, P. J. et al. Fluorescence lifetime imaging of unstained tissues: early results in human breast cancer. J*ournal of Pathology*, v. 199, n. 3, p. 309–317, 2003.

47 COLASANTI, A. et al. MS-2 fibrosarcoma characterization by laser induced autofluorescence. *Lasers in Surgery and Medicine*, v. 26, n. 5, p. 441–448, 2000.

48 PRADHAN, A. et al. Steady state and time-resolved fluorescence properties of metastatic and non-metastatic malignant cells from different species. *Journal of Photochemistry and Photobiology,* v. 31, n. 3, p. 101–112, 1995.

49 GALLETLY, N. P. et al. Fluorescence lifetime imaging distinguishes basal cell carcinoma from surrounding uninvolved skin. *British Journal of Dermatology*, v. 159, n. 1, p. 152–161, 2008.

50 DIMITROW, E. et al. Spectral fluorescence lifetime detection and selective melanin imaging by multiphoton laser tomography for melanoma diagnosis. *Experimental Dermatology*, v. 18, n. 6, p. 509–515, 2009.

51 NELSON, J. S.; MCCULLOUGH, J. L.; BERNS, M. W. Photodynamic therapy of human malignant melanoma xenografts in athymic nude mice. *Journal of National Cancer Institute*, v. 80, n. 1, p.56–60, 1988.

52 SCHUITMAKER, J. J. Bacteriochlorin a, a new photosensitizer in photodynamic therapy. in vivo results. *Investigative Ophthalmology and Visual Science,* v. 31, n. 8, p.1444–1450, 1990.

53 BIOLO, R et al. Effect of photosensitizer delivery system and irradiation parameters on the efficiency of photodynamic therapy of b16 pigmented melanoma in mice. *Photochemistry and Photobiology*, v. 63, n. 2, p.224–228, 1996.

54 BUSETTI, A. et al. Treatment of malignant melanoma by high-peak-power 1064 nm irradiation followed by photodynamic therapy. *Photochemistry and Photobiology,* v. 68, n. 3, p. 377–381, 1998.

55 BUSETTI, A. et al. High efficiency of benzoporphyrin derivative in the photodynamic therapy of pigmented malignant melanoma. *British Journal of Cancer,* v. 79, n. 5–6, p.821–824, 1999.

56 MA, L-W. et al. A new method for photodynamic therapy of melanotic melanoma -- effects of depigmentation with violet light photodynamic therapy. *Journal of Environmental Pathology, Toxicology and Oncology*, v. 26, n. 3, p.165–172, 2007.

57 SHARMA, K. V.; BOWERS, N.; DAVIDS, L. M. Photodynamic therapy-induced killing is enhanced in depigmented metastatic melanoma cells. *Cell Biology International*, v. 35, n. 9, p. 939–944, 2011.

58 MCEWAN, C. et al. Comparing the efficacy of photodynamic and sonodynamic therapy in non-melanoma and melanoma skin cancer. *Bioorganic & Medicinal Chemistry*, v. 24, n. 13, p.3023–3028, 2016.

59 KIM, Y. R. et al. Bioluminescence-activated deep-tissue photodynamic therapy of cancer. *Theranostics*. v. 5, n. 8, p. 805–817, 2015.

60 TUCHIN, V. V. Light propagation in tissues with controlled optical properties. *Journal of Biomedical Optics*, v. 2, n. 4, p. 401, 1997.

61 WEN, X. et al. In vivo skin optical clearing by glycerol solutions: mechanism. *Journal of Biophotonics*, v. 3, n. 1–2, p. 44–52, 2010.

62 SHAN, H. et al. Study on application of optical clearing technique in skin diseases. *Journal of Biomedical Optics*, v. 17, n. 11, p. 115003, 2012.

63 WEN, X. Enhanced optical clearing of skin in vivo and optical coherence tomography in-depth imaging. *Journal Biomedical Optics*, v. 17, n. 6, p.066022, 2012.

64 LIU, C. Enhancement of skin optical clearing efficacy using photo-irradiation. *Lasers in Surgery and Medicine*, v. 42, n. 2, p. 132–140, 2010.

65 STUMPP, O. F.; WELCH, A. J.; MILNER, T. E.; NEEV, J. Enhancement of transepidermal skin clearing agent delivery using a 980 nm diode laser. *Lasers in Surgery and Medicine*, v. 37, n. 4, p. 278–285, 2005.

66 XU, X.; ZHU, Q.; SUN, C. Assessment of the effects of ultrasound-mediated alcohols on skin optical clearing. *Journal of Biomedical Optics*, v. 14, n. 3, p. 034042, 2009.

67 PINKUS, H. Examination of the epidermis by the strip method of removing horny layers. I. observations on thickness of the horny layer, and on mitotic activity after stripping. *Journal of Investigative Dermatology*, v. 16, n. 6, p. 383–386, 1951.

68 GÖPPERT-MAYER, M. Über elementarakte mit zwei quantensprüngen. *Annalen der Physik,* v. 401, n. 3, p. 273–294, 1931.

69 MARCHESINI, R. A study on the possible involvement of nonlinear mechanism of light absorption by HpD with Nd: YAG laser. *Lasers in Surgery and Medicine*, v. 6, n. 3, p. 323–327, 1986.

70 YAMASHITA, Y. et al. Photodynamic therapy using pheophorbide-a and Q-switched Nd:YAG laser on implanted human hepatocellular carcinoma. *Gastroenterologia Japonica,* v. 26, n. 5, p. 623–627, 1991.

71 BHAWALKAR, J. D. Two-photon photodynamic therapy. *Journal Clinical Laser Medicine Surgery*, v. 15, n. 5, p.201–204, 1997.

72 FISHER, W. G, Simultaneous two-photon activation of type-I photodynamic therapy agents. *Photochemistry and Photobiology*, v. 66, n. 2, p.141–155, 1997.

73 WACHTER, E. A.; PETERSEN, M. G.; DEES C. Photodynamic therapy with ultrafast lasers. *Proceedings of SPIE,* v. 3616, p. 66-74, 1999. doi:10.1117/12.351822.

74 KOENIG, K.; RIEMANN, I.; FISCHER, P. Photodynamic therapy by nonresonant two-photon excitation. *Proceedings of SPIE,* v. 3592, p. 43-49, 1999. doi:10.1117/12.351512;

75 GOYAN, R. L.; CRAMB, D. T. Near-infrared two-photon excitation of protoporphyrin IX: photodynamics and photoproduct generation. *Photochemistry and Photobiology,* v. 72, n. 6, p. 821–827, 2000.

76 KAROTKI, A. et al. Simultaneous two-photon excitation of photofrin in relation to photodynamic therapy. *Photochemistry and Photobiology*, v. 82, n. 2, p. 443, 2006.

77 KHURANA, M. et al. Quantitative in vitro demonstration of two-photon photodynamic therapy using photofrin and visudyne. *Photochemistry Photobiology*, v. 83, n. 6, p. 1441–1448, 2007.

78 COLLINS, H. A. et al. Blood-vessel closure using photosensitizers engineered for two-photon excitation. *Nature Photonics*, v. 2, n. 7, p. 420–424, 2008.

79 ZOU, Q. et al. Effective two-photon excited photodynamic therapy of xenograft tumors sensitized by water-soluble bis(arylidene)cycloalkanone photosensitizers. *Journal of Medicinal Chemistry*, v. 58, n. 20, p. 7949–7958, 2015.

80 SHEN, Y. et al. Two-photon excitation nanoparticles for photodynamic therapy. *Chemistry Society Reviews*, v. 45, n. 24, p.6725–6741, 2016.

81 ZHANG, P. et al. Noncovalent ruthenium(II) complexes–single-walled carbon nanotube composites for bimodal photothermal and photodynamic therapy with near-infrared irradiation. *ACS Applied Materials & Interfaces,* v. 7, n. 41, p. 23278–23290, 2015.

82 NOGUEIRA, M. S. *Fluorescence lifetime spectroscopy for diagnosis of clinically similar skin lesions*. 2016. 263 p. Dissertação (Mestrado em Ciências) - Instituto de Física de São Carlos, Universidade de São Paulo, São Carlos, 2016.

83 PIRES, L. et al. Optical clearing of melanoma *in vivo* : characterization by diffuse reflectance spectroscopy and optical coherence tomography. *Journal of Biomedical Optics,* v. 21, n. 8, p. 081210, 2016.

84 RIGEL, D. S.; RUSSAK, J.; FRIEDMAN, R. The evolution of melanoma diagnosis: 25 years beyond the ABCDs. *CA:* a cancer journal for clinicians, v.60, n. 5, p. 301–316, 2010.

85 MORTON, C. A.; MACKIE, R. M. Clinical accuracy of the diagnosis of cutaneous malignant melanoma. *British Journal of Dermatology,* v. 138, n. 2, p. 283–287, 1998.

86 ARGENZIANO, G et al. Epiluminescence microscopy: criteria of cutaneous melanoma progression. *Journal of American Academy Dermatology*, v. 37, n. 1, p.68–74, 1997.

87 GARCIA-URIBE, A. et al. In vivo diagnosis of melanoma and nonmelanoma skin cancer using oblique incidence diffuse reflectance spectrometry. *Cancer Research*, v. 72, n. 11, p.2738–2745, 2012.

88 HARLAND, C. C. et al. Differentiation of common benign pigmented skin lesions from melanoma by high-resolution ultrasound. *British Journal of Dermatology*, v. 143, n. 2, p.281–289, 2000.

89 PRICHARD, R. S. et al. Positron emission tomography for staging and management of malignant melanoma. *British Journal of Surgery,* v. 89, n. 4, p.389–96, 2002.

90 PIRES, L. et al. Time-resolved fluorescence lifetime for cutaneous melanoma detection. *Biomedical Optics Express,* v. 5, n. 9, p.3080, 2014.

91 KIM, A. et al. A fiberoptic reflectance probe with multiple source-collector separations to increase the dynamic range of derived tissue optical absorption and scattering coefficients. *Optics Express,* v. 18, n. 6, p.5580–5594, 2010.

92 MARIAMPILLAI, A. et al. Optimized speckle variance OCT imaging of microvasculature. *Optics Letters*, v. 35, n. 8, p.1257–1259, 2010.

93 RICE, J. A. *Mathematical statistics and data analysis*. 3rd ed. United States of America: Duxbury Press; 2007.

94 PENG, Q et al. Uptake, localization, and photodynamic effect of meso-tetra(hydroxyphenyl)porphine and its corresponding chlorin in normal and tumor tissues of mice bearing mammary carcinoma. *Cancer Research,* v. 55, n. 12, p. 2620–2626, 1995.

95 Photodynamic therapy of subfoveal choroidal neovascularization in age-related macular degeneration with verteporfin: one-year results of 2 randomized clinical Trials—TAP report 1. *Archives of Ophthalmology*, v. 117, n. 10, p.1329, 1999. doi:10.1001/archopht.117.10.1329.

96 MEHRARA, E. et al. Specific growth rate versus doubling time for quantitative characterization of tumor growth rate. *Cancer Research*, v. 67, n. 8, p. 3970–3975, 2007.

97 AYERS G. D., et al. Volume of preclinical xenograft tumors is more accurately assessed by ultrasound imaging than manual caliper measurements. *Journal Ultrasound Medicine*, v. 29, n. 6, p.891–901, 2010.

98 VARGAS, G. et al. Morphological changes in blood vessels produced by hyperosmotic agents and measured by optical coherence tomography. *Photochemistry and Photobiology*, v. 77, n. 5, p.541–549, 2003.

99 SERGEEV, A. M. et al. Melanin effect on light scattering in tissues: from electrodynamics of living cells to OCT imaging. *Proceedings of SPIE, v. 2981,* p. 58–63, 1997. doi: 10.1117/12.274322.

100 SHIRMANOVA, M. In vivo study of photosensitizer pharmacokinetics by fluorescence transillumination imaging. *Journal of Biomedical Optics*, v. 15, n. 4, p.048004, 2010.

101 WEINSTEIN, D. Diagnostic and prognostic biomarkers in melanoma. *Journal Clinical Aesthetic Dermatology*, v. 7, n. 6, p.13–24, 2014.

102 LAJIS, A. F. B. et al. Depigmenting effect of kojic acid esters in hyperpigmented B16F1 melanoma cells. *BioMed Research International*, v. 2012, p. e952452, 2012.

103 LENCIONE, D. et al. The spatial distribution of the photostability of thionine in zeolite L nanochannels investigated by photobleaching lifetime imaging microscopy. *Photochemistry and Photobiology Science,* v. 15, n. 3, p.398–404, 2016.

104 SIMON, J. D. Current challenges in understanding melanogenesis: bridging chemistry, biological control, morphology, and function. *Pigment Cell & Melanoma Research*, v. 22, n. 5, p.563–579, 2009.

105 QIU, K. et al. Crossfire for two-photon photodynamic therapy with fluorinated ruthenium (II) photosensitizers. *ACS Applied Materials & Interfaces,* v. 9, n. 22, p.18482–18492, 2017.

106 DAVIDS, L. M.; KLEEMANN, B. Combating melanoma: the use of photodynamic therapy as a novel, adjuvant therapeutic tool. *Cancer Treatment Reviews,* v. 37, n. 6, p.465-475, 2010. doi: 10.1016/j.ctrv.2010.11.007.

107 CHIARELLI-NETO O, et al. Melanin photosensitization and the effect of visible light on epithelial cells. *PLOS ONE,* v. 9, n. 11, p.e113266, 2014.

108 YOON, H. E. Pheophorbide a-mediated photodynamic therapy induces autophagy and apoptosis via the activation of MAPKs in human skin cancer cells. *Oncology Reports*, v. 31, n. 1, p. 137-144, 2013. doi: 10.3892/or.2013.2856.

109 JI, H-T. et al. 5-ALA mediated photodynamic therapy induces autophagic cell death via AMP-activated protein kinase. *Molecular Cancer*, v. 9, n. 1, p.91, 2010.

110 KARS, M. D. et al. Femtosecond laser induced photodynamic therapy on 5-ALA treated SKMEL-30 cells: an efficient theranostic strategy to combat melanoma. *Biomedicine & Pharmacotherapy*, v. 68, n. 5, p. 657–662, 2014.

111 SCHMIDT-ERFURTH, U. et al. Photodynamic therapy of experimental choroidal melanoma using lipoprotein-delivered benzoporphyrin. *Ophthalmology*, v. 101, n. 1, p. 89–99, 1994.

112 GONZALEZ, V. H. Photodynamic therapy of pigmented choroidal melanomas. *Investigative Ophthalmology Visual Science*, v. 36, n. 5, p.871–878, 1995.

113 LUCENA, E. G.; MILLER, J. W. Benzoporphyrin (verteporfin) photodynamic therapy for choroidal neovascularization in age-related macular degeneration. *Arquivos Brasileiros de Oftalmologia*, v. 63, n. 6, p. 511–518, 2000.

114 Verteporfin in Photodynamic therapy study group. photodynamic therapy of subfoveal choroidal neovascularization in pathologic myopia with verteporfin. 1-year results of a randomized clinical trial--VIP report no. 1. *Ophthalmology*, v. 108, n. 5, p.841–852, 2001.

115 SAPERSTEIN, D. A. et al. Photodynamic therapy of subfoveal choroidal neovascularization with verteporfin in the ocular histoplasmosis syndrome. *Ophthalmology*, v. 109, n. 8, p. 1499–1505, 2002.

116 PORRINI, G. Photodynamic therapy of circumscribed choroidal hemangioma. *Ophthalmology*, v. 110, n. 4, p.674–80, 2003.

117 STEPHAN, H. et al. Photodynamic therapy in retinoblastoma: effects of verteporfin on retinoblastoma cell lines. *Investigative Opthalmology & Visual Science,* v. 49, n. 7, p. 3158, 2008.

118 BLASI, M. PDT for amelanotic choroidal melanoma. *Acta Ophthalmologica*, v. 86, n. s243, 2008. doi: 10.1111/j.1755-3768.2008.6362.x.

119 TSIPURSKY, M. S. et al. A review of photodynamic therapy for intraocular tumors. *Journal of Analytical & Bioanalytical Techniques*, S1:001. doi: 10.4172/2155-9872.S1-001.

120 BARBAZETTO, I. A. et al. Treatment of choroidal melanoma using photodynamic therapy. *American Journal Ophthalmology*, v. 135, n. 6, p.898–899, 2003.

121 CANAL-FONTCUBERTA, I. et al. Clinical and histopathologic findings after photodynamic therapy of choroidal melanoma. *Retina*, v. 32, n. 5, p.942–948, 2012.

122 FABIAN, I. D. et al. Primary photodynamic therapy with verteporfin for small pigmented posterior pole choroidal melanoma. *Eye*, v. 31, n. 4, p. 519–528, 2017.

123 HAMMER, D. X. et al. Experimental investigation of ultrashort pulse laser-induced breakdown thresholds in aqueous media. *IEEE Journal of Qantum Electronics,* v. 32, n. 4, p. 670-678, 1996.

124 SAMKOE, K. S. et al. Complete blood vessel occlusion in the chick chorioallantoic membrane using two-photon excitation photodynamic therapy: implications for treatment of wet age-related macular degeneration. *Journal of Biomedical Optics*, v. 12, n. 3, p. 034025, 2007.

125 KHURANA, M. et al. Drug and light dose responses to focal photodynamic therapy of single blood vessels in vivo. *Journal of Biomedical Optics,* v. 14, n. 6, p.064006, 2009.

126 STARKEY, J. R. et al. New two-photon activated photodynamic therapy sensitizers induce xenograft tumor regressions after near-IR laser treatment through the body of the host mouse. *Clinical Cancer Research*, v. 14, n. 20, p. 6564–6573, 2008.

APPENDIX A – Published paper "Time-resolved fluorescence lifetime for cutaneous melanoma detection"

Biomedical Optics EXPRESS

Time-resolved fluorescence lifetime for cutaneous melanoma detection

Layla Pires,* Marcelo Saito Nogueira, Sebastião Pratavieira, Lilian Tan Moriyama, and Cristina Kurachi

Universidade de São Paulo, Instituto de Física de São Carlos – IFSC/USP, Av. Trabalhador São Carlense, 400 - São Carlos, SP, Brazil

**laylabm@gmail.com*

Abstract: Melanoma is the most aggressive skin cancer type. It is characterized by pigmented lesions with high tissue invasion and metastatic potential. The early detection of melanoma is extremely important to improve patient prognosis and survival rate, since it can progress to the deadly metastatic stage. Presently, the melanoma diagnosis is based on the clinical analysis of the macroscopic lesion characteristics such as shape, color, borders following the ABCD rules. The aim of this study is to evaluate the time-resolved fluorescence lifetime of NADH and FAD molecules to detect cutaneous melanoma in an experimental *in vivo* model. Forty-two lesions were analyzed and the data was classified using linear discriminant analysis, a sensitivity of 99.4%, specificity of 97.4% and accuracy of 98.4% were achieved. These results show the potential of this fluorescence spectroscopy for melanoma detection.

OCIS codes: (300.6500) Spectroscopy, time-resolved; (170.3650) Lifetime-based sensing; (170.3890) Medical optics instrumentation; (170.6510) Spectroscopy, tissue diagnostics; (170.6935) Tissue characterization.

References and links

1. D. S. Rigel, J. Russak, and R. Friedman, "The Evolution of Melanoma Diagnosis: 25 Years Beyond the ABCDs," CA Cancer J. Clin. 60(5), 301–316 (2010).
2. C. Garbe, T. K. Eigentler, U. Keilholz, A. Hauschild, and J. M. Kirkwood, "Systematic Review of Medical Treatment in Melanoma: Current Status and Future Prospects," Oncologist 16(1), 5–24 (2011).
3. R. Marchesini, A. Bono, C. Bartoli, M. Lualdi, S. Tomatis, and N. Cascinelli, "Optical imaging and automated melanoma detection: questions and answers," Melanoma Res. 12(3), 279–286 (2002).
4. S. Seidenari, F. Arginelli, C. Dunsby, P. M. W. French, K. König, C. Magnoni, C. Talbot, and G. Ponti, "Multiphoton laser tomography and fluorescence lifetime imaging of melanoma: morphologic features and quantitative data for sensitive and specific non-invasive diagnostics," PLoS ONE 8(7), e70682 (2013).
5. C. Gerhäuser, "Cancer cell metabolism, epigenetics and the potential influence of dietary components – A perspective," Biomed. Res. 23(1), 1–21 (2012).
6. D. A. Scott, A. D. Richardson, F. V. Filipp, C. A. Knutzen, G. G. Chiang, Z. A. Ronai, A. L. Osterman, and J. W. Smith, "Comparative metabolic flux profiling of melanoma cell lines: beyond the Warburg effect," J. Biol. Chem. 286(49), 42626–42634 (2011).
7. K. Koenig and I. Riemann, "High-resolution multiphoton tomography of human skin with subcellular spatial resolution and picosecond time resolution," J. Biomed. Opt. 8(3), 432–439 (2003).
8. M. C. Skala, K. M. Riching, A. Gendron-Fitzpatrick, J. Eickhoff, K. W. Eliceiri, J. G. White, and N. Ramanujam, "In vivo multiphoton microscopy of NADH and FAD redox states, fluorescence lifetimes, and cellular morphology in precancerous epithelia," Proc. Natl. Acad. Sci. U.S.A. 104(49), 19494–19499 (2007).
9. M. S. Islam, M. Honma, T. Nakabayashi, M. Kinjo, and N. Ohta, "pH dependence of fluorescence lifetime of FAD in solution and in cells," Int. J. Mol. Sci. 14(1), 1952–1963 (2013).
10. R. Martinez-Zaguilán, E. A. Seftor, R. E. Seftor, Y. W. Chu, R. J. Gillies, and M. J. Hendrix, "Acidic pH enhances the invasive behavior of human melanoma cells," Clin. Exp. Metastasis 14(2), 176–186 (1996).
11. M. L. Wahl, J. A. Owen, R. Burd, R. A. Herlands, S. S. Nogami, U. Rodeck, D. Berd, D. B. Leeper, and C. S. Owen, "Regulation of intracellular pH in human melanoma: potential therapeutic implications," Mol. Cancer Ther. 1(8), 617–628 (2002).
12. M. G. Vander Heiden, L. C. Cantley, and C. B. Thompson, "Understanding the Warburg Effect: The Metabolic Requirements of Cell Proliferation," Science 324(5930), 1029–1033 (2009).

#214104 - $15.00 USD Received 16 Jun 2014; revised 8 Aug 2014; accepted 10 Aug 2014; published 22 Aug 2014

APPENDIX B – Published paper "Optical clearing of melanoma *in vivo*: characterization by diffuse reflectance spectroscopy and optical coherence tomography"

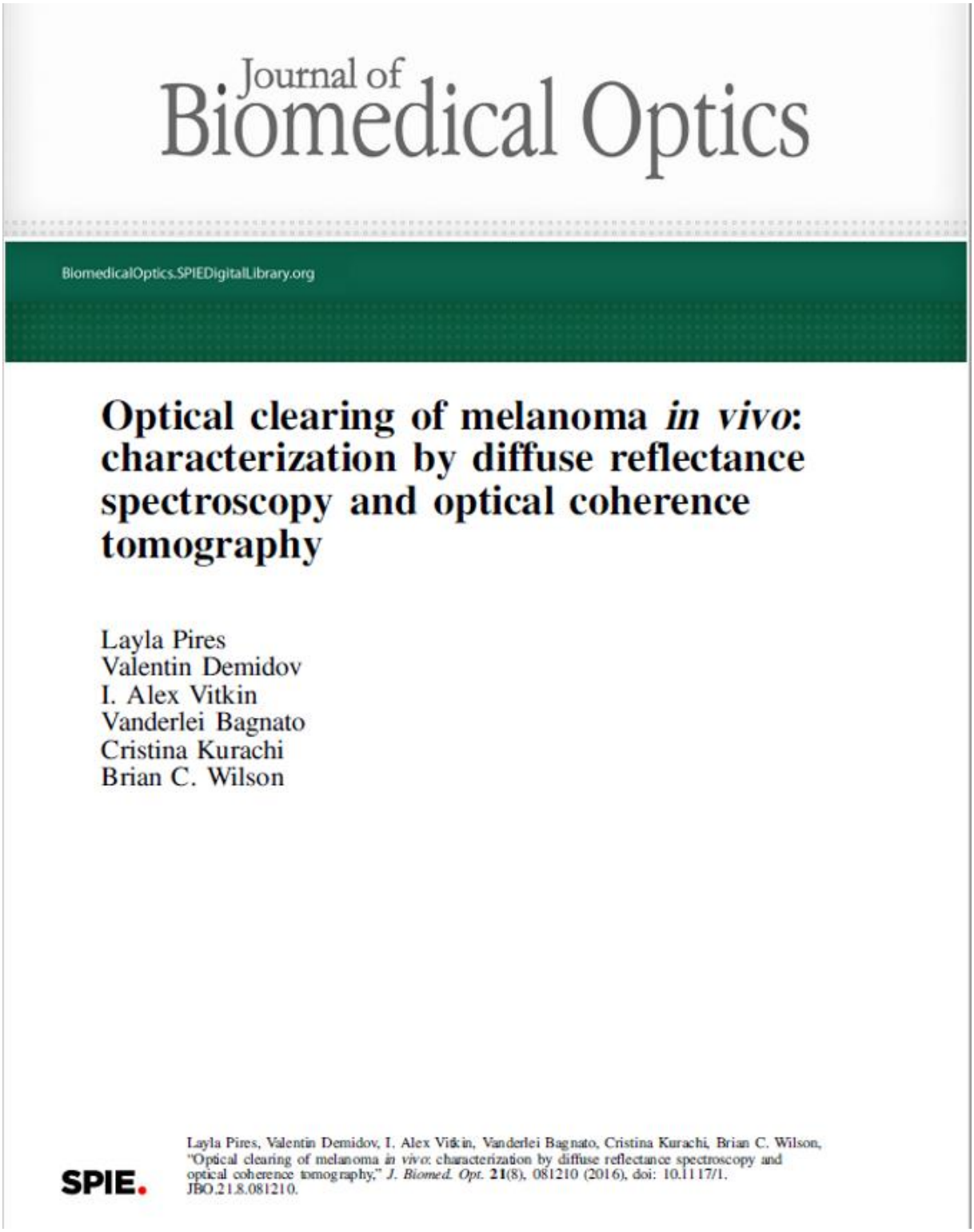

Journal of Biomedical Optics

BiomedicalOptics.SPIEDigitalLibrary.org

Optical clearing of melanoma *in vivo*: characterization by diffuse reflectance spectroscopy and optical coherence tomography

Layla Pires
Valentin Demidov
I. Alex Vitkin
Vanderlei Bagnato
Cristina Kurachi
Brian C. Wilson

SPIE.

Layla Pires, Valentin Demidov, I. Alex Vitkin, Vanderlei Bagnato, Cristina Kurachi, Brian C. Wilson, "Optical clearing of melanoma *in vivo*: characterization by diffuse reflectance spectroscopy and optical coherence tomography," *J. Biomed. Opt.* **21**(8), 081210 (2016), doi: 10.1117/1.JBO.21.8.081210.

ANNEX A – Animal Research Ethics Committee approval – UFSCar

UNIVERSIDADE FEDERAL DE SÃO CARLOS
PRÓ-REITORIA DE PESQUISA
Comissão de Ética no Uso de Animais
Via Washington Luís, km. 235 - Caixa Postal 676
Fones: (016) 3351.8025 / 3351.9679
Fax: (016) 3351.8025
CEP 13560-970 - São Carlos - SP - Brasil
ceua@ufscar.br - www.propg.ufscar.br

Parecer da Comissão de Ética no Uso de Animais

nº 059/2012

Protocolo nº. 055/2012

A Comissão de Ética no Uso de Animais da Universidade Federal de São Carlos - CEUA/UFSCar **APROVOU** o projeto de pesquisa intitulado *"Desenvolvimento de estratégias para terapia fotodinâmica em melanoma."*, submetido pela pesquisadora *Layla Pires.*

São Carlos, 4 de outubro de 2012.

Azair Liane Matos do Canto de Souza

Profa. Dra. Azair Liane Matos do Canto de Souza.

Presidente da Comissão de Ética no Uso de Animais

ANNEX B – Research Ethics Committee approval – IFSC/USP

UNIVERSIDADE DE SÃO PAULO
Instituto de Física de São Carlos

Av. Trabalhador são-carlense, 400 / 13566-590
Caixa Postal 369 / 13560-970
São Carlos - SP, Brasil
Fone: +55 16 3373-9758
www.ifsc.usp.br

PARECER DA COMISSÃO DE ÉTICA PARA O USO DE ANIMAIS – CEUA/IFSC

Protocolo nº 03/2014

A Comissão de Ética para o Uso de Animais do Instituto de Física de São Carlos – CEUA/IFSC, em reunião realizada no dia 24/06/2014, **aprovou** o projeto de pesquisa intitulado "Desenvolvimento de estratégias ópticas para diagnóstico e tratamento do melanoma", submetido pela pesquisadora Layla Pires. Outrossim, informamos que foi aprovada a utilização de 200 camundongos heterogênicos de linhagem balb/c nude, com idade de 6 semanas e peso aproximado de 15g.

São Carlos, 30 de outubro de 2014.

Prof. Dr. Alberto Tannus
Suplente da Presidente em exercício da CEUA/IFSC

ANNEX C – Animal Care Committee approval – Princess Margaret Cancer Centre - UHN

1 AUP Info

Select the Animal Care Committee(ACC) for this AUP submission	OCI
Indicate the Category of Invasiveness (as per CCAC guidelines)	
C - Experiments which cause minor stress or pain of short duration	
Please indicate the purpose of animal use as per CCAC Guidelines, see "Instructions document". Select only one.	• 2 - Medical Studies, including Veterinary Medicine

Title of Animal Use Protocol Application
Please provide a brief title to the protocol which must reflect the content of the application. e.g. "The role of metabolic overload in liver regeneration in the rat after surgical creation of a communication between the common bile duct and the jugular vein and ligation of a branch of the portal vein."

Combination use of optical clearing agents with
Photodynamic therapy for melanoma treatment

This AUP currently has 5 attachment(s). This supplementary documentation includes:

- (PDF Document) attachment 1
- (PDF Document) atachment 2
- (PDF Document) ACC Letter
- (PDF Document) Review 1
- (PDF Document) Review 2

2 Personnel Assignments

Principal Investigator	Brian C Wilson
Associate Scientist(s)	
Research Staff	Layla Pires
Anesthesia	Layla Pires
Surgery	Layla Pires
Procedures	Layla Pires
Monitoring and nursing	Layla Pires
Emergency Personnel	Layla Pires

3 Personnel Details

Full Name:	Brian C Wilson	Office Address:	MaRS Centre Toronto Medical Discovery Tower 15, 314 101 College St., M5G 1L7 Toronto, Ontario, Canada
Lab Address:	MaRS Centre Toronto Medical Discovery Tower 15, 314 101 College St., M5G 1L7 Toronto, Ontario, Canada	Email:	wilson@uhnres.utoronto.ca